

NMR studies of polymer networks under deformation

Dissertation

zur Erlangung des Doktorgrades der Naturwissenschaften
(Dr. rer. nat)

der

Naturwissenschaftlichen Fakultät II
Chemie, Physik und Mathematik

der Martin-Luther-Universität
Halle-Wittenberg

vorgelegt von

Frau Anna Naumova

geboren am 20.07.1989 in Weliki Ustjug

Gutachter:

1. Prof. Dr. Kay Saalwächter (Betreuer)
2. Prof. Dr. Thomas Thurn-Albrecht
3. Prof. Dr. Eike Brunner

Eröffnung des Promotionsverfahrens: 04.09.2019

Öffentliche Verteidigung: 09.12.2019

Contents

1	Introduction	1
2	Polymer networks	5
2.1	Peculiarities of polymers	5
2.2	Polymer melts and solutions	7
2.2.1	Flexibility of a polymer chain	7
2.2.2	Freely jointed chain model and random walk	8
2.2.3	Chain segment - Kuhn monomer	9
2.2.4	Conformation of a polymer coil	10
2.3	Polymer networks: elastic materials	12
2.3.1	Thermodynamics of rubber elasticity	13
2.3.2	Elasticity of a single polymer chain	16
2.3.3	Real vs ideal polymer network	17
2.4	Interaction of polymers with liquids	19
2.4.1	Swelling of polymer melt and polymer network	20
2.4.2	Polymer-solvent interactions	21
2.5	Elasticity models	23
2.5.1	Affine model	24
2.5.2	Phantom model	25
2.5.3	Tube model	26
2.6	Elastic free energy of a polymer network	27
2.7	Isotropic Swelling	29
2.7.1	Swelling Theory	29
2.7.2	NMR of isotropically swollen polymer networks	31
2.8	Small-Angle Neutron Scattering	33
2.8.1	Theory	33
2.8.2	Deformed and swollen polymer networks	34
3	Basics of NMR and application to polymers	37
3.1	General concepts of NMR	38
3.1.1	Spin and Magnetization	38
3.1.2	Hamiltonian and spin-spin interactions	39
3.2	Dipolar interaction in polymer networks	40
3.2.1	Secular approximation for homonuclear dipolar coupling	41
3.2.2	Residual dipolar coupling of polymer networks	42

3.3	DQ NMR experiments of polymer networks	43
3.3.1	Essentials of NMR measurements	43
3.3.2	NMR pulse sequence for measuring dipolar coupling	46
3.3.3	DQ NMR theoretical concepts for polymer networks	48
3.3.4	Data fitting	49
3.3.5	Tikhonov regularization of build-up function I_{nDQ}	51
4	Samples and NMR analysis in dry and swollen state	53
4.1	Samples details	53
4.2	Good solvents for samples	55
4.3	NMR characterisation	57
4.3.1	Dry samples	57
4.3.2	Swollen samples	59
5	Numerical calculations of the NMR response of networks	63
5.1	Calculation of I_{nDQ} for unstretched polymer networks	64
5.2	Model build-up functions	65
5.2.1	\sin^2 function	65
5.2.2	Single-orientation Abragam-like function	67
5.2.3	Effect of distributions	71
5.3	Calculation of I_{nDQ} for different elasticity models	73
	Affine model	74
	Phantom model	74
	Tube model	75
	Meta-data fitting	76
6	Deformation of dry rubber	79
6.1	Uniaxially stretched rubber	80
6.1.1	Experiment	80
6.1.2	Results	81
6.2	Uniaxially compressed rubber	83
6.2.1	Experiment	83
6.2.2	Results	84
6.3	Pure-shear deformation of rubber	85
6.3.1	Experiment	85
6.3.2	Results	85
6.4	Discussion	86
6.4.1	Basic elastic models	86
6.4.2	"Reduced" elastic models	88
7	Deformation of swollen rubber	91
7.1	Swelling of pre-stretched rubber	92
7.1.1	Experiment	92
7.1.2	Degradation test	93
7.1.3	Results	94

7.2	Deformation of pre-swollen rubber	95
7.2.1	Uniaxial compression	95
	Experiment	95
	Results	96
7.2.2	Pure shear	97
	Experiment	97
	Results	98
7.3	Anisotropic swelling	99
	Experiment	99
	Results	100
8	Summary	103
A	Samples	105
	Densities of rubbers and solvents	105
	Molecular weight M_c	105
	Bibliography	107
	Erklärung	119

Chapter 1

Introduction

Elasticity is one of the most important properties of rubber. Owing to this phenomenon, rubber can restore their original shape after large deformation: mechanical stretching, compression or shear. The restoring force of the stretched sample to the original state is entropic in nature. William Thomson (Lord Kelvin) and James Prescott Joule concluded the entropic nature of rubber elasticity already in 19-th century [1], not long after natural rubber was cross-linked for the first time in 1838.

To calculate precisely the forces and the local deformations one should calculate the entropy of the polymer network and set up the relationship between total numbers of possible configurations for the network and the applied external perturbations. For the explanation of the experimental data plenty of models were suggested. The most common one are the two "classical" models: affine and phantom, and the non-classical tube model [2].

The classical affine model is assuming that the microscopic deformation of the network chains are exactly the same as the deformation of the whole sample. It is based on continuum mechanics rather than molecular concepts. Additionally, it does not take the fluctuations of the cross-links into account.

The phantom network model was first proposed by James and Guth [3], and considers cross-links fluctuations. Although some of the assumptions of this model are not quite realistic, the model is a good approximation for different experiments,

such as deuterium nuclear magnetic resonance (NMR) and small-angle neutron scattering (SANS) [4–6]. Burak Erman calculated the expressions for the transformation of the mean-squared chain vector according to the constrained junction model. The experimental data points mostly lies in between the phantom and affine model predictions [4].

It is not possible to measure intrinsic characteristic of isolated chains because the influence of surrounding chains in concentrated polymer melt or in an network could not be separated and ruled out. However neither affine nor phantom network models take into consideration chain entanglements (interaction between chains), which are important in the elasticity phenomenon. Importance of the inter-chain interaction is reflected via nematic-like interaction in swollen networks, observed by deuterium NMR [7].

The idea on how to take into account the effect of surrounding chains (entanglements, excluded volume interactions) for polymer networks, comes from the theory for the polymer melts, the reptation model [8]. In comparison to the melt, the network entanglements have a much stronger effect on the viscoelastic behaviour, because cross-links forestall the reptation motion and thus the constraint release. The concept of the tube model became rather popular among polymer scientist and therefore several tube models were proposed for describing the effect of the surrounding chains [9–13].

Recently two new models were proposed, real elastic network theory (RENT) and the phantom model of Lang [14–17]. The main purpose of these models is the accounting of the defects (loops, dangling ends or free chains) influence on the network elasticity. RENT and Lang’s models take the phantom network model as a starting point and calculate the reduction of the elastic effectiveness due to the defects. These models were supported by the experiments results [15].

Polymer networks are complex systems and measurements of microscopic deformations can only be observed by a few experimental techniques. First attempts to obtain microscopic information were made by SANS experiments [18, 19]. Such experiments are restricted by the labelled networks and in this instance, double-quantum NMR (DQ NMR) experiments as used in this thesis have an advantage, because they do not require labelling of the sample. DQ NMR is based on the anisotropic dipole-dipole interactions of protons. In highly mobile systems like melts, these dipolar interactions are averaged out. While the network chains are

also mobile, they are restricted by the crosslinks, but also the closer the crosslinks are to each other, the less restricted is a segment of the chain [20]. In any case, if the segmental motion is very fast, it will remain anisotropic because of these constraints. This phenomenon is used in DQ NMR, which monitors the motional anisotropy as D_{res} (residual dipolar coupling). D_{res} contains information about the ratio between end-to-end length and contour length of the polymer chain.

By using DQ NMR technique, we could measure the end-to-end distance between the cross-links of the network. From the data, we can obtain information about the microscopic deformation of polymer chains under the deformation and swelling [21–24], thus verify the experimental results with different elasticity models. Previous investigations of our group on uniaxially stretched rubber shows on average a nonaffine behaviour [23, 24], whereas isotropically swollen polymer networks were found to follow an affine expansion in the late stage of swelling [21, 22]. In the current work, I am using DQ NMR measurements in order to investigate microscopic stretching of polymer chains during anisotropic swelling and under different mechanical deformations (uniaxial and as well biaxial) of not only dry, but also swollen polymer networks. The main focus is a comparison of chain deformation in dry and swollen state.

The leading hypothesis for the present work is that the polymer chains of a highly swollen rubber may follow a more affine-like behaviour under deformation. In this study, we checked if chains are deformed at a higher extent in the swollen than in dry state. Our various combinations of swelling and stretching show that in swollen state under mechanical strain the network chains are stretched as weakly as in dry state. The reasons of such weak local deformation are most probably a high inhomogeneity and significant chain reorganization of the swollen network. Comparisons of the MQ NMR data for mechanically deformed dry and then swollen rubber show that the averaged dipolar coupling is not changed, but its distribution is considerably increased. This means that the swelling of the prestretched polymer network does not change the average relative configuration of chains but results instead in significant rearrangements.

The key results of this thesis have been published in two articles in *Solid State Nuclear Magnetic Resonance* [25] and *Macromolecules* [26].

Chapter 2

Elastomers - polymer networks

”Dear colleague, drop the idea of large molecules; organic molecules with a molecular weight higher than 5000 do not exist. Purify your products, such as rubber, then they will crystallize and prove to be low molecular compounds!” wrote Heinrich Wieland, the 1927 Nobel laureate in chemistry in a letter to Staudinger in end of the 1920s.

2.1 Peculiarities of polymers

The theoretical review in this chapter is based on the books of Bartenev [27, 28], Kozlov [29], Rubinstein and Colby [30], Grosberg and Khokhlov [31] and Tanaka [32], [33].

When we hear the word ”polymer”, many of us would imagine plastics. However, plastics is only one representative of the polymer material group. Silk, wool, skin, resin, rubber and many other biological substances are also polymers.

Polymers are high molecular compounds, which consist of repetitive groups made of atoms or molecules. These repetitive groups are called monomers. Monomers in the macromolecule are connected by covalent bonds. Such high molecular compounds are often named macromolecules. The size of one macromolecule could vary from several angstroms up to centimetres.

All macromolecules have three distinct characteristics: large number of monomers, chain-like structure and flexibility. These characteristics enable the macromolecules to exhibit specific properties which are not observed in low molecular materials.

Due to the chain-like structure of polymers, the entropy is lower when compared to a low molecular soft material. The monomers within a polymer chains are spatially restricted by chemical bonds. This means that polymer materials have an extremely low entropy in comparison to the low molecular substances.

The length of macromolecules and the relatively weak interactions of non-neighbouring monomers lead to a high conformational flexibility of the polymer chains. Due to a large amount of monomers, the chain could be considered as a macroscopic linear system: a long uniform flexible thread. The flexibility of a polymer chain is unique, because it is based on the rotation of chemical bonds rather than the variation of bond length or bond angle. In order to describe the physics of such system, methods of statistical physics are commonly applied.

Physical states of polymers also differ from non-polymeric material states. Low molecular materials are found in 4 fundamental states of matter: solid, fluid, gas or plasma. For polymers plasma state is not possible because of the high temperatures and ionisation: the polymer would be degraded into small molecules. A gas is also not possible: polymer chains are too heavy. Single-crystals cannot be formed from a polymer chains either but only semi-crystalline states. Two non-equilibrium solid states of polymers is then possible: glass and semi-crystalline states.

From 4 essential states of matter for low molecular substances only fluid and solid states are possible for polymers. At the same time macromolecules have common polymer specific states: semicrystalline, viscoelastic and elastic. Some non polymeric material could also be in rather viscous (for example glycerol) and glassy states. The most interesting and specific states of polymers are semicrystalline and elastic - there are no such low molecular substances which could be in these states of matter.

In this work we would investigate *elastic property* of polymer materials: polymer networks or elastomers. Polymer networks are complex materials and to understand its properties first we need to "look" at polymer melts.

2.2 Polymer melts and solutions

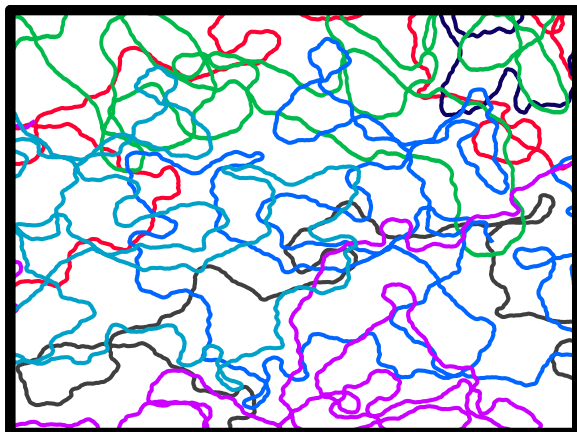


FIGURE 2.1: A polymer melt is a "liquid" consisting of a polymer chains. At temperatures higher than T_g polymer melt has viscoelastic properties and could flow. At lower temperatures the system of polymer chains forms a glass.

Polymer system in normal condition is a polymer "liquid", where polymer chains could move freely with each other. The pool of long chains has a viscoelastic properties. If there are no small molecules in the system, then it is called a polymer melt. When there are solvents present in the system, it is then called a polymer solution.

In order to describe a system of polymer chains, the behaviour of a single polymer chain should be first addressed. An ideal macromolecule is a chain of molecules which does not interact with the molecules of the same chain, molecules of other chains or solvent molecules. Such an approximation is similar to the model of ideal gas: all volume interactions are neglected. The model of an ideal polymer chain is applicable to polymer melts and dilute solutions in the so-called Θ state (corresponding to the Boyle refernce of a real gas) within a good approximation.

2.2.1 Flexibility of a polymer chain

The segments within the polymer chains are not fixed but move relative to each other: displacements, oscillations and rotations. As a result of these motions, chemical lengths and valence bond angles could change within a small range, not more than 3% of magnitude. Among different atom motions in the molecule, *the rotation* of the atoms around chemical bonds is crucial for polymers.

Inter-segmental rotation of a polymer chain is a part of total kinetic energy of a molecule. Consequently, at increasing temperatures, energy is used not only for translational and rotational movement of molecules in space, but also for inner

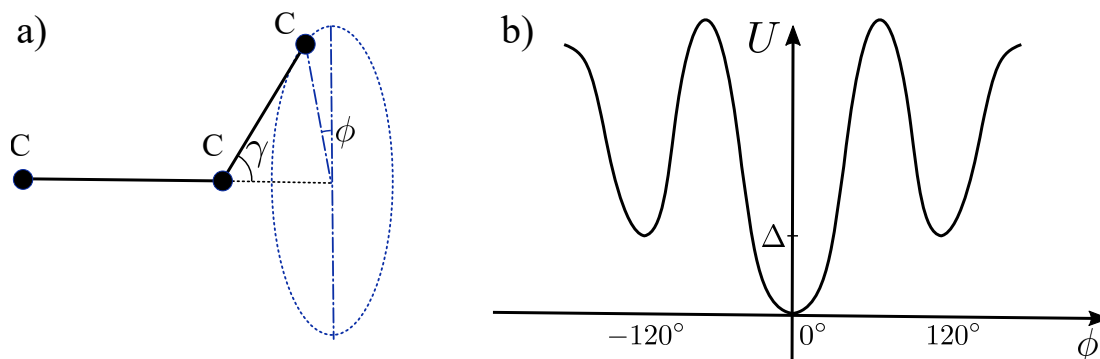


FIGURE 2.2: a) Rotation of the $C-C$ bond (γ is a bond angle, ϕ is an rotational angle); b) Relative energy of the system depending on the rotational angle ϕ .

rotation. At temperatures high enough, inner rotations could become free, when the kinetic energy is enough to make possible for atom groups the full turnover around chemical bonds. In most cases, at normal working temperatures, the maximum rotation angles are limited for the polymer chains. For example for the C-C single bond there are three minima of potential energy: one trans and two gauche states (see fig.2.2b).

Flexibility of the polymer chain could be divided into two types: thermodynamic and kinetic. Thermodynamical flexibility defines the conformation of macromolecule in equilibrium (in melt or diluted solution). Kinetic flexibility characterizes kinetics of the macromolecule transformation from one to another conformation. The kinetic flexibility is not a constant for the polymer chain, but depends on the external force parameters: frequency, load, rate [34].

2.2.2 Freely jointed chain model and random walk

A freely jointed chain model assumes, that torsion angle for every monomer have equal probability for all angles: $-\pi < \phi \leq \pi$, and bond lengths are presumed fixed. Let us consider a polymer chain consisting of n number of monomers with the bond vectors \vec{a}_i identical length a (shown on the fig.2.3a). Due to the fact that the orientations of monomers are independent from each other in the freely jointed chain model, the angles between vectors \vec{a}_i and \vec{a}_j ($i \neq j$) could take a values between 0 up to 2π with equal probability. This means, that mean value of cosine of the angle between the vectors \vec{a}_i and \vec{a}_j (if $i \neq j$) is zero: $\langle \cos \theta_{ij} \rangle = 0$. Then scalar product of the vectors \vec{a}_i and \vec{a}_j if $i \neq j$ is also zero: $\langle a_i a_j \rangle = a^2 \langle \cos \theta_{ij} \rangle = 0$,

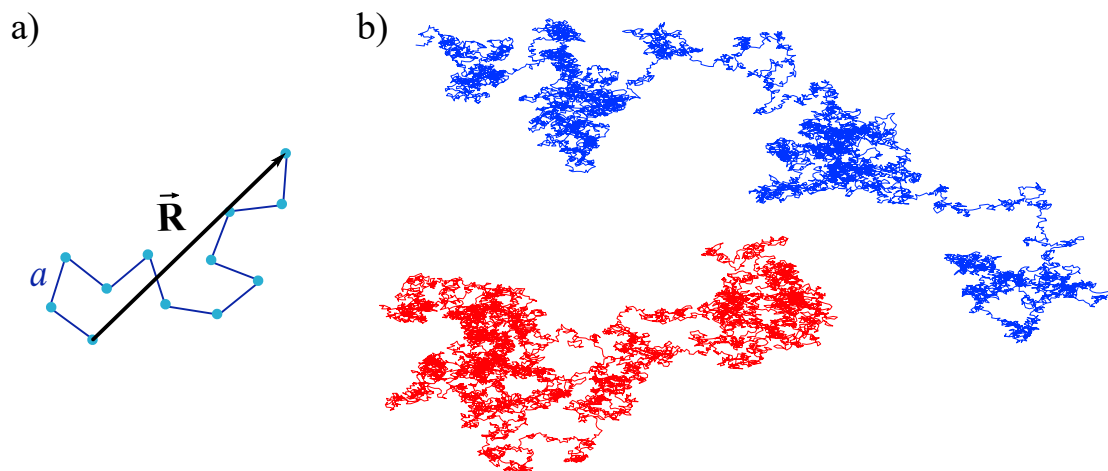


FIGURE 2.3: a) Model of freely jointed chain: a is the length of covalent bond, \vec{R} is end-to-end vector. b) Examples of two polymer chain conformations, according to the freely jointed chain model. The *random walk* calculations were done in MATLAB for 10^4 monomers.

and non zero in case if $i = j$: $\langle a_i a_i \rangle = a^2 \langle \cos 0 \rangle = a^2$. As a result, we get the expression for the mean-square end-to-end distance R :

$$\langle R^2 \rangle = na^2, \quad (2.1)$$

where n is number of monomers in the chain and a - length of the monomer. The averaged size of macromolecule is proportional to the square root of the number of monomers in the chain: $R = \langle R^2 \rangle^{1/2} = n^{1/2}a$. Assuming a large amount of monomers ($n \gg 1$), the averaged end-to-end distance is significantly lower than the contour length of the chain: $L = na$. This infers that the conformation of the polymer chains is more likely to be a tangled coil, rather than a linearly stretched structure of stretched line is negligible.

In fig.2.3b an example is shown of two simulated conformation states of the polymer chain according to the freely jointed chain model. These chains contain 10^4 monomers and are represented by a *random walk*.

2.2.3 Chain segment - Kuhn monomer

A free rotation of monomers is not usually realized in real polymer systems. In reality, every monomer could make only restricted rotation in relations to its own

neighbours, while the model of free jointed chain does not consider this case. Nevertheless any polymer chain could be broken down in segments of few monomers such a way, that these segments correspond to each other as a freely jointed segments. If every monomer could rotate at angle α to it's neighbour, then this monomer could rotate at angle 2α to the subsequent neighbour in the line. The rotation angle between the "first" and monomer number " $360^\circ/\alpha = n_0$ " would be 360° . As a result of these monomer rotation, the polymer chains are able to rotate "freely" at the n_0 -th monomer and the polymer chain could be broken down into many segment which are able to rotate "freely" in relation to each other. Such segment is called *Kuhn monomer* and it's length - *Kuhn length*, b .

Hence the countour length of the chain could be written in terms of Kuhn segments as $L = Nb$ and the mean-square end-to-end distance R would be proportional to the square root of the number of segments which is defined as a Kuhn segment as oppose to a monomer segments: $R = \langle R^2 \rangle^{1/2} = N^{1/2}b$, where N is number of Kuhn monomers in the chain, and b - is a Kuhn length. A longer polymer chain would lead to a more compact coil conformation due to the mean-square end-to-end distance being proportional to the square root of the number of segments.

Depending on the flexibility of the polymer, the Kuhn length varies. A stiffer polymer chain would indicate a lower flexibility of the chains, henceforth, a longer Kuhn length. For example, the Kuhn length of natural rubber contains 5-15 monomers, in PDMS (Polydimethylsiloxane) is has 5 monomers, and in cellulose it has 20-50 monomers [29]. It is important to note that the size of the Kuhn segment is not fixed for a polymer, but it is altered in accordance to the physical conditions: temperature, molecular weight, cross-link density, presence of solvents or other substances. Therefore Kuhn length should be considered as an averaged value of the segment.

2.2.4 Conformation of a polymer coil: end-to-end distance distribution

A polymer chain is flexible, if the number of statistical segments in the chain is large enough to have independent orientations from each other. This infers that for flexible chain number of Kuhn segments N should be large enough: $N > 10$.

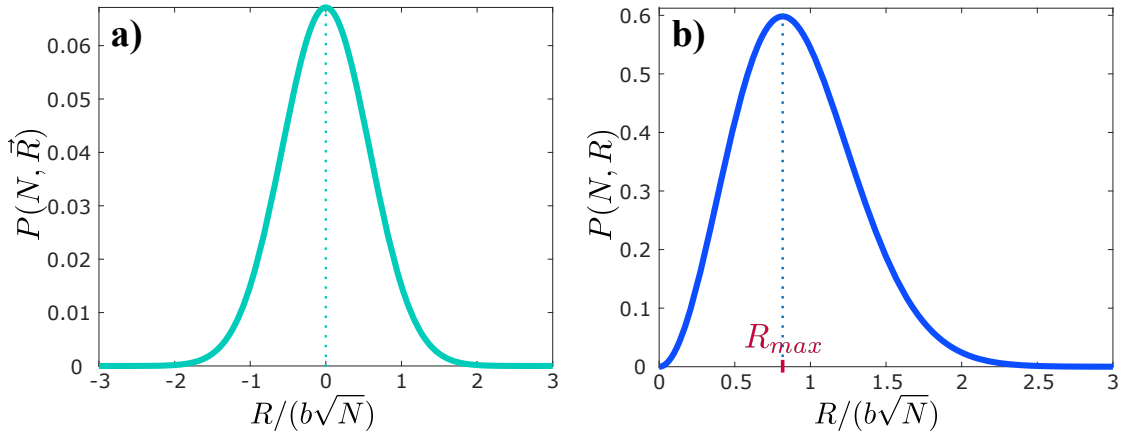


FIGURE 2.4: a) The probability distribution function for end-to-end vector \vec{R} of an ideal linear chain of N monomers b) The probability distribution function for end-to-end distance R of an ideal linear chain of N monomers.

The polymer chain characteristics can be obtained by averaging the whole set of chain conformations. Conformation of the chain is characterized by the mean-square end-to-end distance: $R = \sqrt{\vec{R}^2}$. The distribution function $P(N, \vec{R})$ is describing the probability, that polymer chain with N Kuhn segments has an end-to-end vector \vec{R} . This probability could be defined as averaged over time for one macromolecule or as an averaged over ensemble of identical chains. $P(N, \vec{R})$ proportional to the number of conformations $\Omega(N, \vec{R})$, which could be realized by the chain with end-to-end vector from \vec{R} to $\vec{R} + d\vec{R}$:

$$P(N, \vec{R}) = \frac{\Omega(N, \vec{R})}{\int \Omega(N, \vec{R}) d\vec{R}}. \quad (2.2)$$

The expression for function $P(N, \vec{R})$ could be derived by 3D random walk calculations [30]. The probability distribution function in Cartesian coordinates for the end-to-end vector \vec{R} of a freely jointed chain of N Kuhn segments is shown on the fig.2.4a and the expression for it is:

$$P(N, \vec{R}) = \left(\frac{3}{2\pi Nb^2} \right)^{3/2} \exp\left(-\frac{3\vec{R}^2}{2Nb^2} \right), \quad (2.3)$$

where b is length of Kuhn segment and \vec{R} - is a specific vector with the magnitude R , but not all vectors with this magnitude. $P(N, \vec{R})$ is a Gaussian function. The polymer chains which are obeying the Gaussian distribution are "Gaussian chain".

To get the probability distribution function as a function of the end-to-end distance $R = |\vec{R}|$ we need to multiply the function $P(N, \vec{R})$ with the sphere area $4\pi R^2$:

$$P(N, R) = 4\pi R^2 \left(\frac{3}{2\pi N b^2} \right)^{3/2} \exp \left(-\frac{3R^2}{2N b^2} \right). \quad (2.4)$$

The function $P(N, R)$ (eq.2.4) is not a Gaussian, and its maximum (the most probable end-to-end distance) $R_{max} = b\sqrt{2N/3}$ is less than the mean-square end-to-end distance $\sqrt{\langle R^2 \rangle} = b\sqrt{N}$. On the fig.2.4b the x-scale is normalized by $b\sqrt{N}$ and the most probable end-to-end distance $R_{max} = \sqrt{2/3} \approx 0.8$.

2.3 Polymer networks: elastic materials

Polymers in an elastic state are called elastomers or rubbers. Elastomers are solid amorphous materials and very often referred as soft solids. Essentially they are networks, which can be obtained from polymer melts via the vulcanization process. During vulcanization, chemical reactions occur between the polymer chains and cross-linking agents, which creates bridges between the polymer chains. When sufficient crosslinks are created, the result is a single macroscopic polymer network - rubber. This implies that the polymer chains are not able to move independently with each other and rubber could not flow, such was the case for polymer melts. On the scale smaller than the crosslink distance however, the polymer chain segments are not constrained and have the same behaviour, as in the melts. During elongation these polymer coils straighten oneself and allow the rubber to reach high stretch.

Rubbers are very distinct from ordinary solid materials such as metals, wood, ceramics etc. The main difference is the ability to have large reversible deformations under moderate stress. Natural rubber could return to the original shape even after stretching up to 700%, which exceed about 1000 times the deformation of metals. The ultimate tensile stress values, which is the maximum stress before material fracture are also very different: 2000 MPa for steel, and 30 MPa for rubber. At the same time, the value of the coefficient of thermal expansion for rubber is close to that in liquids.

The flexibility of polymer chains is the key point for the hyperelasticity. If all the bonds are in the trans state, then the chain would be a straight thread: a perfect

zig-zag line. Polymer chains however, are not linear, it is often a combination between trans and gauche states. At room temperature the rate of change between two states is about 10^{10} s^{-1} , and this rate strongly depends on the temperature [35]. If $T < T_g$ (T_g - glass transition temperature), the state-changing time diverges to infinity (at $T_V \approx T_g - 50\text{K}$) and the rubber is no longer elastic. This means that not all polymer networks in our conventional conditions would exhibit rubber-like behaviour, but only those which have glass temperature much lower than the current working temperature.

2.3.1 Thermodynamics of rubber elasticity

A thermodynamic description of a process is possible if the process is reversible (quasi-static). Such description of deformation process is possible if chemical processes and fluidity could be neglected or discount. Rubber is a cross-linked polymer and therefore polymer chains are not flowing during deformation. It means that irreversible ductile deformations are almost absent and a highly elastic stresses arises upon the network deformation. Internal frictional forces are also present during deformation which leads to a hysteresis behaviour that is observable in the stress-strain dependency. When applying low deformation rate on rubber, then the hysteresis becomes smaller and eventually disappears in the case of very slow (quasi-static limit) deformation. In such situation, the rubber acts as a perfectly elastic material and it is in this region that the thermodynamic ratios are applicable.

Elasticity of rubber is connected with the change of conformational entropy while resilience of other materials is due to the change of the internal energy. Thermodynamics of rubber is described by the Helmholtz free energy F , at constant temperature and volume. To describe the polymer network under deformation, we use the following thermodynamic expression:

$$dF = -SdT - pdV + fdL, \quad (2.5)$$

where dF is a free energy change, S - an entropy of the system, p - a pressure, dV - a volume change, f - a force applied to the sample and dL is the elongation due to the applied force. The force could be calculated from the equation 2.5 through the partial derivative:

$$f = (\partial F/\partial L)_{T,V}. \quad (2.6)$$

In the undeformed state at $L = L_0$ the force f is close to zero, which conforms to the condition $(\partial F/\partial L)_{T,V} = 0$. It means that for small deformation, the equation 2.6 could be expanded into Taylor series:

$$f = (\partial^2 F/\partial L^2)_{T,V,L_0}(L - L_0)^2 + \dots \quad (2.7)$$

In the first approximation, the force is proportional to the elongation which is in line with Hooke's law. The first law of thermodynamics for closed system reads:

$$dF = dU - TdS. \quad (2.8)$$

If we substitute first law of thermodynamics (eq.2.8) into the equation 2.6 we get the relation for the force:

$$f = (\partial F/\partial L)_{T,V} = (\partial U/\partial L)_{T,V} - T(\partial S/\partial L)_{T,V} \simeq -T(\partial S/\partial L)_{T,V}, \quad (2.9)$$

where the first term: $(\partial U/\partial L)_{T,V}$ - internal energy variation and second term: $T(\partial S/\partial L)_{T,V}$ - entropy variation. In contrast to the conventional solids, the energetic contribution to the force is negligible for the elastomers: $(\partial U/\partial L)_{T,V} = 0$.

It is the entropic contribution that is the most important in rubbers. Due to the dominance of the entropic term in the energy, polymer networks have a distinct temperature dependence of the force at constant elongation. For other solids (for example metals or ceramics), the force is slightly decreasing with increasing temperature while for while the temperature dependency is reversed for rubbers. The first term in equation 2.9 is zero for ideal networks and the force only contains the entropic contribution: $\partial S/\partial L$. An entropy of the extended polymer network is lower which means that $\partial S/\partial L < 0$. This leads to an increase of the second term in the equation 2.9 as well as the force with increasing temperature.

For small deformation, the volume variation of the rubber sample is negligible because the force required to compress is very high. Hence, rubber is often defined

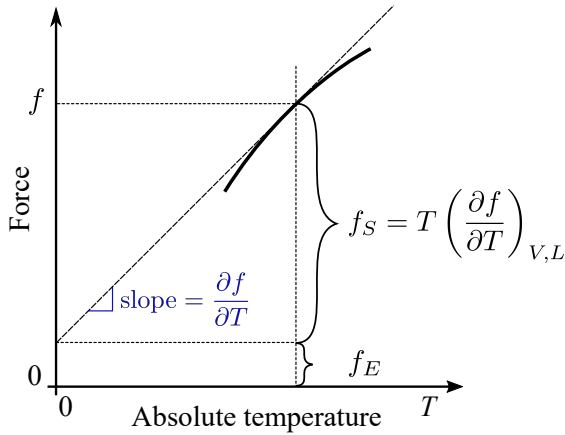


FIGURE 2.5: A schematic representation of the Flory construction for temperature dependency of a force in a polymer network. f_E and f_S are energetic and entropic contributions of the force.

as incompressible. Therefore the change of volume is constant ($V = \text{const}$), and we could neglect the term pdV from the equation 2.5:

$$\begin{cases} dF = -SdT + fdL, \\ V = \text{const} \end{cases} \quad (2.10)$$

Applying properties of the second order partial derivatives to the free energy F :

$$\frac{\partial}{\partial L} \left(\frac{\partial F}{\partial T} \right)_L = \frac{\partial}{\partial T} \left(\frac{\partial F}{\partial L} \right)_T \quad (2.11)$$

and taking into account, that $(\frac{\partial F}{\partial T})_L = -S$ and $(\frac{\partial F}{\partial L})_T = f$ (from eq.2.5), we obtain:

$$(\partial S / \partial L)_T = -(\partial f / \partial T)_L. \quad (2.12)$$

If we substitute eq.2.12 into eq.2.9 we will get:

$$\left(\frac{\partial U}{\partial L} \right)_T = f - T \left(\frac{\partial f}{\partial T} \right)_L. \quad (2.13)$$

Equation 2.12 and 2.13 are very important because it defines the entropic f_S and energetic f_E contributions of force f at constant deformation. In fig 2.5, a schematic representation of Flory construction for temperature dependency of retractive force is shown at constant volume V and at constant elongation L .

2.3.2 Elasticity of a single polymer chain

Equation 2.9 was derived for a polymer system consisting of many polymer chains. The same expression for the elastic force f could be written for a single polymer chain. In the case of melts or chain segments between two crosslinks:

$$\vec{f} = -T \left(\frac{\partial S(N, \vec{R})}{\partial \vec{R}} \right)_T, \quad (2.14)$$

where \vec{R} is end-to-end vector, S - entropy of the chain and T - temperature. The entropy could be calculated according to the Boltzmann law:

$$S(N, \vec{R}) = k \ln \Omega(N, \vec{R}), \quad (2.15)$$

where $\Omega(N, \vec{R})$ is number of realizations and $P(N, \vec{R})$ (eq.2.3) is a thermodynamical probability of the chain with N segments to have end-to-end vector \vec{R} . From eq.2.2 we could calculate $\Omega(N, \vec{R})$: $\Omega(N, \vec{R}) = \left(\int \Omega(N, \vec{R}') d\vec{R}' \right) \cdot P(N, \vec{R})$.

Combining equations 2.15, 2.2 and 2.3, we get an expression for the entropy:

$$S(N, \vec{R}) = -\frac{3k\vec{R}^2}{Nb^2} + \text{Const}(N), \quad (2.16)$$

where k is Boltzmann constant, \vec{R} is end-to-end vector of the polymer chain (or distance between crosslinks in case of rubbers), b is Kuhn length and $\text{Const}(N)$ is a constant, which is independent of the end-to-end vector \vec{R} .

An expression for the elastic force could be calculated from entropy $S(N, \vec{R})$ by the use of equation 2.14:

$$\vec{f} = \frac{3kT}{Nb^2} \vec{R}. \quad (2.17)$$

Therefore, if macromolecule is subjected to a force along the end-to-end vector, then the force is proportional to the distance between the ends. The force proportionality with the absolute temperature indicates the entropic nature of elasticity. Using the relation for contour length: $L = Nb$, one can rewrite the expression for the force:

$$\vec{f} = \frac{3kT}{b} \frac{\vec{R}}{L}. \quad (2.18)$$

From this equation (2.18), the chain strain force is lower when the contour length of the polymer chain is longer or molecular weight (M) is higher. For a given M , the strain force is higher for flexible polymers than for rigid one because Kuhn length b is shorter for the former.

The linear dependence of the force with the end-to-end vector (eq.2.17 and 2.18) is valid only for $|\vec{R}| \ll L$ [36], i.e. in the Gaussian range of deformation.

2.3.3 Real vs ideal polymer network

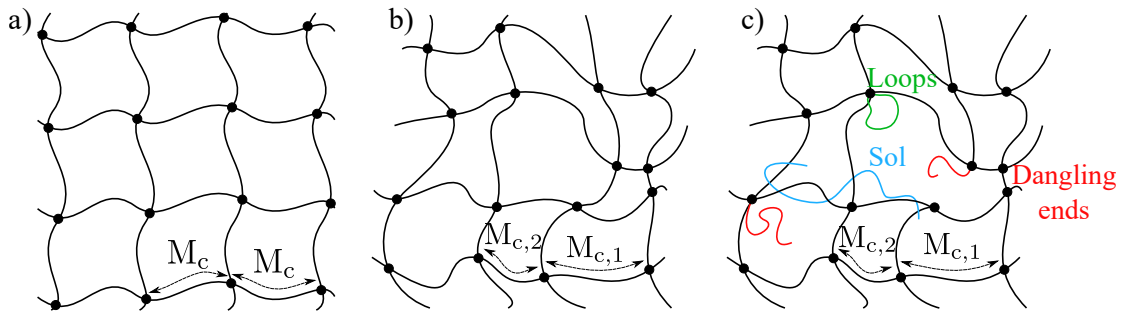


FIGURE 2.6: a) Representation of an "ideal" polymer network. The molecular weight M_c (mesh size) is the same for all polymer strands between crosslinks; b) Representation of a "real" polymer network. The molecular weight is not the same for different segments of the network: $M_c = M_{c,i}$ for i -th strand. c) Representation of a "real" polymer network with defects: loops (green), dangling ends (red) and soluble fraction (blue).

Here we will talk about the "transformation" from ideal polymer network to a real one. First we take an ideal polymer network as a basis for the real network and then add some elements, interactions and modifications for the real network.

Length of polymer network strands

- *Ideal network*: all chain segments have the same length:

$$M_{c,1} = M_{c,2} = \dots = M_{c,N} = M_c.$$

- *Real network*: chain segments have different length:

$$M_{c,i} \neq M_{c,j}.$$

All meshes of an ideal polymer network have the same size (see fig.2.6a). This implies that calculation for one chain with fixed ends, multiplied by the number of polymer strands in the sample could be correct for a non-deformed ideal network.

Real polymer networks are not homogeneous and have different strand lengths(see fig.2.6b). The length of polymer chains between two cross-links is not entirely random, but rather have Gaussian distribution and sometimes could be controlled to have a very narrow distribution [37–39]. The inhomogeneity of the mesh size influences the elastic behaviour of the network. Although it is usually unwanted, a distribution of mesh sizes offers some advantages: such networks dissipate energy more efficiently and have higher recoverability, mechanical strength and toughness. [40–42]

Defects

- *Ideal network*: no defects.
- *Real network*: three types of defects: loops, dangling ends and sol component.

All polymer chain-ends in an ideal network are interconnected chemical bonds, forming one huge macromolecule. In a real polymer network, not all chains are interconnected after the vulcanization process. As a result, there are some *dangling chains*, which are connected by only one side to the rest network (marked red on fig.2.6c). It is also likely, that some chains are not connected to the network at all, and they are defined as *sol fraction* i.e., free polymer chains inside the polymer network (marked blue in fig.2.6c). In addition, some chains form *loops* in the network (marked green on fig.2.6c), which are not elastically active.

Volume interactions \Rightarrow entanglements (see section 2.4.2)

- *Ideal network*: it is assumed, that monomers do not have volume interactions.
- *Real network*: molecules have volume interactions.

Monomers in the polymer chain are connected through covalent bonds. All non-covalent interactions of the atoms in the polymer, which are usually much weaker than the interactions of chemical bond, are referred to as a volume interactions [36] (described in chapter 2.4.2). The absence of such interactions for an ideal polymer network results in a specific unrealistic behaviour: they could go through each other and do not "feel" other chains. Also monomers of the same chain, except of an only close neighbours, do not interact.

In a real networks, polymer chains cannot intersect with each other and subjected to attraction over long distances and repulsion at short distances. Such interactions result in topological constraints, called *entanglements* [30]. The influence of entanglements on the elasticity will be discussed in chapter 2.5.

Crosslinks fluctuations

- *Ideal network*: crosslinks are fixed in the space (no fluctuations).
- *Real network*: crosslinks are less mobile than chains, but nevertheless have fluctuations.

We assumed, that crosslinks of ideal network are fixed (they do not fluctuate) in space and a polymer chains between crosslinks are mobile and could freely move. In a real polymer network, both the polymer chains and crosslinks are mobile, even so they are more restricted than chains between crosslinks. This property of crosslinks is very important for the response on strain and will be discussed detailed in chapter 2.5.

2.4 Interaction of polymers with liquids

The theoretical review in this chapter is based upon the books of Erman, Mark and Roland [43], Dorozhkin [44], Kozlov [29], Grosberg and Khokhlov [36] and Shur [45].

2.4.1 Swelling of polymer melt and polymer network

The dissolution of polymer melts with molecular weight higher than a critical value features a distinctive stage: swelling. The process of polymer volume growth due to the diffusion of small molecules is called *swelling*. When the polymer melt is placed in a solvent, the small molecules diffuse into the polymer phase, while polymer chains are still staying in the polymer phase since they are entangled with other chains and cannot move freely. These constraints are the reason, why polymer melts first swell before they dissolve in the solvent.

The rate of solvent diffusion into the polymer depends on the intermolecular interaction parameter between the polymer and solvent (χ), as well as a temperature.

After initial swelling, a polymer melt will eventually dissolve, thus there is the limit to the swelling process. Polymer networks, however, independent of the polymer-solvent interaction, have a limited swelling. Crosslinks do not prevent solvation of a polymer chain, but they do hinder a polymer chains from diffusing out of the network. While network is swelling, the distances between the crosslinks are increasing and the chains are stretched, and thus the entropy of the system is decreasing. At a certain swelling degree, the deformed system reaches an equilibrium: entropy growth due to the mixing of solvent molecules and polymer counterbalances the entropy decrement due to the chain straightening. When this condition is fulfilled, the network expansion discontinues.

Swelling could be characterized by different parameters, one of them being the *swelling degree*, and it can be defined on the basis of mass (Q_m) or volume (Q):

$$Q_m = \frac{m_{\{\text{swollen polymer}\}}}{m_{\{\text{dry polymer}\}}} = \frac{m_{\{\text{dry polymer}\}} + m_{\{\text{solvent}\}}}{m_{\{\text{dry polymer}\}}}, \quad (2.19)$$

$$Q = \frac{V_{\{\text{swollen polymer}\}}}{V_{\{\text{dry polymer}\}}} = \frac{V_{\{\text{dry polymer}\}} + V_{\{\text{solvent}\}}}{V_{\{\text{dry polymer}\}}}, \quad (2.20)$$

where $m_{\{\text{swollen polymer}\}}$ and $m_{\{\text{dry polymer}\}}$ are masses of the polymer after and before swelling, and $V_{\{\text{swollen polymer}\}}$ and $V_{\{\text{dry polymer}\}}$ are corresponding volumes. Because in experiments we usually measure Q_m , we here link two qualities:

$$Q = 1 + \frac{\rho_r}{\rho_s} (Q_m - 1), \quad (2.21)$$

where ρ_r and ρ_s are densities of rubber and solvent correspondingly.

Swelling of a polymer network does not only lead to the increase of the size and shape distortion, but also to a sharp decrease of strength. Swelling is accompanied by intermolecular bond disruption, chain breakage and the free radicals, which initiate destruction. Solvent effects could be intensified by temperature, mechanical deformations, UV light and other factors [46]. Degradation in swollen state is generally faster than in the dry state.

2.4.2 Volume interactions, solvent quality and excluded volume interactions

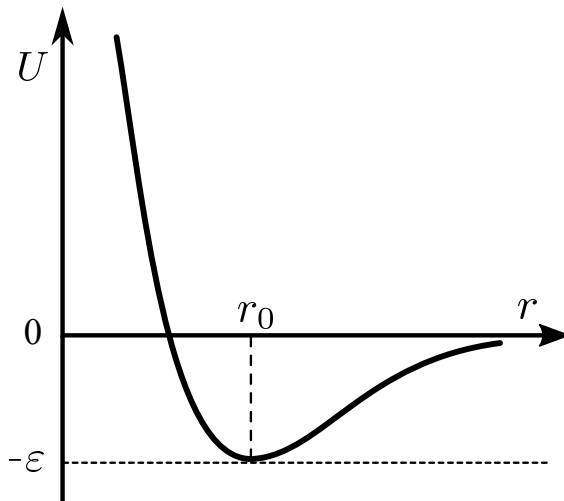


FIGURE 2.7: Typical dependency of an interaction energy U from the distance r between two monomers. Distance $r_0 \approx 10\text{\AA} = 10^{-9}m$ is the order of monomer size.

In section 2.2.2 we considered the model for the ideal polymer chain the freely rotating chain. Such ideal chain is similar to a *random walk* trajectory. A real chain rather follows a *self-avoiding walk*, which is essentially a random walk that never reaches a site previously visited. Monomers of real chain could not occupy the same positions in space and they interact not only with the nearest neighbours but also with other monomers and solvent molecules.

Such volume interactions depend on the chemistry of the monomer. If there are no specific strong interactions (for example electrostatic interactions: polyelectrolytes bridging) between a monomers, then potential energy of the interactions are usually similar to the schematically shown one of the fig.2.7. For a small intermolecular distances, the potential of monomer-monomer interactions is large and

positive, because monomers could not occupy the same space (Pauli repulsion). At large distances the Van-der-Waals attraction dominates, leading to a potential minimum at a monomer-monomer distance $r = r_0$: $U(r_0) = -\varepsilon$. The distance r_0 is of the same order as the monomer size. The former dominates the so-called excluded volume in a polymer system.

In polymer solution, monomers of a polymer chains interact not only with other monomers but also with solvent molecules. Based on the interactions between a monomer and a solvent, we could include it as a correction term for the monomer-monomer interaction potential. In this case, the potential $U(r)$ could be considered as an effective potential between a monomers as if there is no solvent.

An effective attractive interaction means that non-mediated monomer-monomer contact is more beneficial than the contact of monomer with a solvent molecule. In this case polymers have tendency to stick together and accordingly, precipitate eventually. Such solvents are called a *poor solvents*. A negative effective interaction means that monomers have the tendency to be surrounded by the solvent molecules. Such solutions are designated as a *good solvents*.

The solvent quality (poor or good) varies with temperature. Indeed, if the temperature is low, such that $\varepsilon \gg kT$, then the net interaction is usually attractive and the solvent is a poor solvent. In the case of a high temperature ($\varepsilon \ll kT$), the net interaction is repulsive and the solvent is good. At some temperature, attraction and repulsion parts of the potential energy will compensate each other so that a net interaction will be zero and a polymer chains will have no preference to be in contact with other monomers or solvent. In this case, the conformation of the chain will be close to ideal. Such solvents are called an Θ *solvents* and a temperature is called Θ -temperature.

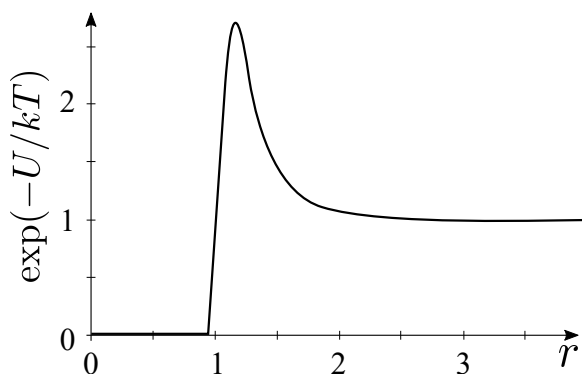


FIGURE 2.8: The relative probability of finding a second monomer at distance r from a given monomer. It is given by Boltzmann factor. The scale for r is normalized by the monomer size.

The probability to find two monomers with a distance r at temperature T from each other is proportional to the Boltzman factor: $\exp\{-U(r)/(kT)\}$. The *Mayer f-function* [30], shown on fig.2.8, is defined as the difference between the Boltzman factor for two monomers by the distance r and at the infinite distance ($e^{\{-U(r)/(kT)\}} = e^0 = 1$):

$$f(r) = e^{\{-U(r)/(kT)\}} - 1. \quad (2.22)$$

The negative integral of the Mayer f -function from 0 to ∞ provides the *excluded volume* v_{exc} (half of the second virial coefficient B):

$$v_{exc}(T) = - \int (1 - e^{\{-U(r)/(kT)\}}) d^3r \quad (2.23)$$

The excluded volume parameter defines the net two-body interaction in a polymer coil. If $v_{exc} > 0$ for a polymer, then the net interaction between a monomers of a polymer is repulsive, if $v_{exc} < 0$, then the net interaction is attractive. The case of $v_{exc} = 0$ is only possible when three-body and higher order interactions are negligible. Indeed, the contribution of the potential energy from these collisions is always infinitesimal, and contribution from two-body interaction is proportional to the excluded volume and equal zero at Θ -point. It means, that at Θ -temperature energetic contribution U of free energy is cancelled out and only entropic part remains.

Polymer chains in the melt generally have an ideal chain conformation (Gaussian chain), because intra-chain and inter-chain excluded volume forces compensate each other. Polymer network is essentially a cross-linked melt and therefore its chains are also ideal.

2.5 Elasticity models

The descriptions of the elasticity models in this section are based on the books or articles written by Rubinstein and Colby [30], Mark, Erman and Eirich [47], Erman [35], Treloar [48], and Doi [49].

²Micro-deformation of the end-to-end distance along (\parallel) or perpendicular (\perp) to the stretching axis for uniaxial deformation

	Affine	Phantom	Tube
crosslink fluctuations	no	yes	yes
entanglements	no	no	yes
micro-deformation ¹	λ	$\sqrt{(1 + \lambda^2)/2}$	$\sqrt{\lambda}$
micro-deformation ² ⊥	$\sqrt{(1/\lambda)}$	$\sqrt{(1 + \lambda)/2\lambda}$	$\sqrt[4]{(1/\lambda)}$

TABLE 2.1: Comparison of the main properties for three models: affine, phantom and nonaffine tube models

There are many different models of elasticity described in the literature, but we will only talk about three of them: affine, phantom and nonaffine tube models. The main distinctions of the models are shown in the table 2.1.

2.5.1 Affine model

The affine elasticity model corresponds to the deformation of an ideal polymer network. The assumptions for this model are quite strict.

- The network is assumed to be built from randomly coiled ideal (Gaussian) chains the same length.
- Upon deformation, the same force is assumed to be applied to the ends of each sub-chain (to the cross-links).
- The cross-links are not fluctuating.

End-to-end distance of every chain according to the affine model deforms in proportion to the macroscopic deformation:

$$\begin{cases} \vec{R}_0 \rightarrow \vec{R}, \\ \vec{R} = \Lambda \cdot \vec{R}_0, \end{cases} \quad (2.24)$$

where \vec{R}_0 is initial end-to-end vector, \vec{R} - end-to-end vector after a deformation and Λ is the macroscopic deformation tensor:

$$\Lambda \equiv \begin{pmatrix} \lambda_x & 0 & 0 \\ 0 & \lambda_y & 0 \\ 0 & 0 & \lambda_z \end{pmatrix}. \quad (2.25)$$

Here λ_x , λ_y and λ_z are macroscopic deformations of the sample along the axes x , y or z , respectively. The affine network theory (or classical theory of rubber elasticity) is thus a molecular theory of rubber elasticity on the basis of affine deformation assumption.

However, the assumption of affine deformation for all chains in a polymer network is not physically justified, because in real situations the external force does not act directly on the junctions or the chain itself, but is redistributed by the chain-chain interactions and by topological and packing confinement. The cross-links are in reality not fixed but fluctuating around their average position.

2.5.2 Phantom model

The idea, that only averaged cross-links positions are moving affinely, was implemented in the *phantom model*, suggested by James and Guth [3, 50]. According to this model all cross-links are fluctuating around their mean positions in such way, that fluctuations $\Delta\vec{R}$ are independent of the deformation, because fluctuations are thermally activated:

$$\langle(\Delta\vec{R})^2\rangle = \frac{2}{f}\langle\vec{R}_{0,\text{mean}}\rangle, \quad (2.26)$$

Here \vec{R}_{mean} is a time-averaged mean end-to-end vector in non-deformed state and f is a functionality of the junctions: how many branches are connected by the junction. The brackets $\langle\cdots\rangle$ in equation 2.26 denote the average over the ensemble of the chain strands in the network sample. The end-to-end vectors in the non-deformed $\langle\vec{R}_0\rangle$ and deformed $\langle\vec{R}\rangle$ states will be then:

$$\begin{cases} \langle\vec{R}_0^2\rangle = \langle\vec{R}_{0,\text{mean}}^2\rangle + \langle(\Delta\vec{R})^2\rangle, \\ \langle\vec{R}^2\rangle = \langle\vec{R}_{\text{mean}}^2\rangle + \langle(\Delta\vec{R})^2\rangle, \end{cases} \quad (2.27)$$

where $\vec{R}_{0,\text{mean}}$ and \vec{R}_{mean} are time-averaged mean end-to-end vectors in non-deformed and deformed states. Like in the affine model the phantom model also assumes, that conformation of every chain is Gaussian and there are no volume interaction between the not neighbour monomers: essentially all chains are ideal.

The affine deformation is realized (valid) only for the surface of the macroscopic sample. It means, that there are two types of junction in the network: fixed on the surface and fluctuating in a bulk. The external forces act on the surface cross-links

but do not directly act on the cross-links from a bulk. Cross-links in the volume (non-surface) receive the stress only transmitted through the surrounding chains. Due to the fluctuations the microscopic deformation for the phantom model is smaller, than for the affine model [51]:

$$\begin{cases} \vec{R}_0 \rightarrow \vec{R}, \\ \langle R^2 \rangle = \left[\left(\frac{\lambda_x^2 + \lambda_y^2 + \lambda_z^2}{3} \right) \left(1 - \frac{2}{f} \right) + \frac{2}{f} \right] \langle R_0^2 \rangle. \end{cases} \quad (2.28)$$

2.5.3 Tube model

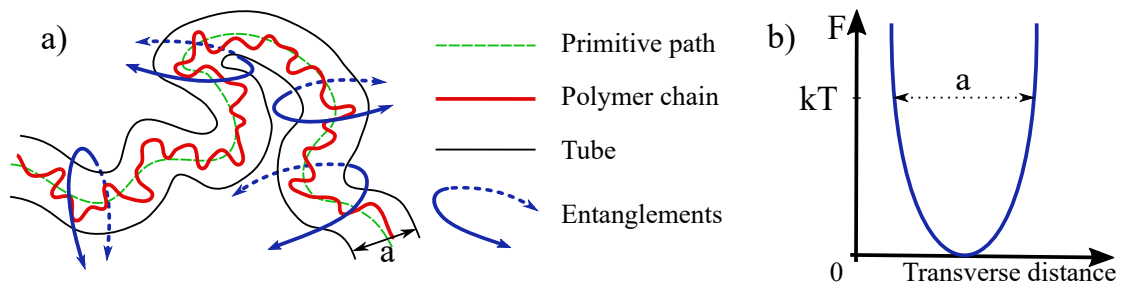


FIGURE 2.9: a) Representation of the tube model for a polymer chain. The chain is constrained in the tube region with diameter a . The primitive path is the shortest path from one chain end to another, which mimics the contour length of tube model. b) The quadratic potential, which defines the tube diameter a depending on the temperature T . F is a free energy of the monomer. The minimum of the function locates the primitive path.

In both models affine and phantom, the chains are assumed to be ideal. This means, that they do not "feel" each other. In real networks polymer strands are constrained in motion and in position by other chains: they are entangled [48]. Edwards showed [49], that entanglement effects could be taken into account by quadratic constraining potential for every monomer of the chain. The minima of the potential map out the primitive path of the polymer strand. Such a potential could be represented as a tube (fig. 2.9), the diameter of which depends on the thermal energy and also on the entanglement length of the polymer ($a \approx bN_e^{1/2}$).

As originally proposed by Edwards, the tube diameter a does not depend on deformation. Rubinstein and Panyukov proposed a *nonaffine tube model* [52, 53], which is a combination of Edwards' tube model and the constrained junction model. According to this model the tube diameter on small scales ($R < bN_e^{1/2}\lambda^{3/2}$

for $\lambda > 1$) changes nonaffinely with the network deformation:

$$a_i \approx bN_e^{1/2}\lambda_i^{1/2} \approx a\lambda_i^{1/2}, \quad (2.29)$$

where a is a tube diameter in undeformed state, b is Kuhn segment and N_e is a number of Kuhn segments between entanglements.

The tube diameter is representing the fluctuation amplitude perpendicular to the contour length. In the nonaffine tube model it coincides with the distance between constraints. This means that according to equation 2.29 the microscopic deformations along the different axes follow the square root of affine deformation values (eq.2.24):

$$\begin{cases} \vec{R}_0 \rightarrow \vec{R}, \\ \vec{R} = \sqrt{\Lambda} \cdot \vec{R}_0, \end{cases} \quad (2.30)$$

where

$$\sqrt{\Lambda} = \begin{pmatrix} \sqrt{\lambda_x} & 0 & 0 \\ 0 & \sqrt{\lambda_y} & 0 \\ 0 & 0 & \sqrt{\lambda_z} \end{pmatrix}. \quad (2.31)$$

Values λ_x , λ_y and λ_z are macroscopic deformations of the sample along the respective axis.

2.6 Elastic free energy of a polymer network

The model-free elastic free energy change due to the deformation is defined by microscopic quantities: $\langle \vec{r}_0^2 \rangle$, $\langle \vec{r}^2 \rangle$ - the average square of end-to-end vectors in the non-deformed and in the deformed network, respectively.

$$\Delta F_{\text{el,mic}} = \frac{3kT}{2\langle \vec{r}_0^2 \rangle} \sum_{\nu} [\vec{r}^2 - \langle \vec{r}_0^2 \rangle] = \frac{3\nu kT}{2} \left[\frac{\vec{r}^2}{\langle \vec{r}_0^2 \rangle} - 1 \right], \quad (2.32)$$

where $\langle \vec{r}^2 \rangle = \sum \vec{r}^2 / \nu$ and ν is the number of chains in the network. End-to-end vectors can be represented in Cartesian coordinates:

$$\begin{cases} \langle \vec{r}^2 \rangle = \langle x^2 \rangle + \langle y^2 \rangle + \langle z^2 \rangle, \\ \langle \vec{r}_0^2 \rangle = \langle x_0^2 \rangle + \langle y_0^2 \rangle + \langle z_0^2 \rangle. \end{cases} \quad (2.33)$$

2.6. Elastic free energy of a polymer network

For isotropic chain dimensions before deformation one can rewrite the expression for the elastic free energy chain in Cartesian coordinates:

$$\Delta F_{\text{el,micro}} = \frac{\nu kT}{2} \left[\frac{\langle x^2 \rangle}{\langle x_0^2 \rangle} + \frac{\langle y^2 \rangle}{\langle y_0^2 \rangle} + \frac{\langle z^2 \rangle}{\langle z_0^2 \rangle} - 3 \right]. \quad (2.34)$$

The elastic part of a free energy depends on the used elastic model. Here we take an example of constrained-junction model, which describes the affine as well as the phantom model in two limits of a constrain parameter. The free energy change for the deformed rubber then described as [43, 51]:

$$\Delta F_{\text{el,con.j}} = \frac{f-2}{f} \cdot \frac{\nu kT}{2} \sum_{i=x,y,z} \left\{ (\lambda_i^2 - 1) + \frac{2}{f-2} [B_i + D_i - \ln(B_i + 1) - \ln(D_i + 1)] \right\}, \quad (2.35)$$

where index i corresponds to the Cartesian coordinates x , y or z , f is the average junction functionality, λ_i is an extension of the sample along the i -axis, ν is the number of crosslinks in the volume V_0 (the number density of crosslinks) and N_A is Avogadro's number.

Terms from the equation 2.35 for free energy, which are containing parameters B_i and D_i , correspond to the elastic free energy due to the instantaneous displacements of the junction from the phantom network center and the constraint center respectively. These parameters are expressed via the constrain parameter κ :

$$\begin{cases} B_i = \frac{\kappa^2(\lambda_i^2 - 1)}{(\lambda_i^2 + \kappa)^2}, \\ D_i = \frac{\kappa\lambda_i^2(\lambda_i^2 - 1)}{(\lambda_i^2 + \kappa)^2}. \end{cases} \quad (2.36)$$

The constrain parameter κ is defined through the relation of averaged displacement of the junction from phantom network $\Delta \vec{R}$, to the displacement from constraints $\Delta \vec{s}$:

$$\kappa = \frac{\langle (\Delta \vec{R})^2 \rangle_{ph}}{\langle (\Delta \vec{s})^2 \rangle_0}. \quad (2.37)$$

In the case of the phantom model there are no constraints acting on the junction and $\langle (\Delta \vec{s})^2 \rangle_0 \rightarrow \infty$, thus $\kappa \rightarrow 0$. For the phantom model both parameters B_i and D_i are zero and the elastic free energy reduces to this expression:

$$\Delta F_{\text{el,ph}} = \frac{f-2}{f} \cdot \frac{\nu kT}{2} (\lambda_x^2 + \lambda_y^2 + \lambda_z^2 - 3). \quad (2.38)$$

In the limit of the affine model there are no fluctuations of junctions and $\langle (\Delta \vec{s})^2 \rangle_0 = 0$, thus $\kappa \rightarrow \infty$. In this case $B_i = \lambda_i^2 - 1$, $D_i = 0$ and the elastic energy reads:

$$\Delta F_{\text{el,aff},\Delta V} = \frac{\nu kT}{2} \left\{ (\lambda_x^2 + \lambda_y^2 + \lambda_z^2 - 3) - 2 \cdot \frac{f-2}{f} \ln(V/V_0) \right\}. \quad (2.39)$$

If during a deformation volume of the sample is not changing, then we obtain the formula for the elastic free energy change according to the affine model:

$$\Delta F_{\text{el,aff}} = \frac{\nu kT}{2} (\lambda_x^2 + \lambda_y^2 + \lambda_z^2 - 3). \quad (2.40)$$

2.7 Isotropic Swelling

2.7.1 Swelling Theory

The theory of swelling process is described in a number of books [33, 43, 48, 51, 54] used for this chapter.

When, a polymer network is placed in a good solvent it starts to swell. The solvent molecules penetrate into the network until an equilibrium between the elastic F_{el} and mixing F_{mix} energy is reached:

$$\Delta F = \Delta F_{\text{el}} + \Delta F_{\text{mix}}. \quad (2.41)$$

The free energy change due to the mixing of polymer chains and solvent molecules is described fairly well by the lattice theory of polymer solutions - *Flory-Huggins theory*:

$$\Delta F_{\text{mix}} = kT \left\{ \frac{\phi}{N} \ln \phi + (1 - \phi) \ln(1 - \phi) + \chi \phi(1 - \phi) \right\}, \quad (2.42)$$

where N is a number of monomers in a polymer chain, T is a temperature, k - Boltzmann constant, ϕ is a volume fraction of polymer network, χ is the Flory interaction parameter, characterising the difference of interaction energies in the mixture.

The free energy change due to the network expansion could be described for the phantom model by eq. 2.38 or for the affine model by eq. 2.39. If we consider

isotropic swelling, then

$$\lambda_x = \lambda_y = \lambda_z = \left(\frac{V}{V_0} \right)^{\frac{1}{3}} = \phi^{-\frac{1}{3}},$$

where V_0 and V are volumes of the sample before and after swelling, respectively.

When the free energy reaches its minimum, the system is in equilibrium. Thus, the first derivative of free energy with respect to the number of solvent molecules (N_s) should be zero in equilibrium :

$$\frac{\partial F}{\partial N_s} = \frac{\partial F_{\text{el}}}{\partial N_s} + \frac{\partial F_{\text{mix}}}{\partial N_s} = \Delta\mu_{\text{el}} + \Delta\mu_{\text{mix}} = 0. \quad (2.43)$$

By differentiating eq. 2.34 we obtain the second term of eq.2.43:

$$\frac{\partial F_{\text{mix}}}{\partial N_s} = kT (\ln(1 - \phi) + \phi + \chi\phi^2) \quad (2.44)$$

For the elastic part we consider two cases: affine (from eq.2.39) and phantom models (from eq.2.38):

$$\begin{cases} \frac{\partial F_{\text{el,ph}}}{\partial N_s} = \frac{\rho V_s}{M_c} \cdot \frac{f-2}{f} \phi^{\frac{1}{3}}, \\ \frac{\partial F_{\text{el,aff}}}{\partial N_s} = \frac{\rho V_s}{M_c} \left(\phi^{\frac{1}{3}} - \frac{2}{f} \phi \right), \end{cases} \quad (2.45)$$

where ρ is a density of non-swollen rubber, V_s is a volume of the solvent, f is an average functionality of the network crosslinks and M_c is an average molecular weight of the chain strand between the crosslinks.

By substituting equations 2.45 into equation 2.43 we obtain an expression to define M_c from equilibrium swelling experiments for the phantom model:

$$M_{c,\text{ph}} = \frac{\rho V_s}{\ln(1 - \phi) + \phi + \chi\phi^2} \cdot \left(\frac{f-2}{f} \right) \phi^{\frac{1}{3}}, \quad (2.46)$$

and for the affine model:

$$M_{c,\text{aff}} = \frac{\rho V_s}{\ln(1 - \phi) + \phi + \chi\phi^2} \cdot \left(\phi^{\frac{1}{3}} - \frac{2}{f} \phi \right). \quad (2.47)$$

Equation 2.47 is known as a *Flory-Rehner equation* and it is widely used for the determination of crosslink density. It presumes the affine behaviour of the network

during swelling: the vector components of the displacement vector scales with the same ratio, as the external dimensions of the network sample. To determine the crosslink density one should to perform additional experiment on solutions of the non-crosslinked polymer to define the Flory interaction parameter χ .

2.7.2 NMR of isotropically swollen polymer networks

Our group previously investigated the process of isotropic swelling via double-quantum (DQ) NMR, which will be addressed in more detail below. In this section the results will be explained only briefly, for more information we refer to the publications [21, 22, 55].

By DQ NMR we measure residual dipolar coupling: D_{res} . It was shown, that D_{res} is proportional to the dynamic order parameter of chain backbone S_b [20]: $D_{\text{res}} \approx S_b = \langle P_2(\cos \Theta) \rangle$. Within the approximation of freely jointed (Gaussian) chain with N Kuhn segments between the cross-links, the order parameter for a non-swollen network is given by [56–58]:

$$S_b = \frac{3}{5N} \frac{R^2}{R_0^2}, \quad (2.48)$$

and hence

$$D_{\text{res}} \approx \frac{R^2}{R_0^2}. \quad (2.49)$$

R is end-to-end distance and R_0 is its unperturbed melt-state value.

Cohen-Addad and co-workers were the first to measure by NMR order parameter of swollen networks [59, 60]. They found that the swelling process could be divided into two stages: the first one is desinterspersion and the second chain expansion. More thorough investigations were performed in our group by Walter Chassé [21, 55].

Gaussian chain statistic predicts a monotonic increase of the D_{res} value with increasing degree of swelling, Q . According to the affine model prediction D_{res} should scale with Q with the power $\nu_{\text{def}} = 2/3$: $D_{\text{res}}(Q) \sim Q^{2/3}$.

It was found, that this affine prediction is in good agreement with experimental data at higher swelling degrees, starting from $Q \approx 2.5$. In the second stage from

2.7. Isotropic Swelling

intermediate up to the equilibrium degree of swelling, the network deformation could be considered as the affine or at least as nearly affine.

During the first stage of swelling, D_{res} was found to increase much less, than the affine prediction, or even to decrease. This could be explained by desinterspersion effects and the release of entanglements or packing constraints. In this stage the chains are barely stretching, but the average distance between crosslinks is increasing. The picture here is that the material undergoes a reorganisation of the chains in order to reduce the overall stress before the system is 'forced' to stretch affinely due to the forces exerted by the solvent.

The results on the fig.2.10 for the second stage are fitted to a power law according to the affine prediction:

$$D_{\text{res}}(Q) = D_{\text{res,c}} \cdot Q^{2/3}. \quad (2.50)$$

The back extrapolated parameter $D_{\text{res,c}}$ then is a residual coupling of a dry network with the assumption that the swelling process is entirely affine and is referred as the "phantom reference state" of a network [55]. This value $D_{\text{res,c}}$ is attributed to the contribution of only crosslinks excluding entanglements contribution to measured D_{res} . The contribution from entanglements and other constraints to the measured coupling of the dry network equals the difference between the $D_{\text{res,c}}$ and $D_{\text{res}}(Q = 1)$. It means, that using DQ NMR for swollen polymer network one can separate the contributions to the order parameter from crosslinks and from constraints.

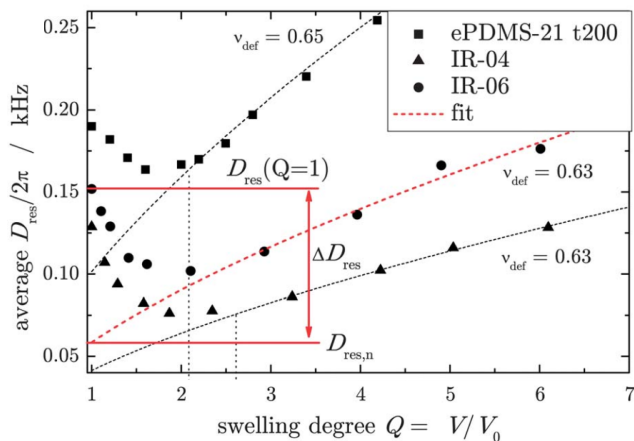


FIGURE 2.10: Isotropic swelling of different polymer networks: end-linked PDMS, Isoprene rubber with two different crosslink densities. The data are fitting by the equation 2.50 for the points after the minimum for swelling degree $Q \approx 2.5 \dots 3$. Figure is reproduced with permission of ROYAL SOCIETY OF CHEMISTRY from [55].

Many experimental methods (SANS, SAXS, NMR, optical microscopy) have revealed that swollen polymer networks possess nano-scale inhomogeneities[55, 61]. High inhomogeneity of swollen networks complicates the measurements of the microscopic deformation of polymer chains during mechanical deformation or isotropic dilation by the swelling process itself. Erman determined that highly swollen polymer networks may be treated as phantom networks [51]. It was also shown by other experiments that the deformation of swollen polymer networks is nonaffine on the scale smaller than the network inhomogeneities [19, 62].

2.8 Small-Angle Neutron Scattering

Polymer networks are complex systems, and measurements of microscopic deformations could only be performed by a few experimental techniques. First attempts to obtain microscopic information were made by Small-Angle Neutron Scattering (SANS) experiments [18, 19]. These are able to give information about polymer conformations on the scale of 1-100 nm. The source of the information of the experiment are the neutrons scattered due to their interaction with nuclei of the atoms under investigation. The scattering strength is quantified by the "scattering cross section". Different nuclei scatter the neutrons with a different strength, which enables the option of tuning the contrast between different types of atoms by isotope labelling. For example, very often the contrast is achieved by deuteration of some part of polymers or few chains among others.

2.8.1 Theory

There are two distinct forms of the neutron scattering: coherent and incoherent. *Coherent* scattering depends on the scattering vector \vec{q} and *incoherent* scattering is independent of \vec{q} . Elastic coherent scattering is proportional to the spatial Fourier transformation of the pair-correlation function. The angular distribution of coherent scattering provide structural and conformational information, while incoherent scattering can be regarded as a background.

Hydrogen ^1H has a very large incoherent scattering cross-section and a small coherent cross-section, while deuterium ^2D has an opposite relation: a large coherent and a small incoherent cross-sections. This property of the scattering provide a

good contrast between ^1H and ^2D , while the substitution ^1H by ^2D has a minimal chemical effect. It means, that various parts of the network could be deuterated in order to get specific conformational information. There are some common examples: network deuterated at cross-links, networks with deuterated chains between two junctions, network with labelled chains extending over several cross-links (labelled path), network swollen in deuterated solvents.

The intensity of a scattered rays $I(q)$ from a collection of n "labelled" atoms is calculated as

$$I(q) = \left\langle \sum_{i,j}^n b_i b_j \exp(i(\vec{q} \cdot \vec{r}_{ij})) \right\rangle, \quad (2.51)$$

where b_i is a scattering cross-section of the i -th scattering center and \vec{r}_{ij} is the vector from i -th to the j -th center. The double summation is performed over all scattering centres and the angular brackets designate that the intensity is coming from all possible configurations of the scattering centres. Using a model-independent Guinier approximation, the radius of gyration R_g can be determined from SANS data:

$$P(q) \equiv \frac{I(q)}{I_0} = \exp\left(-\frac{1}{3}q^2 R_g^2\right), \quad (2.52)$$

where $P(q)$ is a *form factor* - ratio of intensity scattered at angle θ (wave vector \vec{q}) to that extrapolated to zero angle ($\theta \rightarrow 0$) and therefore, zero scattering wave vector ($|\vec{q}| \rightarrow 0$). Scattering data from the ideal chain are described by the Debye function:

$$P(q) = \frac{2}{q^4 R_g^4} \left\{ \exp(-q^2 R_g^2) - (1 - q^2 R_g^2) \right\}. \quad (2.53)$$

2.8.2 Deformed and swollen polymer networks

Robert Ullman [18] performed calculations for scattering function (SANS) for multiple crosslinked networks. He compared his calculation with the previously done experimental data of Clough, Maconnachie, and Allen [63]. In comparison to end-linked networks, randomly crosslinked network chains are deformed to a higher extent and therefore exhibits higher anisotropy. For both types of networks, the deformation is clearly nonaffine. SANS experimental data for randomly crosslinked networks show less microscopic deformation than the phantom network calculations [5].

Wagner [64] showed by analysing SANS data of Beltzung et al. [65], and three sets of mechanical measurements from various sources, that network deformation is nonaffine on the mesh level. This is caused by the restriction of the lateral motion of the network chains due to the deformation of the surrounding chains. He proposed the molecular stress function model and showed that this model fits the SANS and the mechanical data very well [64].

Read and McLeish [66] explained the "lozenge" pattern in contour plots of two dimensional SANS data. They succeeded in explaining the experimental data by including the interaction between relaxed short chains and oriented network chains in the tube model of Warner and Edwards [67]. Experimental data fits very well to this model. An alternative explanation of the "lozenge" shape are the inhomogeneities in crosslink density, which results in nonaffine local deformations [66].

Mendes et.al [68] investigated swollen elongated gels by SANS. They observed the famous "butterfly" pattern on the two dimensional detector. These results can not be explained by classical rubber theories. Three theoretical models: 1) the cluster model, 2) the Onuki model, and 3) the Rabin-Bruinsma model could predict the general features of the experimental data, but only for very small elongation. The effects of elongation are overestimated by all of these models [68].

SANS investigations of networks made of HDH block-copolymer chains with different length scale of deuterated block showed that the scale of affinity is strongly connected with the elastic chain length. On the scale less than the length between crosslinks microscopic deformation is reduced in comparison to affine [69–71] and it is described well by nonaffine tube model [52].

Chapter 3

Basics of NMR and application to polymers

NMR is a very broad conception and depending on the employed NMR methods (pulse programs) and utilized hardware, NMR could be divided into few groups depending on the applied classification. By materials investigated by NMR it could be divided into two groups: solution state NMR (very often referred to just as NMR) and solid-state NMR. Solid-state NMR could be divided into 2 types: static solid-state NMR and MAS (Magic Angle Spinning) NMR. Another classification could be made by the applied data analysis methodology: NMR spectroscopy, time-domain NMR, MQ (Multi Quantum) NMR etc. Hardware classification would divide into groups: high-field NMR, low-field NMR, field-cycling NMR, diffusion NMR etc. There are some other possibilities to classify NMR experiments.

Many NMR methodologies are using different concepts and basic principles of all NMR methods together are numerous. Here I want to explain essential NMR theory for methods applied in my experiments. I would classify it as static solid-state time-domain DQ NMR. The main principles applied in this method, are a dipole-dipole couplings between poles, their measurement by way of generating a double-quantum (DQ) coherence, and their interpretations in terms of an order parameter of a polymer chain. Static in this state refers not to the investigated properties of material, but to the utilized method: sample during experiment is not spinning, but stays static.

The fundamental theory of NMR and DQ NMR of polymers described here is based on the books or papers of Melinda Duer [72], Malcolm H. Levitt [73], Harald Günther [74], S. Szymański and P. Bernatowicz [75], Roger S. Macomber [76], Grit Kummerlöwe and Burkhard Luy [77], Kay Saalwächter [20, 57, 78, 79].

3.1 General concepts of NMR

Nuclear Magnetic Resonance is a unique spectroscopy method relying on the energy level splitting for nuclear spins, which depends on the external magnetic field. An interaction of a nuclear spin with the magnetic field is defining the central Larmor frequency, but the most helpful information is arising from the splitting or other transformations of the resonance peak by the nuclear spin interactions and motions.

3.1.1 Spin and Magnetization

Different isotopes possess a spin - an intrinsic angular momentum. The total spin \vec{I} is proportional to the magnetic dipole moment $\vec{\mu}$ with the proportionality constant γ , gyromagnetic ratio :

$$\vec{\mu} = \gamma \vec{I}. \quad (3.1)$$

It is commonly agreed among NMR specialists and generally used in NMR literature, that an external magnetic field is along the z -axis in Cartesian coordinates and a term "z-component" means that this component is along the external magnetic field B_0 . The same terminology is used here.

As spin is a quantum mechanical property of the nucleus, the z-component of the spin is quantized and could take only discrete values:

$$I_z = m\hbar, \quad (3.2)$$

where m is a magnetic quantum number. Quantity m could take a values between $-I$ and I with step 1: $m = \{-I, -I + 1, \dots, I - 1, I\}$, where I is being a spin quantum number.

3.1. General concepts of NMR

If there is no external magnetic field, then all spins have the same energy. For non-zero external magnetic field $B_0 \neq 0$, energy level is split into several levels, corresponding to every m -value. The potential magnetic energy E_{mag} of a nucleus in the external field B_0 with the magnetic moment μ is then:

$$E_{mag} = -\mu_z B_0 = -\gamma I_z B_0 = -\gamma m \hbar \cdot B_0. \quad (3.3)$$

For the hydrogen nucleus $I = 1/2$, which means, that m can take two values: $m = +1/2$ or $m = -1/2$, and the energy level is split into 2 levels with energy gap $\Delta E_0 = \gamma \hbar B_0$. The resonance frequency ω_0 for the excitation of the energy transition is then proportional to the external magnetic field:

$$\omega_0 = -\gamma B_0. \quad (3.4)$$

This frequency is named **Larmor** frequency ω_0 .

3.1.2 Hamiltonian and spin-spin interactions

The quantum mechanical equivalent of the classical equation 3.3 for the interaction energy between a spin and external magnetic field is the Zeeman Hamiltonian:

$$\hat{H}_z = -\hat{\mu} \vec{B}_0 = -\omega_0 \hat{I}_z. \quad (3.5)$$

Here \hat{H}_z is a Zeeman energy operator, $\hat{\mu}$ is a magnetic moment operator and \hat{I}_z - a z -projection of a full spin-operator \hat{I} .

The Hamiltonian \hat{H}_z describes the interaction of the spin only with the external magnetic field, or the spin system of non-interacting spins. Hamiltonian of interacting spins will contain \hat{H}_z , which is the biggest term, and other Hamiltonians, describing the spin-spin interactions. Notwithstanding that interactions between spins are the same for liquid and solid states, the effects of the interactions are different on account of molecular motion. In the liquid state the molecules are moving fast with the correlation time much shorter than the reciprocal of the NMR frequency. In the solid state the anisotropic contribution to the spin interactions contributes large terms to the Hamiltonian because of the slow motion. The full

Hamiltonian for the spin system could be represented as a sum of Hamiltonians:

$$\hat{H} = \hat{H}_z + \hat{H}_{DD} \left(+\hat{H}_{CS} + \hat{H}_J \right). \quad (3.6)$$

The terms in brackets are chemical shift (\hat{H}_{CS}) and J -coupling (indirect scalar coupling)(\hat{H}_J). They can be measured in the liquid state and by MAS solid-state NMR, because they lead to the resonance line splitting. Direct through-space dipole-dipole interaction does not have an effect on the spectrum, because it is averaged to its isotropic value, i.e. zero, by the Brownian motion and molecular tumbling in case of liquids or solutions and by the spinning in case of MAS NMR. In these cases the residual dipolar coupling is zero. In static solid-state NMR, restrictions of position and orientation of the molecules in the magnetic field are the reason for a large residual dipole-dipole coupling (described by \hat{H}_{DD}). In this case lines are broadened and effects of isotropic chemical shift and J -coupling are hard to measure.

3.2 Dipolar interaction in polymer networks

Rubber or more generally polymer networks are not "solid", but also not "liquid". They can be described as a soft matter: something between the solid and liquid state. Polymer networks possess partially solid-state and partially liquid-state features. They can be deformed and relax under stress on a long time scale, but they do not flow like a liquid, keeping their shape. This is due to restrictions of the polymer chain motion, that dipole-dipole couplings not being averaged to zero. In this section dipolar coupling is explained in more detail as well as the way how could we use it to measure the cross-link density of a polymer network.

3.2.1 Secular approximation for homonuclear dipolar coupling

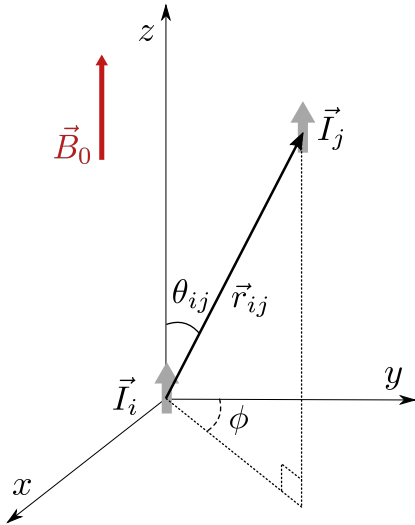


FIGURE 3.1: Two spins \vec{I}_i and \vec{I}_j in external magnetic field \vec{B}_0 along z -axis. θ_{ij} is the angle between two vectors: \vec{B}_0 and \vec{r}_{ij} , where \vec{r}_{ij} is a vector connecting spin \vec{I}_i and spin \vec{I}_j . ϕ is a polar angle.

In the secular approximation dipolar Hamiltonian can be written as:

$$\hat{H}_{DD} = - \left(\frac{\mu_0}{4\pi} \right) \frac{\gamma_i \gamma_j \hbar}{r^3} \cdot \frac{1}{2} (3 \cos^2 \theta_{ij} - 1) \left\{ 3 \hat{I}_{i,z} \hat{I}_{j,z} - \hat{I}_i \cdot \hat{I}_j \right\}, \quad (3.7)$$

where θ is the angle between the internuclear vector and the external magnetic field (see fig.3.1). The product of spin operators can be written via Cartesian coordinates: $\hat{I}_i \cdot \hat{I}_j = \hat{I}_{i,x} \hat{I}_{j,x} + \hat{I}_{i,y} \hat{I}_{j,y} + \hat{I}_{i,z} \hat{I}_{j,z}$.

The coefficient in front of the Hamiltonian in equation 3.7 is the *secular dipole-dipole coupling constant* for the homonuclear case. It depends on the types of nuclei, the distance and orientation of the spin pair; it defines the strength of the dipolar interaction:

$$D_0 = - \left(\frac{\mu_0}{4\pi} \right) \frac{\gamma_i \gamma_j \hbar}{r_{ij}^3} \cdot \frac{1}{2} (3 \cos^2 \theta_{ij} - 1). \quad (3.8)$$

It is very important for us, that the dipolar coupling constant in the secular approximation has an angular dependency, because we could thus define the *dynamic anisotropy* of our samples by measuring an average value of D_0 . The expression for the angular dependency is a second Legendre polynomial:

$$P_2(\cos \theta_{ij}) = \frac{1}{2} (3 \cos^2 \theta_{ij} - 1). \quad (3.9)$$

3.2.2 Residual dipolar coupling of polymer networks

The segmental motion in polymer networks above the glass transition temperature is largely liquid-like, but it is not isotropic because of the topological constraints and permanent cross-links [77]. We consider the dipolar coupling between two protons at fixed distance and angles between them. In the polymer chain it could be for example protons of CH₂ or CH₃ groups. Expression 3.8 gives the instantaneous dipolar coupling between two spins. Because of the rotational motions associated with the segmental dynamics, the dipolar interaction between any two spins is changing due to fluctuations of the angle θ . It means, that the measured dipolar coupling between nuclei i and j will be scaled down (averaged), leaving a *residual dipolar coupling*:

$$D_{\text{res}}^{ij} = - \left(\frac{\mu_0}{4\pi} \right) \frac{\gamma_i \gamma_j \hbar}{r_{ij}^3} \left\langle \frac{(3 \cos^2 \theta_{ij} - 1)}{2} \right\rangle = D_{\text{max}}^{ij} \cdot \left\langle \frac{(3 \cos^2 \theta_{ij} - 1)}{2} \right\rangle. \quad (3.10)$$

In equation 3.10 the brackets $\langle \dots \rangle$ indicate an averaging over motions on time scales short compared to the inverse static dipolar coupling: $1/D_{\text{max}}^{ij}$ [80].

Thus, when we measure a residual coupling in a polymer melt or network, we do not measure the static dipolar coupling between the hydrogen atoms, but rather an average molecular property: the local dynamic order parameter S_b [77, 81]. We actually measure not one coupling between two specific spins D_{res}^{ij} , but an effective dipolar coupling averaged over all *neighbouring* spin pairs in the given chain segment: $D_{\text{res}} = \langle D_{\text{res}}^{ij} \rangle_{i,j>i}$.

The order parameter S_b , determined by the averaged second Legendre polynomial, is uniaxial in nature. It means, that S_b is describing linear system with fixed ends: for example chain strands between crosslinks or entanglements in the approximation of a chain as a freely jointed segments of fixed length. The expression for the uniaxial orientation order parameter for polymer network [58] is thus:

$$S_b = \frac{1}{2} \left[(3 \langle \cos^2 \beta_t \rangle_t - 1) \right]_{str}, \quad (3.11)$$

where $\langle \dots \rangle_t$ denotes the thermal average over all conformations of the polymer network strand and $[\dots]_{str}$ denotes the structural average over all chain segments in the sample. The angle β_t is the instantaneous orientation of the segment vector relative to the end-to-end vector of the polymer chain.

It was shown by Kuhn and Grün [56], that the backbone order parameter is proportional to the square of the end-to-end distance (R) and inversely proportional to the number of statistical polymer segments (N) in the chain. For a Gaussian freely jointed chain at fixed end-to-end distance, S_b is given by:

$$S_b = \frac{3}{5N} \frac{R^2}{R_0^2}, \quad (3.12)$$

where $R_0^2 = \langle R^2 \rangle_0$ is the unperturbed melt-state value of end-to-end distance. Brackets $\langle \dots \rangle$ indicate the structural average over all chains.

Combining equations 3.10, 3.11 and 3.12 we get the relation between the residual dipolar coupling, measured by NMR, and the actual polymer network property, the end-to-end distance,

$$D_{\text{res}} = D_{\text{eff}} \cdot \frac{3}{5N} \left(\frac{R}{R_0} \right)^2, \quad (3.13)$$

where D_{eff} is pre-averaged by fast intra-segmental conformational rearrangements relative to the "static" value D_{max} for a given monomer:

$$D_{\text{eff}} = \frac{D_{\text{max}}}{k}. \quad (3.14)$$

3.3 DQ NMR experiments of polymer networks

By measuring the residual dipolar coupling of polymer networks, we can extract the microscopic properties of the material using eq.3.13: an averaged end-to-end distance (or mesh size) of the network and also a distribution of this value. In this chapter it will be described how D_{res} of a polymer network can be measured.

3.3.1 Essentials of NMR measurements

The basics of NMR measurements, which are necessary for the understanding of DQ NMR experiments, are described in this section. More information can be found in books of Keeler [82], Duer [72], Levitt [73].

NMR pulse:

NMR pulse is an electromagnetic field oscillating with the Larmor frequency in

the xy-plane (perpendicular to the magnetic field B_0). An on-resonance perpendicular magnetic field is usually named B_1 -field. Under the effect of the B_1 -field, the macroscopic magnetization is rotating around the B_1 -vector (which appears static in the rotating frame) and depending on the duration of the RF-pulse t_p , magnetization vector \vec{M} is tilted by the angle θ_p :

$$\theta_p = \gamma B_1 t_p = \omega_1 t_p. \quad (3.15)$$

The **pulse length** t_p is most commonly adjusted to flip angle of 90° or 180° . Another very important parameter of the pulse is its **phase**. For example, a 90°_x -pulse flips the equilibrium magnetization from the z -direction to the $-y$ -direction: $\vec{M} = (0, 0, M_0) = M_z \xrightarrow{90^\circ_x} -M_y = (0, -M_0, 0)$.

FID, T_1 and T_2^* relaxation:

When the magnetization is placed in xy-plane, the state of the system has higher energy, and the spin system will try to minimize it by returning to the equilibrium $M_z = M_0$ magnetization. The transverse component further evolve (precess) and this precession involves an independent decay to zero with the characteristic relaxation time T_2^* - effective **transversal relaxation time**. This decay could be directly observed by NMR as a Free Induction Decay (**FID**), because the transverse magnetization vector is rotating around the magnetic field with the Larmor frequency, resulting in electro-magnetic induction in the receiving coil of the NMR spectrometer. The magnetization component M_z will rise with the **longitudinal relaxation time** $T_1 > T_2^*$. Unlike the transversal magnetization (in the plane perpendicular to the external magnetic field B_0), longitudinal magnetization is undetectable by conventional NMR, because it does not give rise to an induction effect in the receiving coil.

Phase cycling:

The phases of the pulses and the receiver are varied in a systematic way so as to add up wanted signals, and cancel out unwanted signal or imperfections. For phase cycling, the experiment needs to be repeated several times. For example to avoid the imperfections arising from the the pulse and two-phase detector [82], CYCLically Ordered Phase Sequence phase cycle (CYCLOPS), is usually implemented. The cycle has four steps for acquiring the signal from four main directions: x, y,

3.3. DQ NMR experiments of polymer networks

-x and -y. The phase of the pulse as well as the receiver phase proceed in 90°-steps for consecutive scans.

Scan	Pulse	Pulse phase	Receiver phase
$1 \times n$	90_x°	x	x
$2 \times n$	90_y°	y	y
$3 \times n$	90_{-x}°	-x	-x
$4 \times n$	90_{-y}°	-y	-y

TABLE 3.1: CYCLically Ordered Phase Sequence phase cycle (CYCLOPS)

By phase cycling not only imperfections could be eliminated, but it is indispensable for the filtering signal of specific quantum orders. For m -quantum coherence all phases of the RF-pulses have to be shifted by an angle $\frac{\pi}{m}$. Therefore for filtering m -quantum coherence one has to have phase cycling with phase increment $\Delta\phi = \pi/m$.

3.3.2 NMR pulse sequence for measuring dipolar coupling

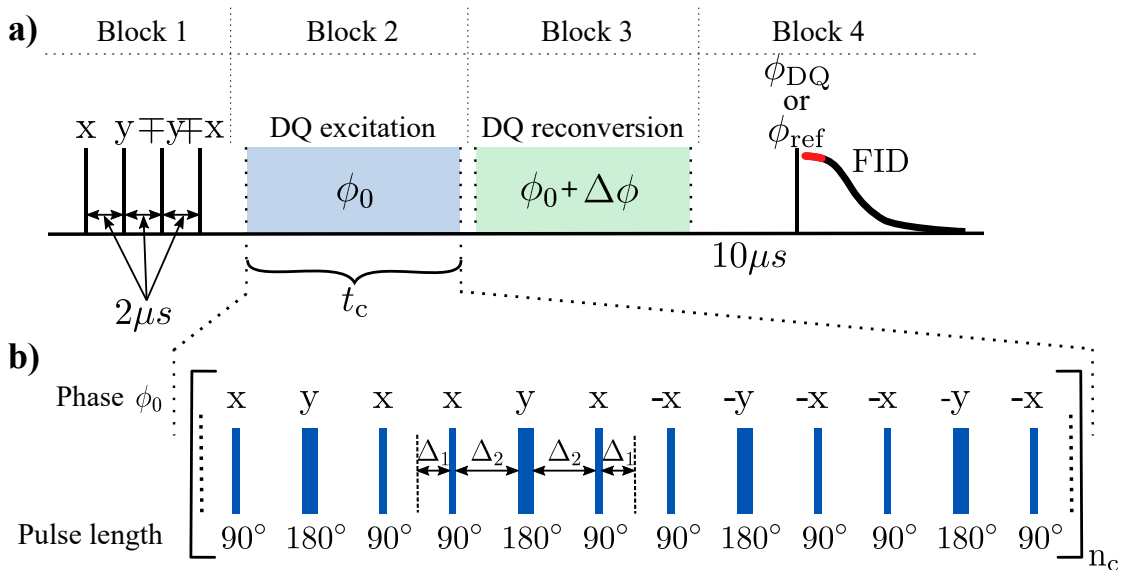


FIGURE 3.2: a) Diagrammatic representation of the DQ NMR sequence used in this work. It could be divided into 4 blocks: 1) spin temperature inversion to suppress T_1 -related artifacts, 2) MQ coherence excitation, 3) MQ coherence reconversion, 4) detection. Block 1 consist of four 90° -pulses, blocks 2 and 3 are complex trains of pulses with special phase cycling for extracting wanted signals. The last block is signal detection by a 90° -pulse. Depending on the phase, we can sample a DQ signal or a reference signal. The part of FID marked in red is the part of the signal to be averaged. At the beginning of FID the curve is almost flat and the maximum value equals the integral of the full NMR spectrum. b) The DQ unit consists of 12 pulses: eight 90° -pulses and four 180° -pulses. Phase ϕ_0 is a set of phases for these 12 pulses: $\{xyx\ xyx\ -x-y-x\ -x-y-x\}$. The experimental time axis equals a product of the cycle time and the number of cycles: $\tau_{DQ} = n_c t_c$.

Multiple-Quantum NMR (MQ NMR) is an NMR method, which excites high-order coherences between two or more coupled (interacting) spins. In this way the averaged dipolar coupling become accessible. Multiple-quantum coherences are not directly observable by the NMR. We need to use special pulse sequences, which excite MQ coherences and then reconvert them into the observable magnetization.

In this work we utilized the pulse sequence of Baum and Pines [83] improved by prof. Saalwächter [57, 84] and it is depicted in the fig.3.2a. This sequence has a pure DQ average Hamiltonian and consists of four blocks:

- 1) suppression of distortions arising from short T_1 relaxation
- 2) excitation of multiple-quantum coherences,
- 3) reconversion of multiple-quantum coherences,

4) detection.

Block 1 in fig.3.2a embodies a two-step phase-cycle controlled polarization inversion, which is suppressing the unwanted effect of additional signal appearing due to the short longitudinal (T_1) relaxation (see section 3.3.1) during the pulse sequence. It consists of four 90° -pulses with fixed intervals of $2 \mu\text{s}$ between them.

Block 2 in fig.3.2a is a DQ excitation pulse sequence and it consists of a pulse train with different phases. The length of every unit is the cycle time t_c . Reference phase for DQ part is denoted as ϕ_0 and it is a set of pulse phases in strict order: {xyx xyx -x-y-x -x-y-x} (shown on the fig.3.2b).

The full duration of the DQ excitation part is $\tau_{\text{DQ}} = n_c t_c$, the DQ coherences evolution time. The times between pulses of the DQ unit are: $\Delta_1 = t_c/24 - t_p/2$, $\Delta_2 = t_c/12 - 3t_p/2$ where t_p is a duration of the 90° -pulse (180° -pulse duration ideally equals $2t_p$). For a time increment in minispec (the low field NMR spectrometer) we usually stretch the pulse train by increasing the duration of cycle time t_c . The other possibility (used in high field NMR) for the time increment is an increasing the amount of cycles n_c in combination with the time increment in order to access the times between nt_c and $(n + 1)t_c$.

Block 3 in fig.3.2a is a DQ reconversion pulse sequence and has the same pulse structure, as the block 2, but differs by the NMR phase shift of $\Delta\phi = n \cdot 90^\circ$ for $n = 0, \dots, 3$, resulting in a four-step phase cycling for filtering double quantum coherences: ($\Delta\phi = 0^\circ, 90^\circ, 180^\circ, 270^\circ$,). Excitation and reconversion blocks together have a total magnetization rotation of 360° (around the axis of 180° -pulse) and consequently do not create an observable magnetization, but excite all $2n$ quantum orders.

Block 4 on the fig.3.2a is simply a detection 90° -pulse with CYCLOPS phase cycling, which has four steps: {x,y,-x and -y}.

$I_{\text{DQ}}(\tau_{\text{DQ}})$ contains information about dipolar coupled spins and reflects the magnitude of homonuclear residual dipolar couplings. It includes all $4n + 2$ quantum orders, but is dominated by DQ coherences. $I_{\text{ref}}(\tau_{\text{DQ}})$ consists of all magnetization that has not evolved into $4n + 2$ coherences, thus containing all $4n$ quantum orders.

3.3.3 DQ NMR theoretical concepts for polymer networks

The acquired data can be theoretically described by simplifying the system to a single coupled spin pair, omitting multiple spin interactions, because couplings involving three and more spins are marginal in comparison with the dominant pair coupling. The pulse sequence used in this study and described above has a pure DQ average Hamiltonian:

$$\hat{H}_{DD} = -\frac{a(\psi)}{2} \sum_{i<j} D_{\text{eff}}^{ij} P_2(\cos \theta_{ij}) \left(\hat{I}_{i,+} \hat{I}_{j,+} + \hat{I}_{i,-} \hat{I}_{j,-} \right). \quad (3.16)$$

A scaling factor $\frac{a(\psi)}{2}$ that is usually included in the time axis scaling, corrects the effects of finite pulses. The intensities $I_{\text{DQ}}(\tau_{\text{DQ}})$ and $I_{\text{ref}}(\tau_{\text{DQ}})$ signals under the Hamiltonian \hat{H}_{DD} after the evolution time τ_{DQ} will be evolved into forms:

$$\begin{cases} I_{\text{DQ}}(\tau_{\text{DQ}}) = \langle \sin \phi_1 \sin \phi_2 \rangle, \\ I_{\text{ref}}(\tau_{\text{DQ}}) = \langle \cos \phi_1 \cos \phi_2 \rangle, \end{cases} \quad (3.17)$$

where ϕ_1 and ϕ_2 are phase factors for DQ coherence for excitation and reconversion periods, which are obtained as:

$$\phi_1 = D_{\text{eff}} \int_0^{\tau_{\text{DQ}}} P_2(\cos \theta_t) dt \quad \text{and} \quad \phi_2 = D_{\text{eff}} \int_{\tau_{\text{DQ}}}^{2\tau_{\text{DQ}}} P_2(\cos \theta_t) dt. \quad (3.18)$$

The angle θ_t is an instantaneous angle between the magnetic field and the inter-nuclear vector. The time dependence of θ_t reflects the full spectrum of motions: from statistical segment orientation fluctuations up to slow cooperative motions of the chains as a whole.

The sum of the DQ and reference signal functions gives a sum function

$$I_{\text{MQ}}(\tau_{\text{DQ}}) = I_{\text{ref}}(\tau_{\text{DQ}}) + I_{\text{DQ}}(\tau_{\text{DQ}}) = \langle \sin \phi_1 \sin \phi_2 \rangle + \langle \cos \phi_1 \cos \phi_2 \rangle,$$

which is fully dipolar refocused. The sum function decays only due to the motions, as phase factors for excitation and reconversion periods due to the motions of the segment may not be the same ($\phi_1 \neq \phi_2$).

The main advantage of DQ NMR experiment consist in the fact, that the signal from the dynamically anisotropic segments of polymer network (chain strands

between crosslinks) is well separated from the signal from isotropically moving segments: dangling chains, sol and unrestricted loops. Experimentally obtained DQ data contain two data sets as a functions of the DQ evolution time τ_{DQ} : decaying reference signal $I_{\text{ref}}(\tau_{\text{DQ}})$ and the build-up curve - DQ signal $I_{\text{DQ}}(\tau_{\text{DQ}})$ (see fig.3.3a).

For data fitting we will use the advantage of good separation of isotropic and anisotropic parts by relaxation times. It is also very important for us, that the relaxation decay of the DQ and reference signals are the same in good approximation. This allows us to normalize DQ intensities thus removing effects of relaxation.

Further details of the theoretical background of DQ NMR can be found in papers of our group [20, 57, 78, 85].

3.3.4 Data fitting

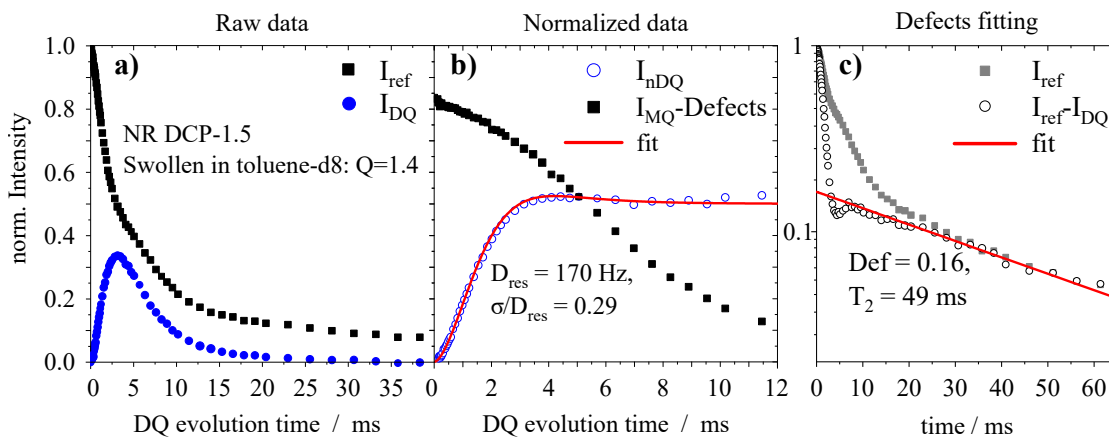


FIGURE 3.3: MQ NMR data of sample NR DCP-1.5 swollen in toluene-d8 at swelling degree $Q = 1.4$. a) **Raw DQ data** consisting of two data sets: reference (I_{ref} : black squares) and DQ (I_{DQ} : blue circles) signals. b) **Normalized data**: here the decaying function is not I_{ref} , but the multiple quantum signal I_{MQ} (sum of reference and DQ signals) after subtraction of the defect fraction. The normalization of the DQ signal is performed by point-by-point division of the DQ raw signal (I_{DQ}) by the ($I_{\text{MQ}} - \text{Defects}$) data (here black squares). c) **Defects fitting**: The long decaying part of the reference signal is arising from isotropically mobile parts of the system, here referred as **defects**: sol, loops, dangling ends. A monoexponential decay is assumed, fitting $I_{\text{ref}} - I_{\text{DQ}}$ in a time interval of 20...60 ms.

The signal function $I_{\text{DQ}}(\tau_{\text{DQ}})$ (shown by blue circles on the fig.3.3a) is referred to DQ values arising from a residual dipolar coupling, which is non-zero only for the

motionally restricted part of the polymer network. The signal function $I_{\text{ref}}(\tau_{\text{DQ}})$ (shown by black squares on the fig.3.3a) reflects the transversal magnetization decay signal from the all parts of the sample. We can separately fit the decay for the isotropic part from the difference between reference and DQ functions $I_{\text{ref}} - I_{\text{DQ}}(\tau_{\text{DQ}})$ (shown on the fig.3.3c). Then, the defect fraction is subtracted from the reference function to perform the normalization of the I_{DQ} signal. The reference function without the isotropic part (defects) will be then $I_{\text{ref,aniso}}(\tau_{\text{DQ}}) = I_{\text{ref}}(\tau_{\text{DQ}}) - f_{\text{def}} \cdot \exp\left[-\frac{2\tau_{\text{DQ}}}{T_{2,\text{iso}}}\right]$, where $T_{2,\text{iso}}$ is a T_2 (or transverse) relaxation time of the isotropic part of the sample (in fig.3.3c $T_2 = T_{2,\text{iso}}/2 = 49$ ms). In the polymer network, the subtracted signal is associated with the small molecules (sol fraction, solvent, other free additives) and from network defects, such as dangling ends and loops.

In networks the relaxation contribution of the anisotropic part is nearly equal for $I_{\text{DQ}}(\tau_{\text{DQ}})$ and for $I_{\text{MQ}}(\tau_{\text{DQ}})$. Thus the effect of a slow motions and multi-spin interaction contributions can be removed from the DQ function signal by point-by-point division assuring that the temperature is high enough for averaging all inter-segmental motions:

$$I_{\text{nDQ}}(\tau_{\text{DQ}}) = \frac{I_{\text{DQ}}(\tau_{\text{DQ}})}{I_{\text{MQ}}(\tau_{\text{DQ}}) - f_{\text{def}} \exp[-2\tau_{\text{DQ}}/T_{2,\text{iso}}]}. \quad (3.19)$$

The normalized DQ function (shown by open blue circles in fig.3.3b) then only contains information about structure, but not dynamics. The function $I_{\text{nDQ}}(\tau_{\text{DQ}})$ can be analysed in terms of the residual couplings in the network, which is proportional to the square of the end-to-end distance. Using a static second-moment approximation [57, 86, 87], the normalized DQ data can be analysed by the function

$$I_{\text{nDQ}}(\tau_{\text{DQ}}, D_{\text{res}}) = 0.5 \left(1 - \exp\left[-\left\{\frac{2}{5}D_{\text{res}}\tau_{\text{DQ}}\right\}^2\right]\right), \quad (3.20)$$

where D_{res} represent not a pair coupling but a second-moment-type quantity proportional to $(\sum D_{\text{eff}}^{ij})^{1/2}$. This simple DQ function fits actual data only for short and intermediate times, up to a value of $I_{\text{nDQ}}(\tau_{\text{DQ}}) \approx 0.45$.

In the current work we used empirically derived *Abragam-like* function[88], which is an improved version of the function described by the eq.3.20:

$$I_{\text{nDQ}}^{A-l}(\tau_{\text{DQ}}, D_{\text{res}}) = 0.5 \left(1 - \exp[-\{0.378D_{\text{res}}\tau_{\text{DQ}}\}^{1.5}] \right) \cdot \cos[0.583D_{\text{res}}\tau_{\text{DQ}}]. \quad (3.21)$$

This function was used to fit the experimental data with an assumed Gaussian distribution of the D_{res} value by using the integration in fitting function from -5σ up to $+5\sigma$, where σ is the width of the distribution. In the fig.3.3b DQ data were fitted with this function. For given sample averaged dipolar coupling D_{res} is 170 Hz with a distribution width $\sigma = 0.29 \cdot 170 \text{ Hz} = 49.3 \text{ Hz}$.

3.3.5 Tikhonov regularization of build-up function I_{nDQ}

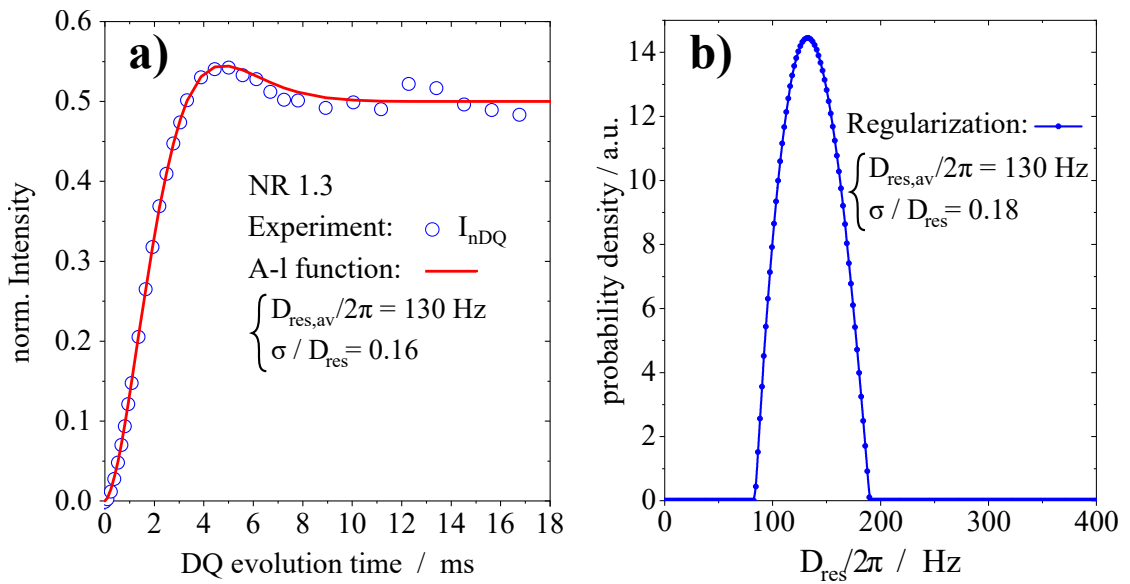


FIGURE 3.4: a) NMR data I_{nDQ} for sample NR-1.3 fitted upon A-l function
 b) Distribution of residual dipolar coupling obtained by the Tikhonov regularization procedure with A-l kernel function ($K(t, D_{\text{res}})$ in eq.3.22).

Every single value of $D_{\text{res},i}$ corresponds to specific $I_{\text{nDQ},i}$ build-up curve. If there are many different couplings, then the experimental I_{nDQ} build-up curve is a superposition of all $I_{\text{nDQ},i}$ functions corresponding to the specific $D_{\text{res},i}$. If a distribution of the D_{res} is continuous, then the experimental I_{nDQ} signal is an integral over D_{res} of the product of $f(D_{\text{res}})$ distribution function and kernel build-up function $K(t, D_{\text{res}})$. To get the distribution function, one has to solve the next integral equation:

$$I_{\text{nDQ}}(t) = \int_0^{D_{\text{max}}} K(t, D_{\text{res}}) f(D_{\text{res}}) dD_{\text{res}}, \quad (3.22)$$

where $I_{\text{nDQ}}(t)$ is an experimentally measured build-up function, $K(t, D_{\text{res}})$ is a kernel function and $f(D_{\text{res}})$ - distribution function of D_{res} , which has to be calculated.

Equation 3.22 is a Fredholm integral equation of the first kind, which could be solved numerically. For this purpose we used program *ftikreg* [89, 90], which is based on Tikhonov regularization method.

The program performs regularization within a given error interval and calculate the distribution of D_{res} , which is proportional to distribution of R^2 in case of polymer networks. To check the goodness of regularization, *ftikreg* calculates back an integral given by eq.3.22 and obtains the I_{nDQ} function corresponding to the calculated distribution.

In order to get the D_{res} distribution one has to define the kernel function, which is the basis curve. Similar to the prior fitting procedure we use Abragam-like function as a kernel function. As was shown in [88] this approach gives good results for all kind of networks in terms of homogeneity.

Chapter 4

Samples and NMR analysis

4.1 Samples

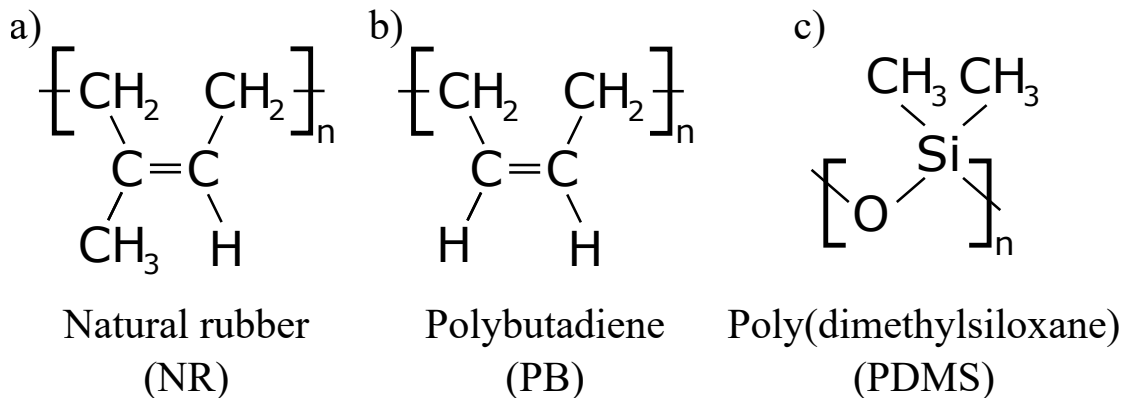


FIGURE 4.1: Chemical structure of samples.

In this study, three different types of lowly cross-linked polymer networks were used: NR (Natural Rubber, SMR-CV60 by Malaysian Rubber), BR (Butadiene Rubber (98% *cis* from Polimeri Europa) and PDMS (telechelic vinyl-modified poly(dimethylsiloxane) from United Chemical Technology, Inc.). The chemical structure of the polymers are shown in fig.4.1. and preparation details are summarized in tables 4.1, 4.2 and 4.3.

Linear elasticity, high strength, fatigue life and excellent adhesion to metals of NR makes it well suited for laminated bearings used for vibration isolation and earthquake of heavy superstructures [91]. NR is irreplaceable part of tires due to its high durability and grip: automotive tires are made up of 50% NR, and tires

4.1. Samples details

used for aircraft are made out of 100% NR [92]. Natural rubber is not only the fundamental raw material used in production most tyres, it is also crucial for the safety and performance of driving, and ecological requirements [93]. In order to use the maximum benefits from NR, we have to gain a deeper understanding of the molecular structure of NR, thus improved materials can be developed in NR products.

BR is the second most produced synthetic rubber following the styrene butadiene rubber (SBR). Annual consumption of BR is ca. 2.8 million metric tons with four major areas of the use. The largest portion is applied in tires ($\approx 70\%$), mostly side walls and tire treads. Other areas of BR use are thermoplast modification ($\approx 25\%$), technical rubber goods ($\approx 4\%$) and golf ball cores ($\approx 1\%$) [94, 95].

PDMS is the most widely used siloxane polymer [96]. PDMS elastomers have numerous and widespread applications such as membranes [97], adhesives [98], dielectric elastomers [99] and biomedical applications.

Chemical composition and synthesis details of our samples are given in tables 4.1, 4.2 and 4.3.

Sample name	Polymer	ZnO	Stearic Acid	CBS	Sulphur	time t_{97}
NR-1.3	NR	5	2	0.26	1.3	17.91
NR-3.1	NR	5	2	0.62	3.1	14.04
NR-7.4	NR	5	2	1.48	7.4	11.46
BR-1.3	BR (98 % cis)	5	2	0.26	1.3	94.29
BR-3.1	BR (98 % cis)	5	2	0.62	3.1	35.07
BR-7.4	BR (98 % cis)	5	2	1.48	7.4	27.20

TABLE 4.1: Recipes for networks, cured with sulphur as a crosslinker. Amount of ZnO, stearic acid, delayed action sulfenamide accelerator: N-cyclohexyl-2-benzothiazole sulfenamide (CBS) and sulphur are given in phr (parts per hundred rubber i.e. grams per 100 grams rubber). NR - natural rubber, BR - butadiene rubber. During the vulcanization time t_{97} samples were kept at temperature $T = 150^\circ\text{C}$.

4.2. Good solvents for samples

Sample name	Dicumyl peroxide (DCP) content / phr	time t_{97} / min
NR DCP-0.5	0.5	130.12
NR DCP-1.0	1.0	114
NR DCP-1.5	1.5	110.33
NR DCP-2.0	2.0	105.68
NR DCP-3.0	3.0	103.91
BR DCP-0.045	0.045	-

TABLE 4.2: Recipes for natural rubber and butadiene rubber samples, cured with dicumyl peroxide (DCP) as a crosslinker. Vulcanization was performed at 150°C. t_{97} is a duration of the vulcanization time.

Sample name	M_n (g/mol)	M_w/M_n
PDMS-A3-7.8k	7900	2.8
PDMS-A3-18.9k	18900	1.6
PDMS-A4-7.8k	7900	2.8
PDMS-A4-18.9k	18900	1.68

TABLE 4.3: Properties of the B_2 precursor chains in end-linked PDMS networks. The number 2 in B_2 means that the both ends of the chains are vinyl modified, so that they could react with the crosslinker. Two types of crosslinker were used: A_3 - three-functional, and A_4 - four-functional. Values 7.8k and 18.9k in the name of B_2 PDMS precursor mean the average molecular weight. The last column is a polydispersity of a precursor chains.

4.2 Good solvents for samples

In order to perform a mechanical experiment with the swollen rubber we need to choose appropriate solvents. Toluene is a good solvent for all our samples and could be used for isotropic swelling or for uniaxial swelling. For all these experiments the deuterated version of toluene was used. A disadvantage of toluene is its volatility, which does not allow us to use the solvent for the other experiments: swelling of mechanically deformed rubber or mechanical deformation of pre-swollen rubber. For the last experiments we needed to find a good non-volatile solvent for NR and BR.

As an indicators of the evaporation rate we compared the vapour pressure of possible good solvents, taken from the website <https://pubchem.ncbi.nlm.nih.gov>:

- DMSO (dimethyl sulfoxide) [0.417 mmHg at 20°C],

4.2. Good solvents for samples

- DOP (dioctyl phthalate) [$1 \cdot 10^{-7}$ mmHg at 25°C],
- DBP (dibutyl phthalate) [$7 \cdot 10^{-5}$ mmHg at 20°C],
- pyridine [16 mmHg at 20°C],
- DMF (dimethylformamide) [3 mmHg at 25°C],
- DBS (dibutyl sebacate) [$4.7 \cdot 10^{-6}$ mmHg at 25°C],
- cyclohexanone [5 mmHg at 26°C].

The vapour pressure of toluene (28.4 mmHg at 25°C) is higher than that of water (17.5 mmHg at 20°C). This means, that toluene vaporize faster than water. For sufficiently low volatility the vapour pressure should be about or less than 17.5 mmHg.

We performed swelling experiments of our samples in solvents with vapour pressure less than 1 mmHg: DOP, DBP, DBS and cyclohexanone. Equilibrium swelling at room temperature for DOP, DBP, DBS and cyclohexanone for NR-1.3 are 2.9, 1.5, 4.1 and 6.4, whereas for NR-1.3 swollen in toluene equilibrium swelling it is about 6.4. From these 4 solvents the best solvents is thus DBS, which we were using for the combined swelling and mechanical experiments.

4.3 NMR characterisation

Sample	Bulk			Q	Swollen			Trapped defects	Ph.ref. D_{res}
	$D_{avg}/2\pi$	σ/D_{avg}	Defects		$D_{avg}/2\pi$	σ/D_{avg}	Defects		
NR-1.3	130	0.25	0.08	4.9	130	G	0.35	0.27	40
NR-3.1	240	0.1	0.04	4.4	300	G	0.09	0.05	110
NR-7.4	450	0.15	0.01	1.7	390	G	-	-	-
BR-1.3	170	0.4	0.17	4.4	190	G	0.44	0.27	-
BR-3.1	280	0.3	0.07	Q*	450	G	0.15	0.08	-
BR-7.4	430	0.28	0.02	Q*	703	G	0.05	0.03	-
NR DCP-0.5	120	0.1	0.13	4.4	94	G	0.50	0.37	-
NR DCP-1.0	160	0.1	0.08	Q*	210	G	0.32	0.24	50
NR DCP-1.5	200	0.1	0.06	4.4	210	G	0.17	0.11	90
NR DCP-2.0	240	0.16	0.05	4.2	265	G	0.13	0.08	110
NR DCP-3.0	300	0.23	0.04	Q*	370	G	0.09	0.05	-
BR DCP-0.045	170	0.34	0.14	5.9	190	G	0.46	0.32	80
PDMS-A3-7.8k	190	0.28	0.07	Q*	290	G	0.13	0.08	120
PDMS-A3-18.9k	50	0.47	0.36	Q*	136	G	0.58	0.22	-
PDMS-A4-7.8k	250	0.33	0.06	Q*	380	G	0.11	0.05	170
PDMS-A4-18.9k	49	0.45	0.39	Q*	110	G	0.58	0.19	-
PDMS-2003y-5k	250	0.47	0.04	3.2	380	G	0.05	0.01	-
PDMS-2003y-58k	170	0.22	0.04	3.2	250	G	0.12	0.08	-

TABLE 4.4: Samples: list of all samples, used in this work. D_{avg} is an average dipolar coupling (given in Hz) and σ/D_{avg} is a variance of the D_{res} distribution, normalized to the D_{avg} . For swollen samples distribution width is denoted by letter "G", which means, that fitting was done by Gamma distribution.

Before stretching and swelling experiments, an NMR characterisation of all networks in the bulk and swollen states (by deuterated solvent) was performed. The fitting procedure of DQ NMR data was explained in section 3.3.4. The results of the sample characterization are summarized in table A.2.

4.3.1 Dry samples

All nDQ data were fitted by the original Abragam-like function (eq.3.21) and D_{res} values were assumed to have a Gaussian distribution with averaged value of $D_{avg}/2\pi$ and standard deviation σ . Almost all our samples are very homogeneous, because their normalized variance $\sigma/(D_{avg}/2\pi) \leq 0.3$ [88]. Average value of dipolar coupling is a measure of the cross-link density of the sample, since it

is proportional to the reciprocal of a chain segments number (N) between the cross-links (see eq.3.13).

In order to compare cross-link densities of different polymers, we need to consider a relations of D_{res} (bulk) with molecular weight of the chains between cross-links (M_c) for NR [46, 78, 100], BR [78, 101] and PDMS [78, 102, 103].

$$M_c^{\text{NR}} = \frac{617 \text{ Hz}}{D_{\text{res}}/2\pi} \cdot \frac{f-2}{f} \text{ kg/mol} \quad (4.1)$$

$$M_c^{\text{BR}} = \frac{656 \text{ Hz}}{D_{\text{res}}/2\pi} \cdot \frac{f-2}{f} \text{ kg/mol} \quad (4.2)$$

$$M_c^{\text{PDMS}} = \frac{1266 \text{ Hz}}{D_{\text{res}}/2\pi} \cdot \frac{f-2}{f} \text{ kg/mol}, \quad (4.3)$$

where f - is functionality of cross-linker. These conversion factors are model dependent and depend on rather simplifying assumptions [78], but have been shown to be accurate within about 30% [46, 101, 102].

In the dry state D_{res} gives not M_c , but rather $M_{c,\text{apparent}} = \left(\frac{1}{M_c} + \frac{1}{M_e}\right)^{-1}$, where M_e is the entanglement molecular weight. This value is dependent on the chemistry of polymer chains and differs quite significantly for NR, BR and PDMS (table 4.5). If $M_c \gg M_e$, then network behaviour would be more influenced by entanglements and D_{res} would reflect M_e , rather than M_c . If $M_c < M_e$, then the entanglements contribution is weaker but still influences the average chain configuration by hindering the chain motion. This means that D_{res} measured for dry state would be higher than D_{res} corresponding to actual molecular weight. To obtain the D_{res} value corresponding to the real molecular weight between crosslinks, we can measure MQ NMR for different degree of swelling up to the equilibrium swelling (Q^*) and back-extrapolate the assumption of the affine expansion [55].

Polymer	M_e (kg/mol)	$D_{\text{res}} / 2\pi(M_e)$	
		A_4	A_3
NR	3.890	80 Hz	-
BR	2.930	110 Hz	-
PDMS	12.000	50 Hz	35 Hz

TABLE 4.5: Entanglement (critical) molecular weight [104] for polymers, used in this work. D_{res} values are calculated by eqs.4.1, 4.2 and 4.3 for polymer networks, if $M_c = M_e$.

The defects fraction measured in dry polymer networks is underestimated due to the trapping of some defects [46, 101]. These rather than the tail have anisotropic behaviour and contribute to the nDQ signal. Defects apparent in dry state then represent only those parts of defects which have isotropic motion on the time scale of the DQ NMR experiment i.e., the millisecond range. These could be dangling ends, loops and possibly some sol fraction, which are not affected by the network. It was shown before [101], and is supported by our data, that the amount of defects declines with increasing cross-link density. This is most probably due to the more compact packing and because dangling chains are statistically shorter for higher cross-linked systems. The same trend is valid for our samples. The same trend is valid for our samples.

4.3.2 Swollen samples

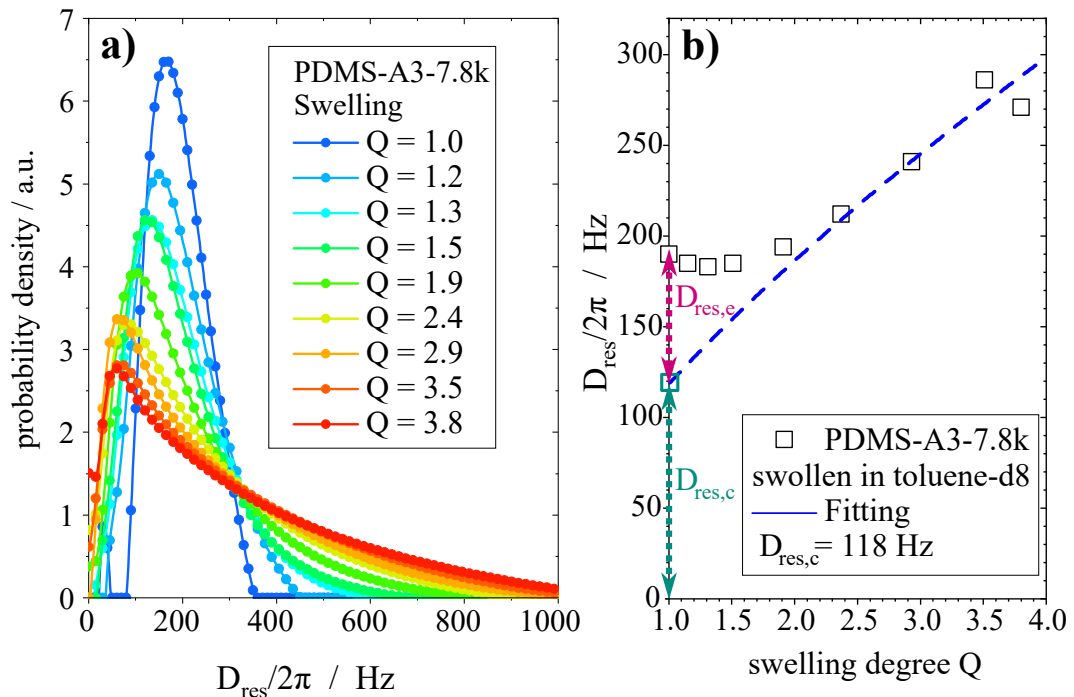


FIGURE 4.2: Example of experimental data for PDMS-A3-7.8k at different degree of isotropic swelling in deuterated toluene. (a) D_{res} distributions for every swelling degree. (b) D_{res} vs swelling degree and back-extrapolation assuming affine deformation for high swelling ($Q \geq 2$). The back-extrapolated value $D_{\text{res,c}}$ corresponds to the pure cross-link density contribution, and the difference of $D_{\text{res}}(Q = 1.0)$ and $D_{\text{res,c}}$ gives the entanglement contribution to the measured residual coupling $D_{\text{res,e}}$.

Distribution of D_{res}

In the swollen state networks are very inhomogeneous. In table A.2 in rows for the distribution width of swollen sample the letter "G" is stated, which means, that nDQ build-up curves were fitted under the assumption of a Γ distribution. It has a width σ that is related to its average and therefore it has no additional fitting parameter for the standard deviation. It was found, that such a distribution describes the typical inhomogeneities in swollen gels rather well [105].

In the fig.4.2a distributions of D_{res} at different swelling degree are shown. These distribution profiles were calculated by improved Tikhonov regularization procedure [88]. The distribution width is significantly increasing upon swelling of the polymer network. Very broad distribution of D_{res} complicate an analysis and therefore the error of the $D_{\text{res,avg}}$ determination is increasing with the swelling degree.

"Phantom reference network"

The term "phantom reference network" was introduced in a paper [55] from our group. It refers to the non-swollen reference state of the network with "switched-off" entanglements. By back-extrapolation of D_{res} versus swelling degree Q to the non-swollen state we can obtain the pure cross-link contribution D_{res} of the network (see fig.4.2b). Such an extrapolation assumes affine deformation during the network strands expansion, and it is thus applied only for the late stage of swelling ($Q \geq 2$), where the disentanglement effects are already absent. As it was noted before, the dry-state D_{res} value corresponds not only to the cross-link density M_c^{-1} , but rather to the sum of cross-link density and entanglement contributions: $D_{\text{res}}(\text{dry}) = D_{\text{res,c}} + D_{\text{res,e}}$, corresponding to $1/M_{c,\text{apparent}} = 1/M_c + 1/M_e$,

Defects

In order to measure the actual defect content we measured all our samples in the swollen state. We know that the constraint release complete for high swelling degrees: $Q \geq 3$. This means, that amount of network in such system is less than 33%. If we would use the usual solvent, then signal from the solvent dominate over the signal from network. Therefore we used deuterated toluene for all measurements.

The amount of defects in the swollen state is shown for all samples in table A.2 except NR-7.4. The defects content is higher in the swollen state, as expected. The difference between the defect content in the dry and swollen states is shown also in the table A.2 in the row "Trapped defects". Such defects have anisotropic motion in dry networks and move isotropically in the swollen state. They could be represented by dangling ends or loops, trapped by entanglements. In addition, in stretched samples some defects could behave non-isotropically due to the via nematic-like behaviour [7].

Chapter 5

Numerical calculations of the NMR response of networks

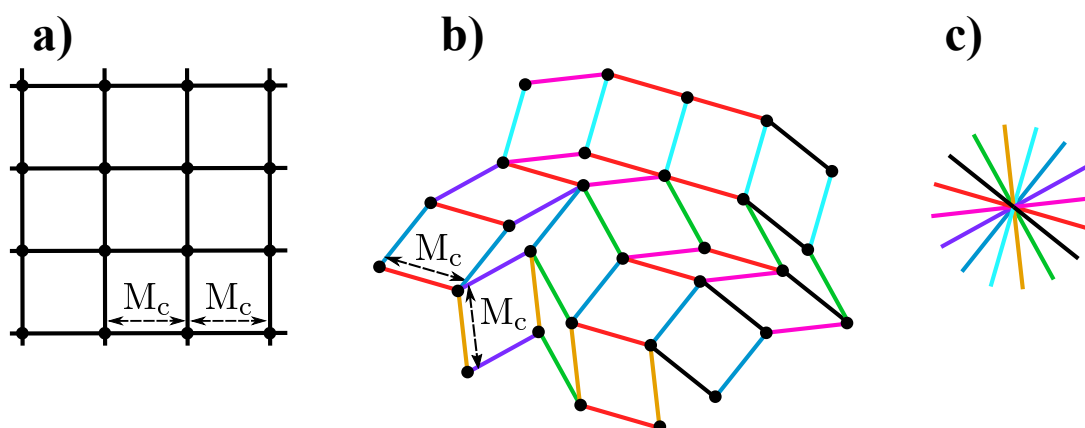


FIGURE 5.1: a) Ideal polymer network in 2D space, where networks are represented by straight lines between crosslinks. The functionality f of the network is 4. b) Ideal network representation with network strand orientations uniformly distributed. c) Representation of the polymer network as a vectors set with central point. Ends of the vectors are on a circle in 2D or common on a sphere in 3D.

In order to analyse the experimental data we need to calculate build-up curves I_{nDQ} based upon different models. We can assume different microscopic deformation specific for different elasticity models and calculate build-up curves I_{nDQ} for every model. A comparison of the calculated NMR data for specific model with experimental data could show us which model is closer to real data. Because polymer networks are generally complex systems, we have to make simplifications in the network description.

5.1 Calculation of I_{nDQ} for unstretched polymer networks

We assume, that all network chains are the same length and there are no defects. In this case we represent the network by identical vectors connected to each other by cross-links, see fig.2.6a, but with the distinction, that polymer strands between the cross-links are represented by straight lines, as shown in the fig.5.1a. It is not possible in 2D to build a network in which all cross-links have the same functionality and the network strands orientations are random and have uniform distribution of angles. Therefore in fig.5.1b the network is represented with randomly distributed orientation of polymer chains, but the functionality equals 4 of cross-links only on average, for some cross-links $f = 3$ or $f = 5$. To clearly see the angle distribution of polymer chains, we "disassemble" the network from the fig.5.1b and put all chains together, starting from a common point, as shown in the the fig.5.1c. In 2D the other ends of the end-to-end vectors reside on a circle with radius $R \propto M_c$, in 3D we have a sphere.

As was explained before, residual dipolar coupling of one polymer chain with fixed ends is proportional to the order parameter of the chain, which is in its turn proportional to the end-to-end chain distance (see section 3.2.2). Then build-up curve I_{nDQ} for a whole polymer network will be a sum of I_{nDQ} from every chain:

$$I_{\text{nDQ}}(\tau_{\text{DQ}}) = \frac{1}{N} \sum_{i=1}^N f_{\text{nDQ}}(\tau_{\text{DQ}}, D_{\text{res},0} \cdot R_i^2, \theta_i), \quad (5.1)$$

where f_{nDQ} - model build-up function (here we will examine two functions: \sin^2 function and Abragam-like function), τ_{DQ} - evolution time of the DQ signal, R_i - end-to-end distance for chain number "i", θ_i - angle between i-th chain and external magnetic field B_0 . Signal from every chain depends not only on length the chain, but also on the chain orientation relative to the external magnetic field.

I_{nDQ} build-up curves from polymer network was calculated in Matlab by representing the network by 100,000 chains with orientations covering the surface of a sphere (see the circle analogy for 2D shown in fig.5.1c). The Chain orientations are isotropically distributed, meaning that vector ends distribution is homogeneous on the sphere surface . For bulk reference samples, the radius of the sphere is always taken to equal unity, $R = 1$.

5.2 Model build-up functions

5.2.1 \sin^2 function

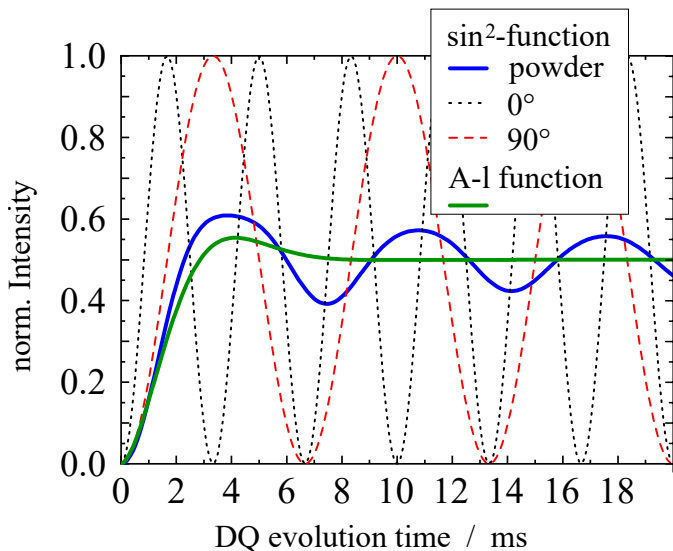


FIGURE 5.2: Comparison of DQ build-up functions: \sin^2 function, (eq.5.2 for I_{nDQ}), for single orientations 0° and 90° as compared to its powder average and the empirical A-l function (Abragam-like function), eq.3.21.

Key results of this section are published in ref. [25]. In previous investigations of our group [23, 24] the \sin^2 -function was used for calculation of DQ NMR data for different models of rubber elasticity. It is supported by the theory of a spin pair, because in polymers, at temperatures much higher than glass temperature, segments of the chain are moving fast and the residual dipole-dipole coupling is essentially dominated by spin-pair DQ coherences of the monomer unit. The exact solution for the $1/2$ -spin pair therefore could be used as a first order approximation for the polymer systems. The solution for I_{nDQ} , as already described in section 3.3.3 by eq.3.17, is a \sin^2 -function: $I_{\text{nDQ}}(\tau_{\text{DQ}}) = \langle \sin \phi_1 \sin \phi_2 \rangle$.

In polymer networks "intermediate motions", which are of the order of an NMR time-scale ($\tau_{\text{DQ}} \approx$ milliseconds), are absent. In this case the phase factors ϕ_1 and ϕ_2 are equal: $\phi_1 = \phi_2 = \phi$. This leads to the simplification

$$I_{\text{nDQ}}(\tau_{\text{DQ}}) = \langle \sin^2 \phi \rangle, \quad (5.2)$$

where $\phi = D_{\text{eff}} \int_0^{\tau_{\text{DQ}}} P_2(\cos \theta_t) dt$. Fast segmental chain motions lead to the averaging of the instantaneous orientation θ_t so that the observed D_{res} corresponds to the quasi-static interaction. Such interaction depends not on the instantaneous orientation θ_t but on the network end-to-end vector orientation θ relative to the

5.2. Model build-up functions

external magnetic field. The expression for the phase factor is then

$$\phi(\tau_{\text{DQ}}) = D_{\text{eff}} S_b P_2(\cos \theta_i) \tau_{\text{DQ}}. \quad (5.3)$$

In fig.5.2 the \sin^2 -function is displayed as powder averaged data (blue line) for the isotropic end-to-end vectors distribution and for two angles θ : 0° (black dot-line) and 90° (red dash-line). The green line in fig.5.2 represents the Abragam-like (A-1) function, corresponding to eq.3.21. The A-1 function is used as a fit function for nDQ data and fits data for homogeneous rubbers best in comparison to the Gaussian fit function.

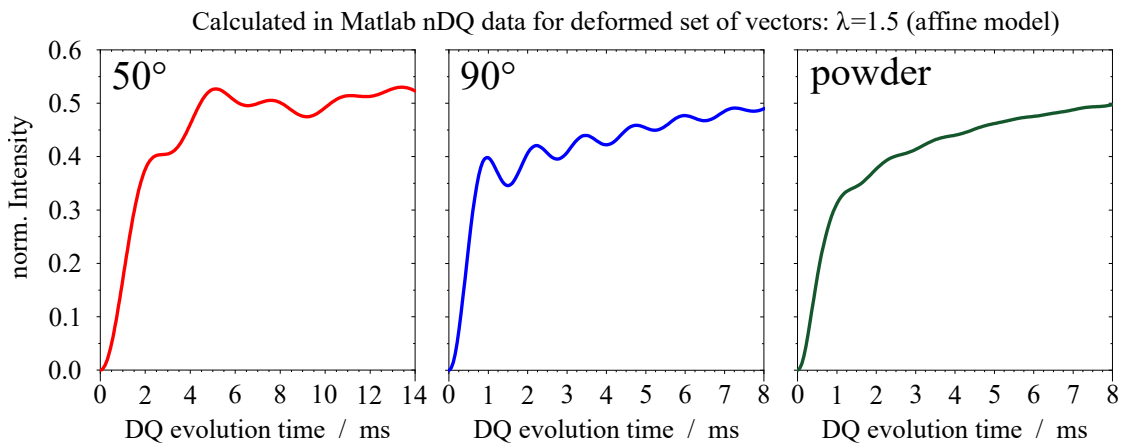


FIGURE 5.3: Examples of calculated data by using \sin^2 -function for affine uniaxial deformation of a vector set ($\lambda = 1.5$) for two orientation angles: $\Omega = 50^\circ$, $\Omega = 90^\circ$; and for powder averaged data. Ω is the angle between the axis of strain and the external magnetic field.

For numerical calculation of I_{nDQ} , based on the \sin^2 -function, we have to calculate a sum of \sin^2 -functions for every chain and normalize by the number of chains:

$$I_{\text{nDQ}}(\tau_{\text{DQ}}) = \frac{1}{N} \sum_{i=1}^N \sin^2(D_{\text{res},0} \cdot R_i^2 \cdot \frac{1}{2}(3 \cos^2 \theta_i - 1) \cdot \tau_{\text{DQ}}). \quad (5.4)$$

Here N - is a number of polymer chains, R_i - length of the i -th vector $R_i = 1$ for all vectors in the non-stretched system. They are modified in different ways corresponding to the deformation models; $\frac{1}{2}(3 \cos^2 \theta_i - 1) = P_2(\cos \theta)$ - second Legendre polynomial, which represents an angular dependency for the dipolar interaction; τ_{DQ} is a DQ evolution time. All these parameters were explained in more detail in section 3.3.

Because the \sin^2 -function suffers from oscillations, due to the spin pair bring an oversimplification on the long times, we could not fit the build-up curve of calculated data for intermediate and long times (longer than 2 ms). Such oscillations become even more troublesome for data of deformed sets of vectors (examples are shown on the fig.5.3). While this oscillations are not a big problem for powder-averaged data (see the right panel of fig. 5.3), they challenge the data analysis for single orientation data and become more pronounced for higher deformations.

As clearly seen in the middle panel (for 90°) of fig.5.3, I_{nDQ} for deformed vectors set have two components: two pronounced slopes in the build-up curve. A \sin^2 -function could not be analysed in the region $t \gtrsim 2$ ms, where the second slow component of the build-up is seen, corresponding to a component with low dipolar coupling. Therefore we need an improved model function, which would produce the theoretical DQ data without oscillations.

5.2.2 Single-orientation Abragam-like function

In order to analyse data for longer DQ evolution time, we need a function, which would have an angular dependence and whose numerical powder integral would be equal to the Abragam-like function (eq.3.21 in section 3.3.4). The Abragam-like function was introduced in our group by Walter Chassé [88] as an empirical fit function describing homogeneous polymer network samples.

$$I_{\text{nDQ}}^{A-l}(\tau_{\text{DQ}}, D_{\text{res}}) = 0.5 \left(1 - \exp[-\{0.378 D_{\text{res}} \tau_{\text{DQ}}\}^{1.5}]\right) \times \cos[0.583 D_{\text{res}} \tau_{\text{DQ}}]. \quad (5.5)$$

This function fits experimental DQ data for our samples in the virgin state very well. Our new function is essentially an Abragam-like function with introduced empirical angle dependence.

We take the A-l function itself as a starting point for a new empirical single-orientation Abragam-like function (soAl). There are two main distinctions between the original A-l and soAl functions:

1. Coefficients in front of D_{res} and power of expression in exponent (from eq.5.5) are represented as three unknown parameters, which have to be fitted: coefficient 0.378 $\rightarrow a$, power 1.5 $\rightarrow b$ and coefficient 0.583 $\rightarrow c$.

5.2. Model build-up functions

2. Residual dipolar coupling D_{res} is now orientation-dependent:

$\omega_{\text{res}} = D_{\text{res}}P_2(\cos \theta)$. The angular dependency is represented by a second Legendre polynomial $P_2(\cos \theta)$ because the phase factor for dipolar interaction has this dependency.

An expression to be solved to obtain the soAl function is then written as:

$$I_{\text{nDQ}}^{\text{soAl}} = 0.5 \left(1 - \exp[-\{a \cdot D_{\text{res}}P_2(\cos \theta)\tau_{\text{DQ}}\}^b] \right) \times \cos[c \cdot D_{\text{res}}P_2(\cos \theta)\tau_{\text{DQ}}]. \quad (5.6)$$

The coefficients a , b and c from the eq.5.6 should be selected such way, that the soAl function will satisfy the condition that a powder-averaged function $I_{\text{nDQ}}^{\text{soAl}}$ is equal to the original A-l function:

$$\int_0^{\pi/2} I_{\text{nDQ}}^{\text{soAl}}(\tau_{\text{DQ}}, D_{\text{res}}, \theta) \sin \theta \, d\theta = I_{\text{nDQ}}^{A-l}(\tau_{\text{DQ}}, D_{\text{res}}). \quad (5.7)$$

In order to obtain these three unknown parameters (a , b and c) we can fit the original A-l function by integrating left part of eq.5.7 numerically. For the fitting procedure two types of spacing between the data points were used: linear or logarithmic. The result was similar except the exponent (unknown b), which was 2 for linear and 1.4 for logarithmic spacing. We choose to use further the exponent $b = 2$, because the initial parabolic rise is supported by the second-moment approximation. Therefore the final result for soAl function is:

$$I_{\text{nDQ}}^{\text{soAl}} = 0.5 \left(1 - \exp[-\{0.455 \cdot D_{\text{res}}P_2(\cos \theta)\tau_{\text{DQ}}\}^2] \right) \times \cos[1.86 \cdot D_{\text{res}}P_2(\cos \theta)\tau_{\text{DQ}}]. \quad (5.8)$$

For illustration, the soAl function is plotted in fig.5.4a for two orientations of 0° and 90° , and the numerical powder-average of all orientations. The latter (blue dash-dot line) coincides well with the original Al function plotted by green squares.

In fig.5.4b the powder-averaged soAl function is not calculated by a linear numerical integral, but is represented by the sum normalized for 100000 vectors with isotropically distributed orientations:

$$I_{\text{nDQ}}^{\text{soAl}}(\tau_{\text{DQ}}) = \frac{1}{N} \sum_{i=1}^N 0.5 \left(1 - \exp[-\{0.455 \cdot D_{\text{res},0}R_i^2 \cdot P_2(\cos \theta_i)\tau_{\text{DQ}}\}^2] \right) \times \cos[1.86 \cdot D_{\text{res},0}R_i^2 \cdot P_2(\cos \theta_i)\tau_{\text{DQ}}]. \quad (5.9)$$

5.2. Model build-up functions

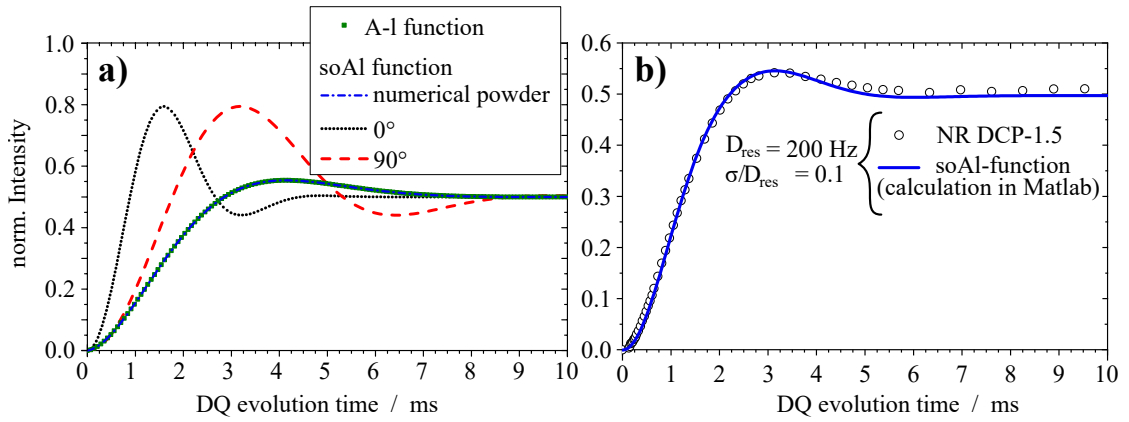


FIGURE 5.4: a) The soAl function for two orientations as compared to its powder average: the A-l function (Abragam-like function). A comparison similar to that, which is shown for the \sin^2 function on the fig.5.2. Angle Ω is an angle between the axis of strain and external magnetic field. b) Comparison of calculated for 100000 vectors DQ build-up function (based on soAl function: eq.5.8) with experimental data for NR DCP-1.5.

The simulated signal is compared with experimental data for the non-deformed rubber sample NR DCP-1.5 (i.e., $R_i = 1$), and shows very good agreement.

Data for nDQ function, shown on the fig.5.4b, was calculated by eq.5.9, where $D_{\text{res},0} = 2\pi \times 200 \text{ Hz}$ with distribution width $\sigma/D_{\text{res}} = 0.1$. These values were obtained by the data fitting for NR DCP-1.5 at temperature 80°C . With the soAl function now we are able to reproduce experimental data for non-stretched samples.

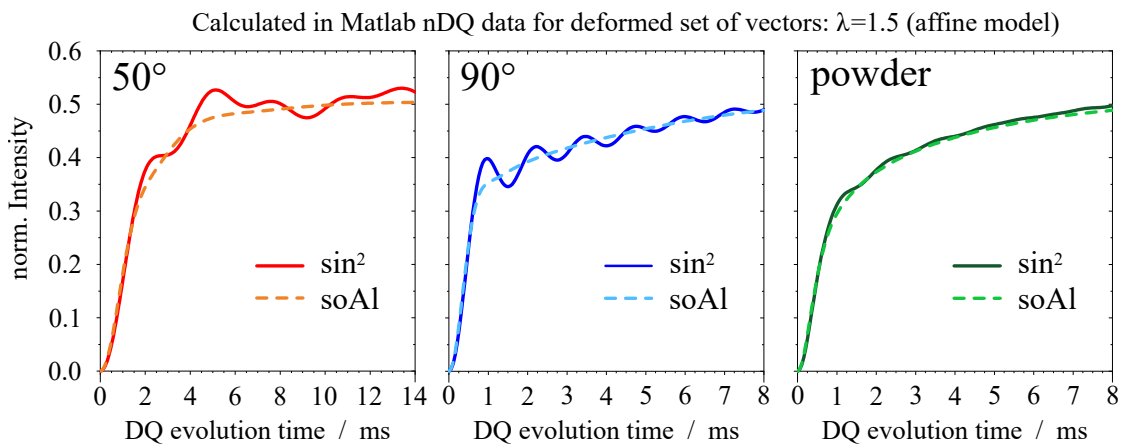


FIGURE 5.5: Example of calculated data using a \sin^2 -function (lines) and the Abragam-like function (dashed lines) for affine uniaxial deformation of a vector set ($\lambda = 1.5$) for two orientation angles: $\Omega = 50^\circ$, $\Omega = 90^\circ$; and for powder averaged data. Ω is the angle between the axis of strain and external magnetic field.

5.2. Model build-up functions

In fig.5.5 the \sin^2 function (solid lines) is compared with the soAl function (dashed lines) in the case of a uniaxially and affinely deformed set of network chains (vectors). The new function has the same shape, as the theoretically supported \sin^2 function but it does not feature oscillations. This allows us to fit the full range of the simulated data.

The simulated data again show two distinct component. For example, in the graph for $\Omega = 90^\circ$, the build-up curve has two components with low and high slopes. This motivated us further to analyse the experimental data for deformed samples by two-component fitting. Experimental data also show bimodal behaviour, but sometimes not as obvious as simulated data.

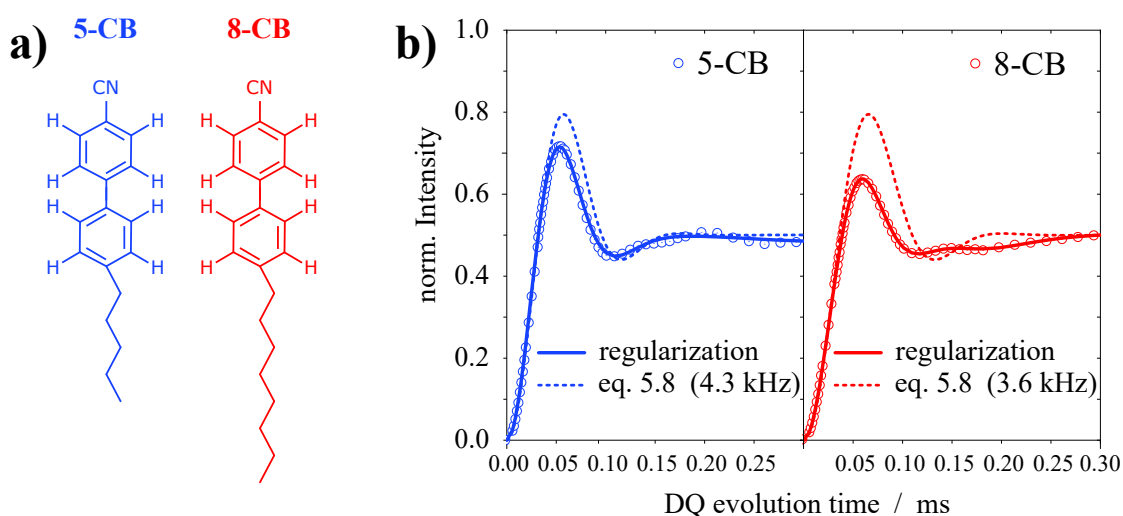


FIGURE 5.6: a) Chemical structures of the investigated liquid crystals. b) DQ build-up curves for two liquid crystal samples. Lines correspond to the fits from eq.5.8 and dashed lines obtained by regularization procedure.

As a test for soAl function we performed a DQ NMR measurements on nematic liquid crystals, because they could be easily oriented along the magnetic field, i.e. $\Omega = 0^\circ$ for all molecules. Chemical structure of samples is shown in fig.5.6a. DQ NMR measurements were performed by Prof. Dr. Saalwächter [25]. The experimental results for I_{nDQ} build-up curves together with fitting by eq.5.8 and regularization are shown in fig.5.6b. 5-CB and 8-CB samples have eight aromatic protons with similar distances thus the distributions of dipolar coupling for these samples are expected to be narrow particularly for the 5-CB sample. This is indeed observed by NMR data: the higher the oscillation, the more homogeneous the system. A dashed lines in fig.5.6b correspond to a system with a single dipolar coupling value (zero distribution width) described by the eq.5.8.

5.2.3 Effect of distributions

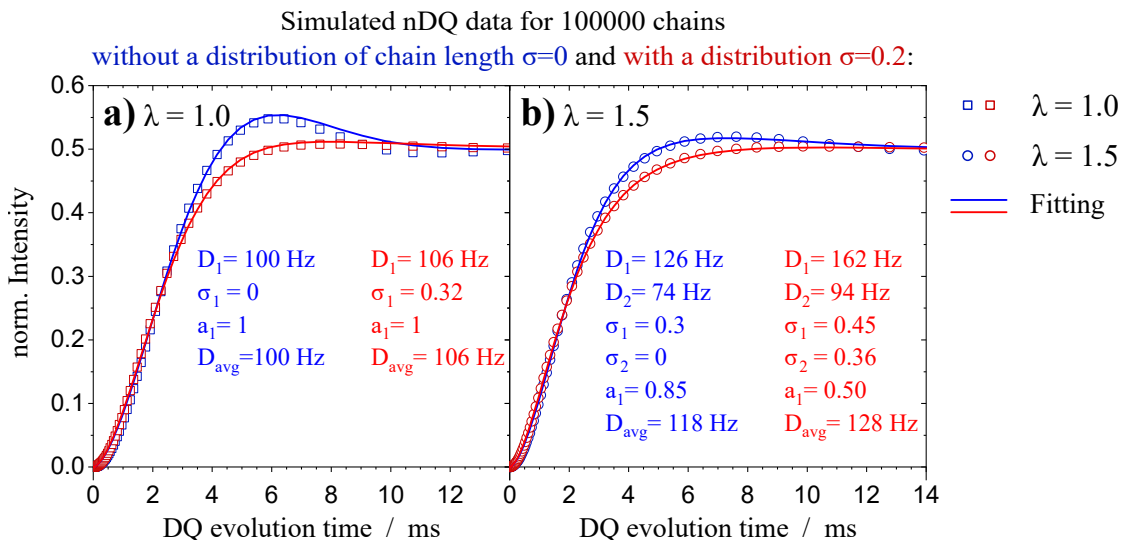


FIGURE 5.7: nDQ functions calculated for a simulated "polymer network" of 100000 chains. The effect of distribution width for end-to-end distances of the network is shown for a) an unstretched sample and b) for an uniaxially stretched sample with strain $\lambda = 1.5$. In the letter case data were fitted with a two-component Abragam-like function. Blue color corresponds to the data without a distribution for chain strands, and red - for data with initial relative distribution width $\sigma = 0.2$.

Distribution width of end-to-end vectors has an effect on the nDQ build-up curve. Here we illustrate this effect for uniformly distributed vectors with reference value of dipolar coupling of 100 Hz. In fig.5.7a is shown an example of data without applied deformation and in fig.5.7b - with applied uniaxial strain $\lambda = 1.5$. Blue squares and circles correspond to the initial vector sets without distribution (all vectors have the same length) and red squares and circles corresponds to the data for initially uniformly distributed vectors of average length $R = 1$ with distribution width $\sigma = 0.2$.

The distribution is considered here for the vector lengths, but not for D_{res} . As $D_{\text{res}} \sim R^2$, the distribution width of resulting D_{res} value should be larger than the distribution width of vector lengths. Fitting curves are shown as lines in fig.5.7: blue lines for data with $\sigma = 0$ and red lines for data with $\sigma = 0.2$. Fittings for both data sets are well converged and were done by assuming a bimodal distribution, because for following analysis we used it as a default.

As expected, for non-stretched vectors without length distribution, fitting results give the same values as the reference: $D_{\text{res}} = 100$ Hz ($\sigma = 0$). For non-stretched

5.2. Model build-up functions

vector sets with distribution the best fit provides a somewhat higher value for D_{res} (106 Hz) than $D_{\text{res},0}$ (100 Hz). The distribution width of D_{res} is expected to be larger, than the distribution width for simulated vectors: in the case of the non-stretched sample $\sigma_{D_{\text{res}}} = 0.32$ while $\sigma_R = 0.20$.

The deformation of the vector set was taken to be affine, as described in the next section. In this case nDQ data for both initial vector sets (without and with the distribution of vector lengths) have two components: the first apparent component has higher D_{res} than $D_{\text{res},0}$ and the second slightly lower $D_{\text{res},0}$. The value a_1 , shown in the plots is a fitting parameter corresponding to the first component fraction. As expected, the averaged value of D_{res} is higher than for the non-stretched sample. Same as in the case of the non-stretched sample, the averaged D_{res} value is higher if a vector length distribution is assumed. The averaged D_{res} is calculated as $D_{\text{res,avg}} = a_1 \times D_{\text{res},1} + (1 - a_1) \times D_{\text{res},2}$.

	$\sigma = 0.0$	$\sigma = 0.2$
$\lambda = 3.0$	330 Hz	340 Hz
$\lambda = 3.5$	420 Hz	390 Hz
$\lambda = 4.0$	530 Hz	450 Hz

TABLE 5.1: The dependence of D_{res} values on the length distribution of vectors. While for small deformation ($\lambda \lesssim 3$) data with R distribution have somewhat increased D_{res} , strains $\lambda \gtrsim 3$ lead to the opposite: $D_{\text{res}}(\sigma = 0.2) < D_{\text{res}}(\sigma = 0)$.

For small deformations the averaged D_{res} is higher for vector sets with length distribution, but for strain $\lambda \gtrsim 3$ the effect of vector length distribution is reversed. Even though not all our samples have a narrow distribution of D_{res} (swollen samples in particular), for the numerical model calculation of build-up curves I_{nDQ} we choose to use vector sets without length distribution. Such data provide more stable fits.

5.3 Calculation of I_{NDQ} for different elasticity models

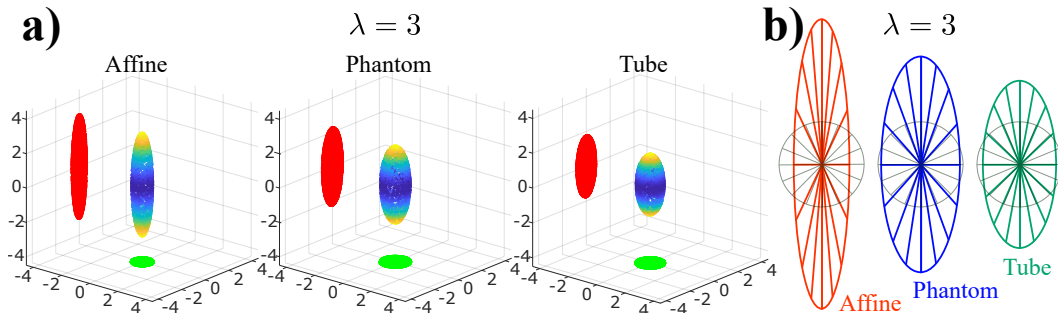


FIGURE 5.8: Representation of the microscopic-level stretching of the chains for uniaxial elongation with strain $\lambda_{\text{exp}} = 3.0$. a) 3D graphs of elongated spheres: result of uniaxial deformation according to three different models. b) Representation of stretched polymer network strands in $\{xy\}$ -plane for the 3 elastic models: affine (red), phantom (blue) and tube (green).

The expected build-up curves I_{NDQ} for the bulk (non-stretched) sample, were calculated as described above in section 5.2. A polymer network is represented by a set of unit vectors originating from a common point. The end points of vectors form a unit sphere and are uniformly distributed over its surface. Such a set-up describes a polymer network in the non-deformed state, where every vector represent a polymer chain strand between two cross-links.

The deformation of polymer chain strands of a network on the microscopic level under external forces is not well established. There are many theories treating the deformation of a polymer network chains under load (see section 2.5). Every theory assumes a specific transformation matrix for the network on the micro-level, which are also described in section 2.5. Now we apply these transformation to the set of the unit vectors, thus simulating a deformed polymer network.

We examined 3 models of rubber elasticity: two classical models (affine and phantom) and a nonaffine tube model. The last one was originally developed for the description of polymer melt rheology [8].

For the mathematical description of the models we consider in this chapter the example of uni-axial deformation. It is the most common and easy way to perform tension testing: one has to push or pull the specimen in one direction. Usually the tensile test is performed by elongation of the rubber piece at a defined strain rate

until the sample breaks or up to some predefined elongation ratio. The macroscopic strain matrix for uniaxial stretching is written as

$$\Lambda_{\text{exp,uni}} = \begin{pmatrix} \frac{1}{\sqrt{\lambda_{\text{exp}}}} & 0 & 0 \\ 0 & \frac{1}{\sqrt{\lambda_{\text{exp}}}} & 0 \\ 0 & 0 & \lambda_{\text{exp}} \end{pmatrix}, \quad (5.10)$$

where λ_{exp} - experimental elongation along the z-axis.

Fig. 5.8 shows a visual representation of the microscopic deformation of chains calculated for different models for the case of uni-axial elongation along the z -axis. In panel 5.8a a 3D-plot of elongated spheres formed by vector ends is shown. In panel 5.8b a projection of the chains on the $\{xy\}$ -plane is depicted for the three models of rubber elasticity: affine, phantom and tube.

Affine model

The classical affine model of elasticity assumes an ideal network. The strands of such a network are deformed according to the macroscopic deformation: $\lambda_{\text{microscopic}} = \lambda_{\text{macroscopic}}$. This presumes, that junction points (or cross-links) of the network move identically to the macroscopic deformation. According to this model, fluctuations of the cross-links are fully suppressed and chains are non-interacting. Even though most experiments show that the affine model overestimates the microscopic deformation of chains [4, 67, 69, 106], it still remains to be a very important model, describing the highest limit of microscopic deformation. Mathematically, we have

$$\Lambda_{\text{affine,uni}} = \Lambda_{\text{exp,uni}} \quad (5.11)$$

where $\Lambda_{\text{exp,uni}}$ - experimental (macroscopic) deformation matrix, described by eq.5.10.

Phantom model

The phantom model was initially proposed by James and Guth [3, 107, 108]. This elasticity model takes into account junction fluctuation, but chains are assumed to be non-interacting with the surrounding chains and even allowed to cross each

other. The average position of the cross-links is assumed to follow the affine theory. Nevertheless, under the mechanical load the chain strands stretch less than affinely due to the fluctuations [64, 109]:

$$\Lambda_{\text{phantom,uni}} = \begin{pmatrix} \left(\frac{1+\lambda_{exp}}{2\lambda_{exp}}\right)^{1/2} & 0 & 0 \\ 0 & \left(\frac{1+\lambda_{exp}}{2\lambda_{exp}}\right)^{1/2} & 0 \\ 0 & 0 & \left(\frac{1+\lambda_{exp}^2}{2}\right)^{1/2} \end{pmatrix}, \quad (5.12)$$

where λ_{exp} - macroscopic strain measured in an experiment.

Tube model

The tube model was originally proposed for describing dynamics in polymer melts. Using a mean field approach, it is possible to take into account not only junctions but also entanglements and other constraints of the surrounding chains. The topological constraints are applied for every monomer in the form of a quadratic potential around the chain: the tube potential. It restricts the fluctuation, such that all monomers are allowed to fluctuate only inside the tube region around every chain. The form of the potential could be described in different ways. In this work we consider the nonaffine tube model [52, 110], which assumes the tube diameter (strength of tube constraints) to be proportional to deformation. The microscopic strain matrix is:

$$\Lambda_{\text{tube,uni}} = \begin{pmatrix} \frac{1}{\sqrt[4]{\lambda_{exp}}} & 0 & 0 \\ 0 & \frac{1}{\sqrt[4]{\lambda_{exp}}} & 0 \\ 0 & 0 & \sqrt{\lambda_{exp}} \end{pmatrix}. \quad (5.13)$$

Fitting of meta-data

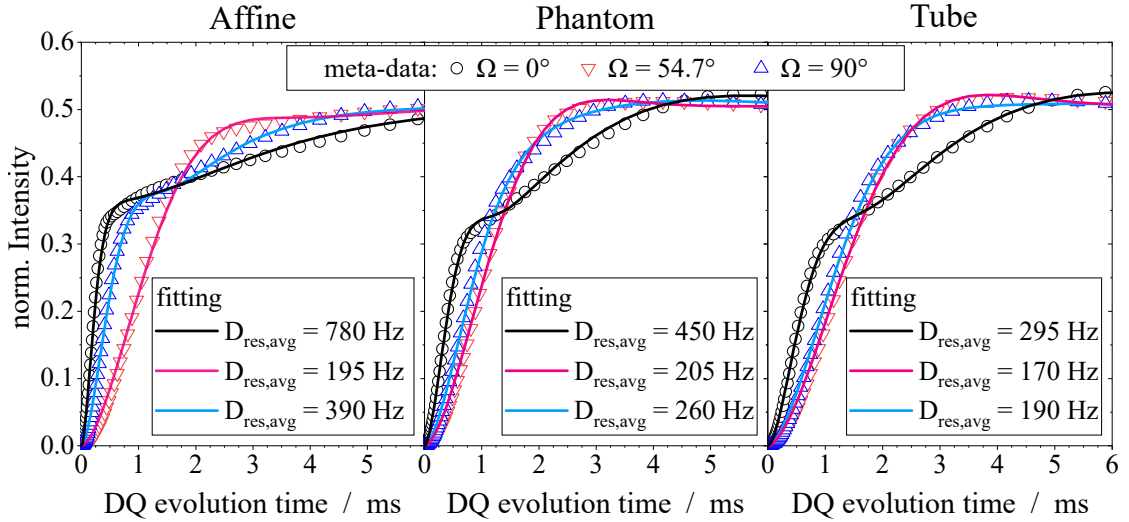


FIGURE 5.9: Fitting of meta-data corresponding to three models, investigated here: affine, phantom and tube. Data are shown for uniaxial elongation with strain $\lambda = 2.4$ of vector set with $D_{\text{res},0} = 150\text{Hz}$.

Examples of fitting are shown in fig.5.9 for all models and three orientation angles: $\Omega = 0^\circ$, $\Omega = 54.7^\circ$, and $\Omega = 90^\circ$. In case of uniaxial elongation, Ω corresponds to the angle between the stretching axis and the external magnetic field B_0 .

For fitting of calculated angle-dependent data we used a two-component original Abragam-like function with Gaussian-distributed values of residual dipolar coupling. Such a fitting function has 5 free parameters: $D_{\text{res},1}$, σ_1 , $D_{\text{res},2}$, σ_2 , and a_1 , where $D_{\text{res},i}$ and σ_i are the average residual dipolar coupling and distribution width of i -th component and a_1 is a content of first component. In fig.5.9 only the average fitted value of D_{res} is shown: $D_{\text{res,avg}} = a_1 \cdot D_{\text{res},1} + (1 - a_1) \cdot D_{\text{res},2}$.

Fitting of meta-data converges well and visually looks good, but it has a slight dependency on the initial parameters. For data analysis we were using for all orientations in one run the same set of initial parameters and boundary restrictions for σ , therefore for some curves the fits were not optimal. For a data reliability check we made few runs with different initial parameters sets and estimated the inaccuracy of the result - $D_{\text{res,avg}}$ - to be less than 5%.

Examples of fitting variations are shown in Table 5.2.

5.3. Calculation of I_{NDQ} for different elasticity models

Model(Ω)	$D_{\text{res},1}$ Hz	$\sigma_1/D_{\text{res},1}$	$D_{\text{res},2}$ Hz	$\sigma_2/D_{\text{res},2}$	a_1	$D_{\text{res,avg}}$ Hz	Result $D_{\text{res,avg}}/\text{Hz}$
Affine(90°)	581	0.08	113	0.3	0.58	385	388 ± 3
	591	0	130	0.36	0.56	389	
	592	0	130	0.36	0.56	390	
Phantom(54.7°)	232	0	164	0.36	0.64	208	206 ± 3
	231	0	163	0.35	0.65	207	
	232	0	121	0.28	0.73	203	
Tube(70°)	194	0	131	0.38	0.72	177	176 ± 2
	194	0	101	0.3	0.78	174	
	194	0	131	0.38	0.72	176	

TABLE 5.2: Examples of a fitting accuracy for meta-data: for every model one build-up curve I_{DQ} was chosen at some orientation angle. Usually data for $\Omega > 45^\circ$ have higher inaccuracy, therefore in the table are chosen examples with angles $\Omega = 54.7^\circ$, $\Omega = 70^\circ$ and $\Omega = 90^\circ$.

Chapter 6

DQ NMR experiments of deformed dry polymer networks

The main goal of the current work is to understand, if deformation on the microscopic level is different in the dry and swollen states. It builds upon the previous work on stretched dry rubber [23] and isotropically swollen rubber [55], as investigated in our group. Maria Ott performed the NMR experiments and simulations to understand, which model follows the deformation of end-to-end distance in rubber. She found that the deformation of network strands is highly nonaffine and that no model provides a very good agreement for all observations. Even earlier Walter Chassé performed NMR investigations of isotropically swollen polymer networks. He found that the swelling phenomenon has two stages as a function of the degree of swelling. In the first stage we have rearrangements of cross-links, so that chain stretching is not observable, and in the second stage the polymer strand expansion is following the affine prediction.

The aim of the current investigation is to understand, how swelling affects the deformation of polymer strands, i.e., how the network is deformed when the packing constraints are minimized by the solvent.

In order to check the validity of elasticity models, we compare several types of deformation for dry and swollen polymer networks: uniaxial stretching, compression and pure-shear deformation. We additionally carried out swelling expansion of uniaxially stretched samples and anisotropic swelling along a single axis.

All experiments were performed on three mq20 BRUKER minispec low-field NMR relaxometers. The length of 90° -pulses for these spectrometers are $1.5 \mu\text{s}$, $2.5 \mu\text{s}$ and $2.8 \mu\text{s}$. We used the Baum-Pines pulse sequence described in section 3.3.2 to measure the evolution of DQ coherences in deformed samples of rubber.

I will first discuss the NMR results for dry samples in this chapter, and then those for swollen deformed samples in the next chapter. The results will be analysed for dry and swollen states in comparison with three elasticity models: affine, phantom and nonaffine tube. Key results of this chapter are published in ref. [26].

6.1 Uniaxially stretched rubber

6.1.1 Experiment

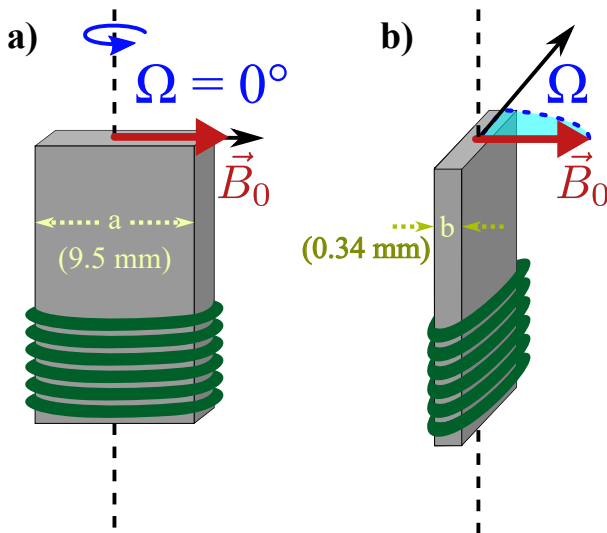


FIGURE 6.1: Uniaxial stretching of rubber rings is performed by stretching them on a thin ceramic plate. a) Angle $\Omega = 0^\circ$ corresponds to the position of the plate with the long side along the permanent magnetic field. b) By rotation of the Teflon plate we could change the orientation and measure the I_{DQ} build-up curve versus angle Ω .

In order to carry out uniaxial deformation, we prepared rubber rings with different diameters (d_1 - inner diameter, d_2 - outer diameter) and rim thickness ($c = d_2 - d_1$). All rubber rings were cut from rubber sheets of 2 mm thickness. The rings were elongated and fixed on the thin ceramic plate with width $a = 9.5 \text{ mm}$ and thickness $b = 0.34 \text{ mm}$. The perimeter length of the ceramic plate is then $L = 2(a + b)$. The macroscopic experimental elongation (λ_{mac}) was calculated using the following equation [23]:

$$\lambda_{exp} = \frac{L [1/d_1 - 1/d_2]}{\pi \ln(d_1/d_2)}, \quad (6.1)$$

the deformation matrix is correspondingly:

$$\Lambda_{\text{exp,uni}} = \begin{pmatrix} \frac{1}{\sqrt{\lambda_{\text{exp}}}} & 0 & 0 \\ 0 & \frac{1}{\sqrt{\lambda_{\text{exp}}}} & 0 \\ 0 & 0 & \lambda_{\text{exp}} \end{pmatrix}, \quad (6.2)$$

the same as already described in the previous chapter by eq.5.10.

Stretched rubber rings were attached to a Teflon rod connected to a computer-controlled servo motor (MSR 0020/L2-45-0, Mattke AG, Freiburg, Germany). The rings were placed into the NMR Bruker-m20 Minispec such way, that the orientation angle $\Omega = 0^\circ$ conforms with the elongation axis being in parallel to the permanent magnetic field B_0 (see fig.6.1a). Ω corresponds the angle between the elongation axis (long side of the ceramic plate) and the magnetic field.

To calibrate frequency and phase of the NMR signal, we first measured FID signals (see section 3.3.1). Because the calibration parameters depend on the sample shape and its orientation, we have to perform a calibration procedure for every orientation of stretched rubber to the magnetic field. For every sample T_1 , the longitudinal relaxation time (description in section 3.3.1) was measured in order to adjust the waiting time between scans. Usually a waiting time between two consequent scans was chosen in the range $T_1 - 5T_1$. DQ NMR data were measured by the Baum-Pines sequence up to 50-100 ms (the sequence is described in section 3.3.2).

6.1.2 Uniaxial elongation: results

Results for 6 different samples of NR (Natural Rubber) and BR (Butadiene Rubber) are shown on the fig. 6.2. Specifically, we address the experimental angular dependency of D_{res} and compare with numerically calculated predictions for three different elasticity models under 3 different deformation strains $\lambda = 2.4, 3.3, 4.1$. All experimental results for D_{res} were normalized by $D_{\text{res},0}$ - the values of residual coupling at the non-stretched state. The values of $D_{\text{res},0}$ are written in the brackets for every sample: the higher the $D_{\text{res},0}$ the higher the cross-link density of the sample. For a strain of 2.4 results are shown for 6 samples, whereas for higher strain experiments were possible only for softer, less crosslinked rubbers. The higher the cross-link density of the samples the easier they are rupturing because

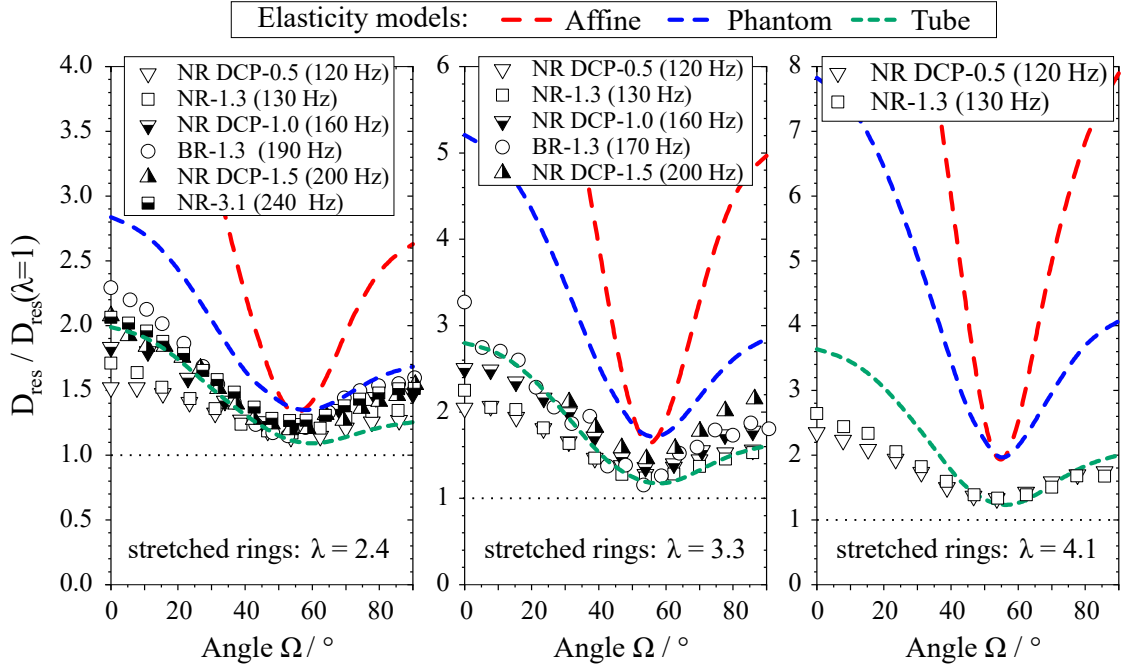


FIGURE 6.2: Angular dependency of dipolar coupling of stretched rubber rings is shown here for 6 samples. Experimental data are shown in comparison with the prediction of three elasticity models: affine (red dash line), phantom (blue dash line) and tube (green dash line) models.

of the deformation. For example at $\lambda = 4.1$ for we were able to put rings on the plate only for two the softest samples: NR DCP-0.5 and NR-1.3.

The dispersion of the measured coupling D_{res} , the angular dependence for different samples is quite significant. For example for $\lambda = 2.4$ values of D_{res} at $\Omega = 0^\circ$ are spread in a range from 1.5 up to 2.3. Lower cross-linked NR samples exhibit a less pronounced dependency on orientation (flatter curves), than the higher cross-linked NR samples. The angular dependency of D_{res} for some lowly cross-linked systems is even weaker than the tube model prediction. This could be a sign, that elasticity is dependent also on chain length between cross-links or by analogy on molecular weight M_c . In all models, which are applied here, this dependency was however not accounted for. The defect fraction can be also a reason for the higher crosslined system to behave more phantom-like [14, 16, 17], because they have less defect fraction (see table A.2).

The affine model prediction for uniaxially stretched samples does not match the experimental data satisfactorily and therefore an affine behaviour of chains on average could be excluded. The experimental data are mostly spread between the phantom and the tube model predictions; similar conclusions were drawn by Erman [4].

Butadiene rubber shows a somewhat more significant angle dependency in comparison with NR with similar crosslink density. The influence of entanglements could be excluded, because both samples have very similar entanglement length (see table 4.5). It could be influenced by topology of chains due to the different chemical reactions of BR and NR with the crosslinker.

6.2 Uniaxially compressed rubber

6.2.1 Experiment

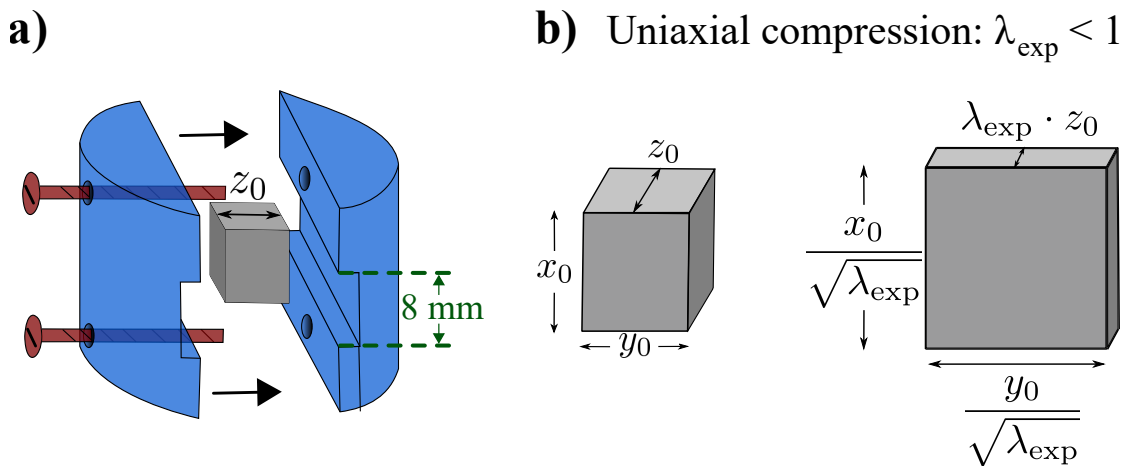


FIGURE 6.3: a) Cylindrical compression device made from ceramics. The diameter of the tool is about 10 mm. The z -axis of the sample is parallel to the compression axis. b) Graphical representation of the original sample dimensions (left) and after an uniaxial compression (right).

Uniaxial compression was performed in order to compare fitting elasticity models results with uniaxially stretched data. It is very important to compare results for different types of deformation, because very often some models fit very well one type of deformation, but do not fit well for others. For example, it was shown by Mott and Roland [111], that a constrained-chain theory of Flory and Erman [112] fits the experimental results for both stress and birefringence data in the case of tension, but fails in case of compression. The same issue arises also for a diffused-constraint theory of rubber elasticity [113].

The strain matrix for uniaxial compression is the same as for uniaxial stretching (eq.6.2), but $\lambda_{\text{exp}} < 1$. The axes $\{x, y, z\}$ in fig.6.3 correspond to the deformation

matrix from eq.6.2. Small pieces of rubber were cut from a rubber sheets of 2 mm thickness and placed between two parts of a cylindrical device shown in the fig.6.3a, and then compressed. To realize different deformations, spacers from Teflon sheets of different thickness were additionally located in-between the rubber and the device. Width and length of the initial piece of rubber to be deformed were calculated prior such that width and length of the deformed sample were not bigger than the dimensions of the slot in the device.

6.2.2 Uniaxial compression: results

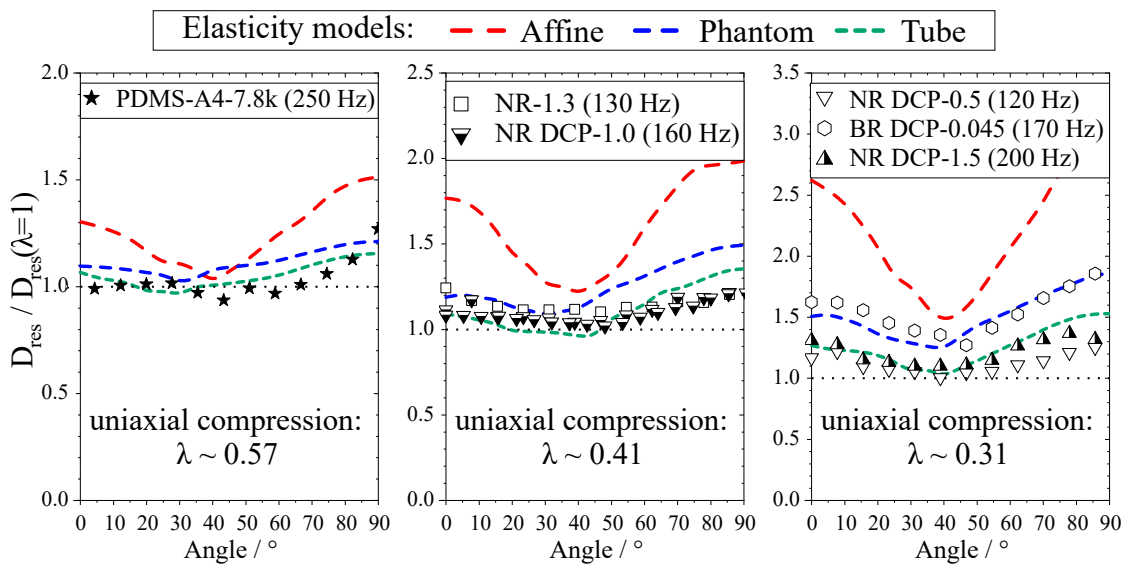


FIGURE 6.4: Angular dependence of dipolar couplings in rubber under compression for 6 samples. The dipolar coupling is normalized to the value of non-deformed state, shown in the brackets. Experimental data are shown in comparison with the prediction of three elasticity models: affine (red dash line), phantom (blue dash line) and tube (green dash line) models.

Fig.6.4 shows experimental data as compared to the model predictions. The results are very similar to the uniaxial stretching: experimental points are placed mostly around the tube model up to the phantom model predictions. As in the case for uniaxial tension, butadiene rubber (here BR DCP-0.045) results are showing more pronounced angular dependence, which corresponds better to the phantom model prediction, whereas experimental data for all NR sample measured here are close to the tube model prediction. This means that, under deformation the order parameter of butadiene rubber chains increases relatively to its bulk state more, than the order parameters for NR or PDMS.

6.3 Pure-shear deformation of rubber

6.3.1 Experiment

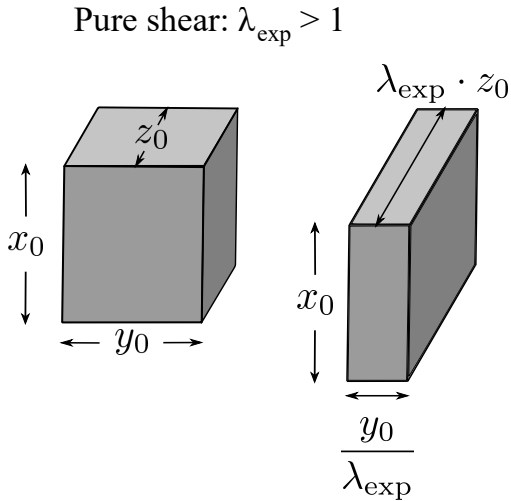


FIGURE 6.5: Graphical representation of original sample dimensions (left) and after pure-shear deformation (right). Compression is here along the y -axis.

This type of deformation is not uniaxial, as the previous two, but it is biaxial, meaning that all three deformation components λ_x , λ_y and λ_z , are different. All shear deformation components are equal to 0. The strain matrix of such a deformation is written as

$$\Lambda_{\text{ps}} = \begin{pmatrix} \lambda_x & 0 & 0 \\ 0 & \lambda_y & 0 \\ 0 & 0 & \lambda_z \end{pmatrix} = \begin{pmatrix} 1 & 0 & 0 \\ 0 & \frac{1}{\lambda_{\text{exp}}} & 0 \\ 0 & 0 & \lambda_{\text{exp}} \end{pmatrix}, \quad (6.3)$$

where λ_{exp} - is the experimentally defined macroscopic deformation i.e., the elongation along the slot of the compression tool (fig.6.3).

Experimental deformations of the samples were performed in a similar way as for uniaxial compression. The difference to uniaxial compression was the initial sample sizes. In order to keep the sample dimension along the x -axis constant, the x_0 -length of the original sample (fig.6.5b left) was 8 mm: corresponding to the compression tool slit (shown on the fig.6.3a).

6.3.2 Pure shear: results

DQ NMR results in comparison with numerically calculated model predictions are shown in fig.6.6. As for uniaxial deformation (elongation as well as compression)

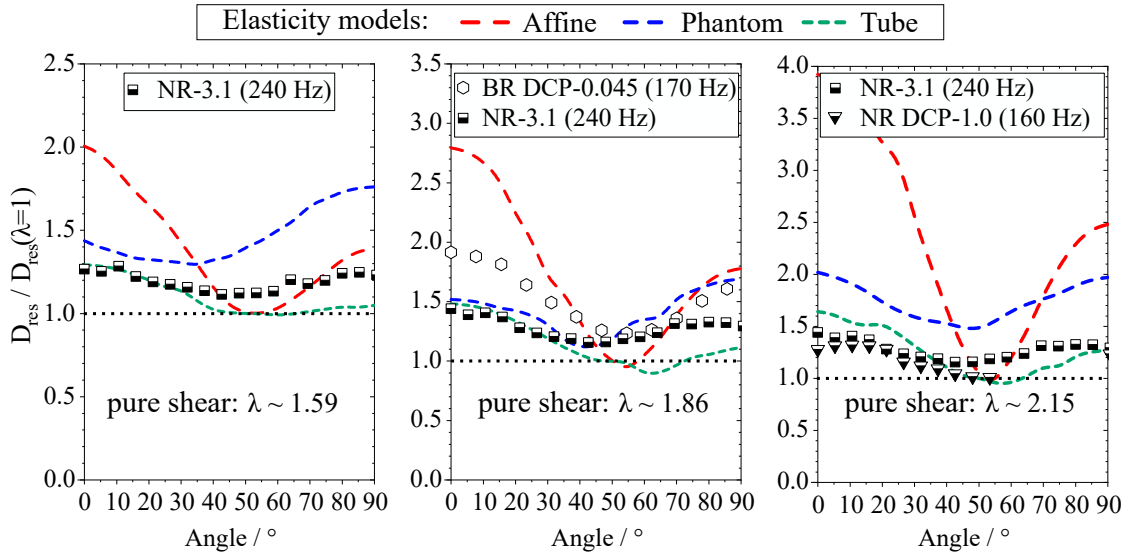


FIGURE 6.6: Angular dependence of dipolar coupling of rubber under pure-shear deformation for 3 samples. The dipolar couplings are normalized to the values for the non-deformed state shown in a brackets. Experimental data are shown in comparison with the prediction of three elasticity models: affine (red dash line), phantom (blue dash line) and tube (green dash line) models.

the experimental results are very far from the affine model prediction (shown by the red dashed line in fig.6.6). Results for NR samples are placed between the tube and phantom models, but do not follow either one of them. In the correspondence with the uniaxial compression BR has again stronger angle dependence in comparison to NR.

6.4 Discussion

6.4.1 Basic elastic models

As we have seen in sections 6.1, 6.2 and 6.3, the affine and phantom model predictions differ significantly from the experimental results for dry rubber and the tube model fits the data better for NR samples and for BR in case of uniaxial extension. For uniaxial compression and biaxial deformation, data for BR are closer to phantom network behaviour.

Such results stand for the homogeneous network but the assumption of high homogeneity can overestimate the average micro-deformation of the network, i.e. average dipolar coupling. As we know from the DQ NMR raw data for swollen

and dry states (table A.2), all our samples have a significant amount of trapped defects, which are not elastically active, but contribute to the total I_{DQ} signal in the dry state. Even though the large part of the trapped defects becomes anisotropic upon mechanical loading, they are deformed less extent than the polymer network chains. Additionally, inhomogeneities and entanglements in the network could affect the deformation pattern. Some chains could be long enough so that during deformation they are stretching much less than shorter chains, which are highly deformed and hold the stress. Possibly also some fraction of the chains behave as predicted by the affine or phantom models, and another part of the chains are only slightly or not affected by a deformation. Such models, in which not 100% of the chains are deformed, are referred to as "reduced" models and are considered in the following section.

A similar behaviour was predicted by simulations made by Everaers and Kremer [114]. They showed, that without entanglements network chains are stretched homogeneously, while entanglements result in highly unequal elongation of different polymer chains under a load. Recently Hsu and Kremer also showed by molecular dynamics simulations in melts, that overall large scale conformations of chains follow affine deformation while the distribution of the entanglement points does not deform affinely [115].

6.4.2 "Reduced" elastic models

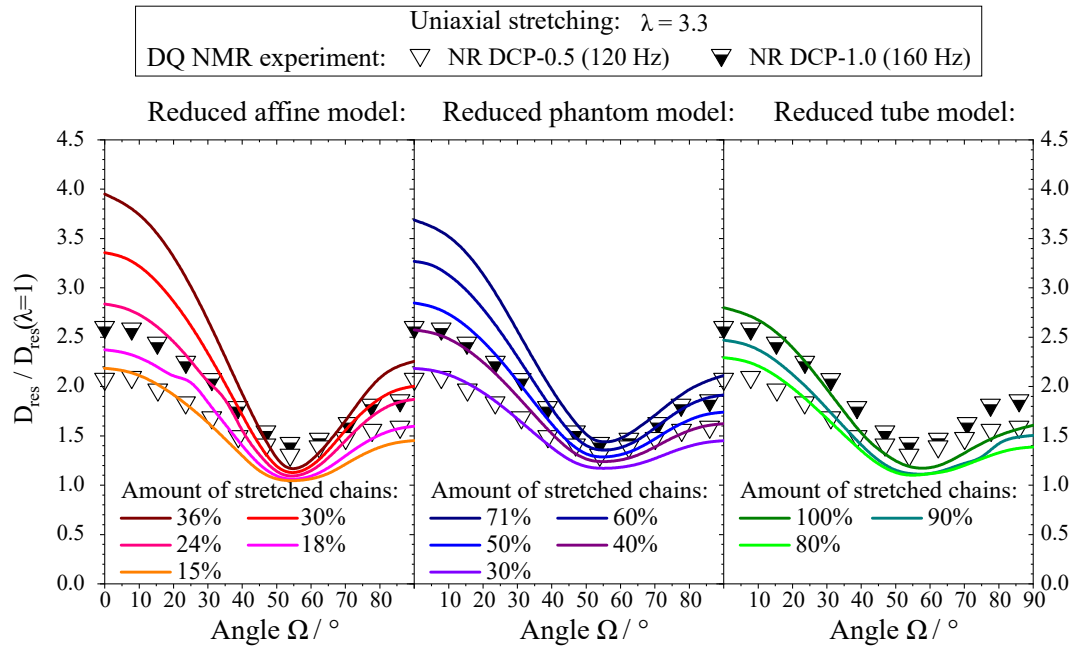


FIGURE 6.7: Calculations for the three main elasticity models (affine, phantom, tube) with partial chain stretching in comparison to experimental data for two NR samples.

Fig.6.7 shows calculated angular dependences for "reduced" models. Two experimental data sets for uniaxially elongated NR at strain $\lambda = 3.3$ of two different cross-link densities are compared with sets of "reduced" models. The lowly cross-linked rubber (NR DCP-0.5) has a weaker angular dependence, than a highly cross-linked sample (NR DCP-1.0). The affine model with 24% and 15% of stretched chains is close to experimental data for NR DCP-1.0 and NR DCP-0.5 respectively. The phantom model fits experimental data best with 50-40% and 30% for NR DCP-1.0 and NR DCP-0.5 respectively. The tube model with all stretched chains fits data for higher cross-linked rubber (NR SCP-1.0) quite well, but for the lower cross-linked sample, a "reduced" tube model with 80% of stretched chains fits data better.

A comparison between the best "fit" of the reduced models for experimental data shows that the different models all provide similar good fits at different reductions of elastic chains. Every model could be adjusted to experimental data by suitable reduction of stretched chains. For example for uniaxial stretching NR DCP-0.5, the best adjustments for "reduced" affine, phantom and tube models are indistinguishable. For the higher cross-linked NR sample (NR DCP-1.0) the best "fits" for

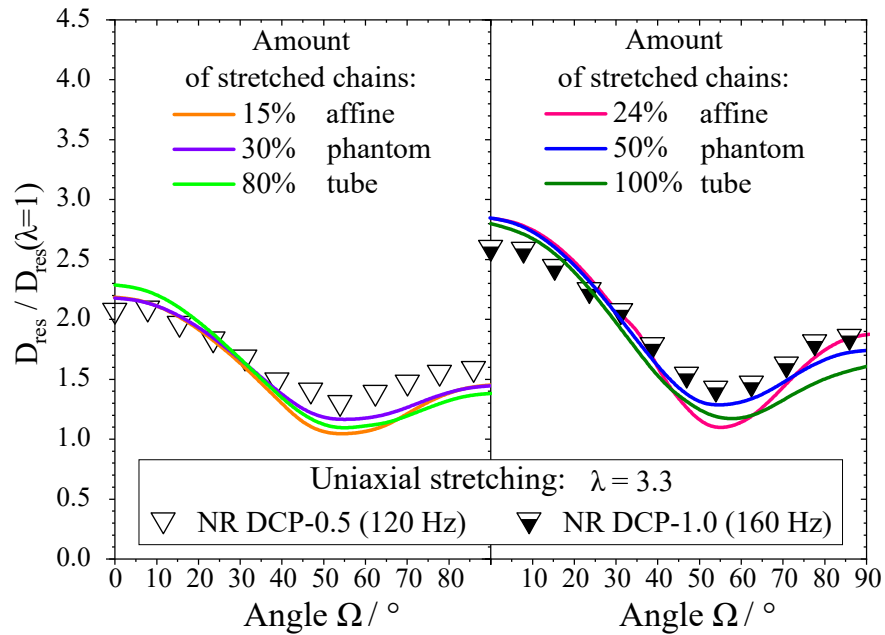


FIGURE 6.8: Comparison of reduced models based on affine, phantom and tube models. The best fit for every basic model corresponds to a different fraction of stretched chains.

the three models are similar for small angles, but diverge for larger angles $\Omega > 40^\circ$. In this case the "reduced" phantom model with 50% of stretched chains provides the best match of experimental data.

Chapter 7

DQ NMR experiments of deformed swollen samples

How swelling of the network influences the stretching and arrangement of the network chains during mechanical deformation is an open question. Solvent accelerates the dynamics of polymer chains and decrease the inter-chain interactions by dilution. Do accelerated dynamics and dilution of the polymer network chains influence the behaviour of the polymer strands and its microscopic deformation during strain? Do network chains behave in different ways upon stretching when they are in the swollen state, or are they not influenced by the solvent?

In this chapter we try to answer these questions by performing a combination of mechanical deformation and swelling. Three possible combinations of swelling and mechanical load are considered here:

- swelling of the pre-stretched rubber,
- mechanical deformation of pre-swollen rubber,
- uniaxial swelling of a rubber piece along one direction i.e., simultaneous swelling and non-isotropic deformation.

Key results of this chapter are published in ref. [26].

7.1 Swelling of pre-stretched rubber

7.1.1 Experiment

Swelling of stretched rubber could be carried out only for the rubber rings, because they have enough contact area with the solvent. At first rubber rings were prepared as described in section 6.1. DQ NMR experiments of stretched (non-swollen) rubber was done first, and then the ceramic plate with stretched rings ($\lambda = 2.4$) was placed in the solvent DBS (dibutyl sebacate) for about 10 minutes.

The swelling experiment of the stretched rings was performed several times, because rings broke frequently due to from the increased tension upon swelling. That is why several observations of the swelling process were necessary to estimate a safe swelling time. Rings at strain $\lambda = 2.4$ usually broke after swelling times no longer than 10 minutes, whereas rings at higher strains broke immediately. Also BR samples could not be measured because they broke immediately, and even at lower deformation and swelling degrees, and even if the samples did not break immediately, they were found broken after the NMR experiment (thus not providing reliable data). Because of the swelling degree limitation the highest possible swelling degree was quite low: $Q = 1.8$, before the second affine regime of swelling (see section 2.7.2). This means, that one can not check the behaviour of the network beyond sub-affine swelling regime by way of this experiment. But at least we could analyse data for swollen stretched rubber in the first stage of swelling.

Assuming a constant Poisson's ratio, the deformation matrix for this experiment reads

$$\Lambda_{\text{us, is}} = \begin{pmatrix} \sqrt[3]{Q} \cdot \frac{1}{\sqrt{\lambda_{\text{mac}}}} & 0 & 0 \\ 0 & \sqrt[3]{Q} \cdot \frac{1}{\sqrt{\lambda_{\text{mac}}}} & 0 \\ 0 & 0 & \sqrt[3]{Q} \cdot \lambda_{\text{mac}} \end{pmatrix}, \quad (7.1)$$

where $\lambda_{\text{mac}} > 1$ - experimental mechanical deformation and Q - swelling degree.

7.1.2 Degradation test

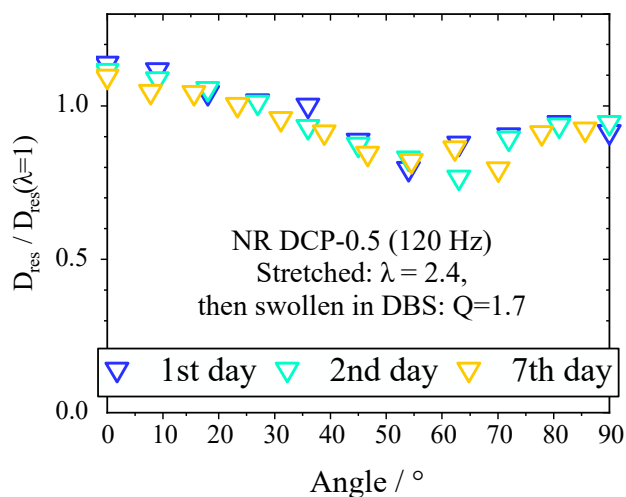


FIGURE 7.1: DQ NMR measurement for stretched rings swollen in DBS after the first, second and seventh day of swelling.

Because the residual dipolar couplings in this experiment were quite low and the angular dependence weak, we decided first to check, whether a destruction effect is active during swelling. NR DCP-0.5 was chosen for the test, a rubber with lowest crosslink density and thus the most vulnerable sample. DQ NMR data for swollen pre-stretched rings were sampled after the first, second and seventh day of swelling. The results shown in fig.7.1 are not indicating any significant degradation over 7 days. There is a trend for data after 7 days (yellow symbols) to be a bit lower, but this difference is insignificant, because it is still inside the limits of error.

7.1.3 Results

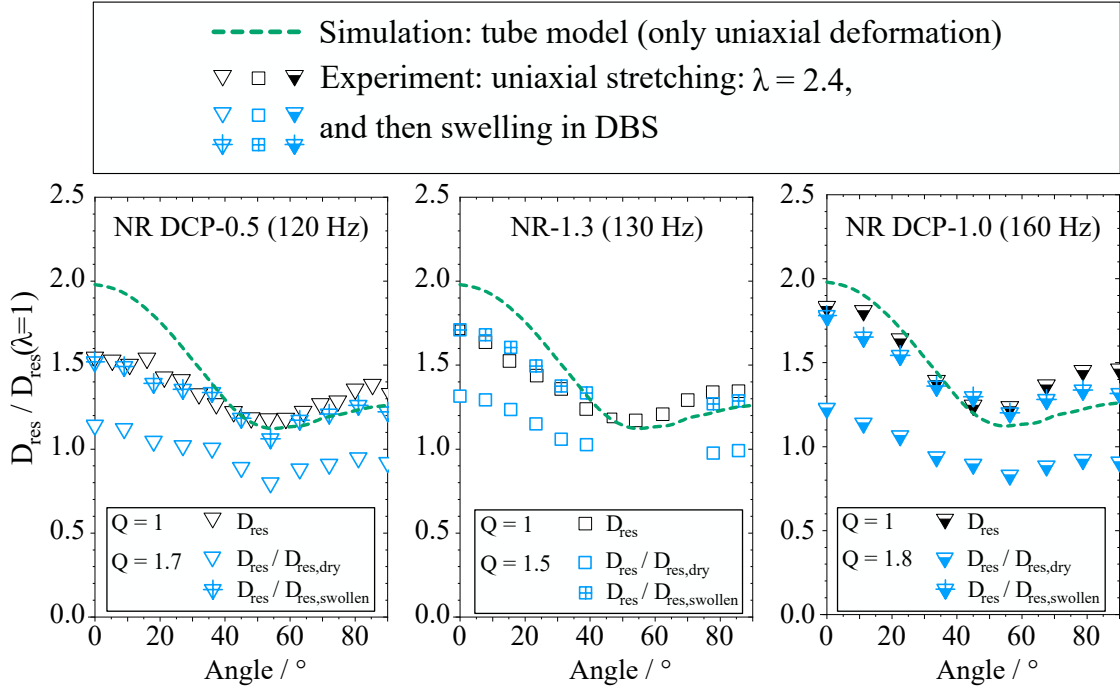


FIGURE 7.2: Orientation dependence of normalized residual coupling for swollen in DBS pre-stretched rings ($\lambda = 2.4$) for three samples. Black symbols represent the data for stretched samples without swelling and blue symbols correspond to the data of swollen and deformed rubber rings.

In fig.7.2 the blue symbols represent data for swollen stretched samples of NR DCP-0.5, NR-1.3 and NR DCP-1.0. Open symbols correspond to the data normalized by the value of D_{res} (dry), i.e. in the virgin (non-swollen, non-stretched) state, and crossed symbols correspond to the data normalized by the value of D_{res} (swollen), i.e. in the isotropically swollen non-stretched state. The actual dipolar coupling value is lower for the swollen state due to the desinterspersion effect discussed in section 2.7.2. This effect can be taken into account by normalization not to the dry value of D_{res} , but to D_{res} in the swollen (non-deformed) state at the same swelling degree.

Data normalized to the swollen match almost perfectly the experimental data for the stretched sample before swelling. This means that the swelling of stretched polymer network at least up to degree of swelling $Q = 1.8$ ($\lambda_Q = \sqrt[3]{Q} \sim 1.2$) does not change the relative configuration of pre-stretched polymer chains. This could mean, that at that swelling degree disentanglement and constraint release is not complete. Rubber, the overall topology and its response to deformation appears conserved.

7.2 Deformation of pre-swollen rubber

The first step of this experiment was the swelling of a rubber piece up to a degree of swelling between 1.5 and 2.8. This to the end of the nonaffine and the beginning of the affine stage of swelling (see section 2.7.2).

Mathematically, isotropic swelling is represented

$$\Lambda_{\text{is}} = \begin{pmatrix} \lambda_x & 0 & 0 \\ 0 & \lambda_y & 0 \\ 0 & 0 & \lambda_z \end{pmatrix} = \begin{pmatrix} \sqrt[3]{Q} & 0 & 0 \\ 0 & \sqrt[3]{Q} & 0 \\ 0 & 0 & \sqrt[3]{Q} \end{pmatrix}. \quad (7.2)$$

After swelling, two types of the deformation of the swollen rubber were carried out: uniaxial compression or pure shear, described in the following sections. Here we only investigate the DCP crosslinked NR samples, because data for the NR with sulphur cross-linking are not reliable due to the fast degradation of the swollen rubber. BR and PDMS in turn are quite brittle in the swollen state.

7.2.1 Uniaxial compression

Uniaxial compression of swollen rubber: experiment

The experimental set-up for uniaxial compression is described above in section 6.2, with the only distinction, that here the initial state is not the dry but the swollen state in DBS. The matrix for uniaxial compression of swollen rubber is a direct product of the isotropic swelling and uniaxial compression matrices:

$$\Lambda_{\text{uc, is}} = \begin{pmatrix} \sqrt[3]{Q} \cdot \frac{1}{\sqrt{\lambda_{\text{exp}}}} & 0 & 0 \\ 0 & \sqrt[3]{Q} \cdot \frac{1}{\sqrt{\lambda_{\text{exp}}}} & 0 \\ 0 & 0 & \sqrt[3]{Q} \cdot \lambda_{\text{exp}} \end{pmatrix}, \quad (7.3)$$

where the strain is $\lambda_{\text{exp}} < 1$.

Uniaxial compression of swollen rubber: results

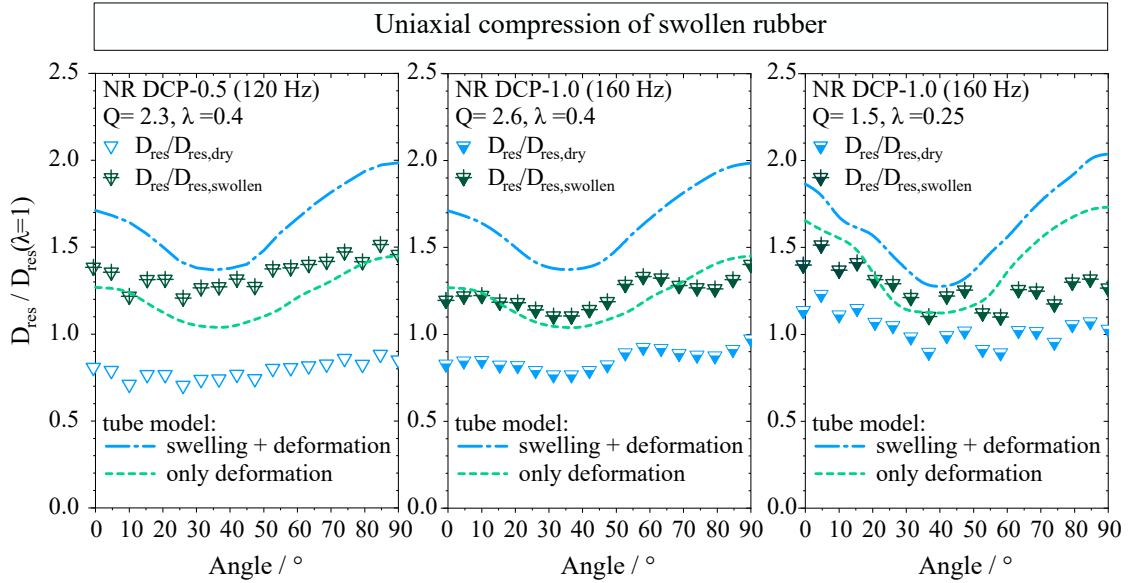


FIGURE 7.3: Angle dependence of normalized dipolar coupling for uniaxially compressed swollen rubber. Comparison of experimental data (triangles) for two different normalizations with tube models (dashed and dot-dash lines) for each normalized data set. Blue lines correspond to the simulations for blue symbols, green lines correspond to the dark green symbols.

To understand how the chains are stretched and possibly rearranged, we need to predict the results according to different deformation models and also choose the right starting condition for the network. All models except the tube model are far from the experimental data for this experiment. In fig.7.3 we show thus only tube model predictions. First consider the blue triangles: these are the experimental data normalized to the dipolar coupling of the network in the dry non-swollen non-stretched (virgin) state. For this data normalization, even the tube model prediction is too high in comparison to the experimental data if we consider both swelling and compression (blue dashed line in fig.7.3). Such a big difference between experiment and simulation is apparently due to the wrong assumptions by normalization of experimental data and deformation matrix by simulation.

Firstly we have to renormalise the experimental data, because in the swollen state the equilibrium end-to-end distance R_0 from eq.3.13 is nominally larger than in the dry state. But D_{res} in the swollen state is lower than in the dry state (in the first stage of swelling). For example D_{res} of NR DCP-0.5 is 120 Hz in the dry state, but in the swollen state at swelling degree $Q = 2.3$, $D_{\text{res}} = 70$ Hz only. Should we now take 70 Hz or 120 Hz as the reference for the experimental data? I chose 70 Hz,

because the equilibrium state is changed in the swollen state. Data normalized to the swollen state are shown in fig.7.3 as green crossed symbols. They are placed above blue symbols, but still are not reaching the simulation curve for the tube model.

Secondly, we need to adjust the simulation for normalized data. A swollen network has an equilibrium state which is distinguished from the dry network state. This new equilibrium state could not be described just by the degree of swelling due to the complex processes of expansion, disentanglement and constraint release (desinterspersion). We have to take into account the new value for the reference D_{res} and assume that our network is in equilibrium. In the simulation we therefore need to consider only the uniaxial compression, because swelling is already taken into account by the normalization by D_{res} of the undeformed network in the swollen state. The deformation matrix 7.3 should be changed accordingly to the one described for the dry state in the previous section, eq.6.2, where $\lambda_{\text{exp}} < 1$. Simulations for uniaxial compression without swelling are shown in fig.7.3 by the green dash lines, which are located below simulations for deformation and swelling, and approximately match the experimental data, normalized to the swollen state D_{res} .

7.2.2 Pure shear

Pure shear of swollen rubber: experiment

The experimental set-up for pure shear is described above in section 6.3 but applied for pre-swollen rubber. The matrix for pure shear deformation of swollen rubber, like for compression of swollen rubber, is also a direct product of matrices for isotropic swelling and pure shear deformation. However, swelling we will not be considered in the simulations for the same reason as describe above in section 7.2.1. Therefore we are simulating only pure shear deformation by the matrix expressed by the eq.6.3.

Pure shear of swollen rubber: results

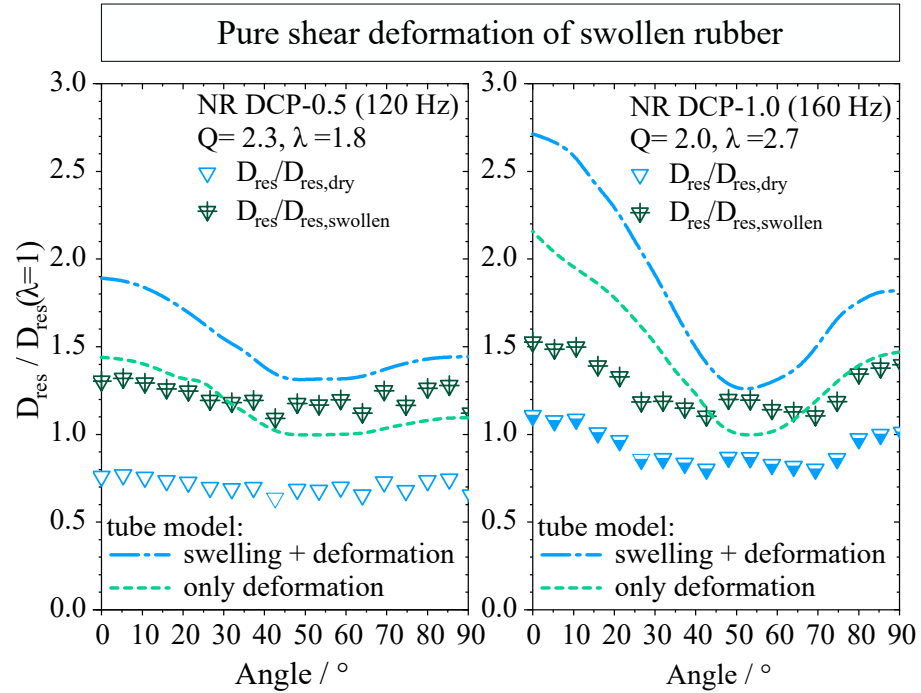


FIGURE 7.4: Angular dependence of normalized dipolar couplings for pre-swollen samples under pure shear deformation. Comparison of experimental data (triangles) for two different normalizations with tube model predictions (dashed lines) for each normalized data set. Blue lines correspond to the simulations for blue symbols, green lines correspond to the dark green symbols.

The results for the second type of the deformation for swollen network were performed to confirm the results for uniaxial compression. Pure-shear experimental data are shown in fig.7.4 by blue (normalization to the D_{res} of the dry state) and by dark green crossed (normalization to the D_{res} of the swollen state) symbols. Re-normalization of the experimental data as well as of the calculated predictions of tube model were made the same way as was done for uniaxial compression in section 7.2.1. The results for pure share agree with the results for uniaxial compression of swollen networks. We could confirm, that in both our experiments the end-to-end distance of swollen rubber does not follow the affine model prediction, but shows on average behaviour corresponding to the tube model prediction for swelling degrees at the beginning of the affine swelling stage.

7.3 Anisotropic swelling along one axis

Uniaxial swelling: experiment

In this experiment, swelling and mechanical deformation of the sample are happening at the same time, as in the case of isotropic swelling. Unlike isotropic swelling, uniaxial swelling sample expansion occurs only along one direction and not along all three directions. We performed this experiment by immersing 3-mm-diameter disc of a polymer network sample inside a tube with the inner diameter $d = 3$ mm. The tube with the sample inside was immersed in deuterated toluene. After a few days of swelling we flame sealed the sample inside the glass test-tube for DQ NMR measurements. We defined Ω as the angle between the direction of elongation of the sample and magnetic field of a spectrometer. The sample could swell only along the tube axis so that deformation along the axis equals degree of swelling $\lambda = Q$. The experimental swelling degree (Q) was estimated from the length of the swollen sample inside the tube. Due to a small size of samples measured Q values have large uncertainty.

The experiment could be described by simulation in two ways, as with the previous experiments with swelling: mechanical deformation of a swollen sample and swelling of an uniaxially stretched sample. In the first method, it is assumed that chains are stretching during swelling. In this case, the expansion along one axis equals degree of a swelling Q . This description of the experiment is represented by

$$\Lambda_{\text{us}} = \begin{pmatrix} 1 & 0 & 0 \\ 0 & 1 & 0 \\ 0 & 0 & Q \end{pmatrix}, \quad (7.4)$$

where Q is degree of swelling, or elongation of the sample along the tube. For such a description of the deformation, we have to *normalize experimental data by the phantom reference* value of D_{res} . Simulations for this representation are then described by the elasticity models *for the dry network state*, neglecting entanglement contributions, corresponding to the $D_{\text{res,c}}$ value of the experimental data from the phantom network reference extrapolation.

The second possibility to describe the uniaxial deformation is to assume the swollen state as the initial state. In this case we avoid describing what is happening during the first stage of swelling, which is anyway uncertain. In order to calculate the

predictions for different elasticity models, we represent our deformation matrix as a product of two matrices, isotropic dilation of the sample and deformation:

$$\Lambda_{\text{us}} = \begin{pmatrix} \sqrt[3]{Q} & 0 & 0 \\ 0 & \sqrt[3]{Q} & 0 \\ 0 & 0 & \sqrt[3]{Q} \end{pmatrix} \cdot \begin{pmatrix} \frac{1}{\sqrt[3]{Q}} & 0 & 0 \\ 0 & \frac{1}{\sqrt[3]{Q}} & 0 \\ 0 & 0 & \sqrt[3]{Q^2} \end{pmatrix} = \begin{pmatrix} \sqrt[3]{Q} & 0 & 0 \\ 0 & \sqrt[3]{Q} & 0 \\ 0 & 0 & \sqrt[3]{Q} \end{pmatrix} \cdot \begin{pmatrix} \frac{1}{\sqrt{\lambda}} & 0 & 0 \\ 0 & \frac{1}{\sqrt{\lambda}} & 0 \\ 0 & 0 & \lambda \end{pmatrix}, \quad (7.5)$$

where Q is the degree of swelling and $\lambda = \sqrt[3]{Q^2}$. According to this representation of the uniaxial swelling, we have to normalize experimental data by the value of $D_{\text{res}}(Q)$ in the swollen state. For the simulation, we are neglecting the matrix of isotropic expansion, because it is taken into account by the normalization. The matrix, which we have to apply for simulation, is the matrix of uniaxial deformation with strain λ , eq.7.5. The simulation for this representation is described by the elasticity models *for the swollen state*.

Uniaxial swelling: results

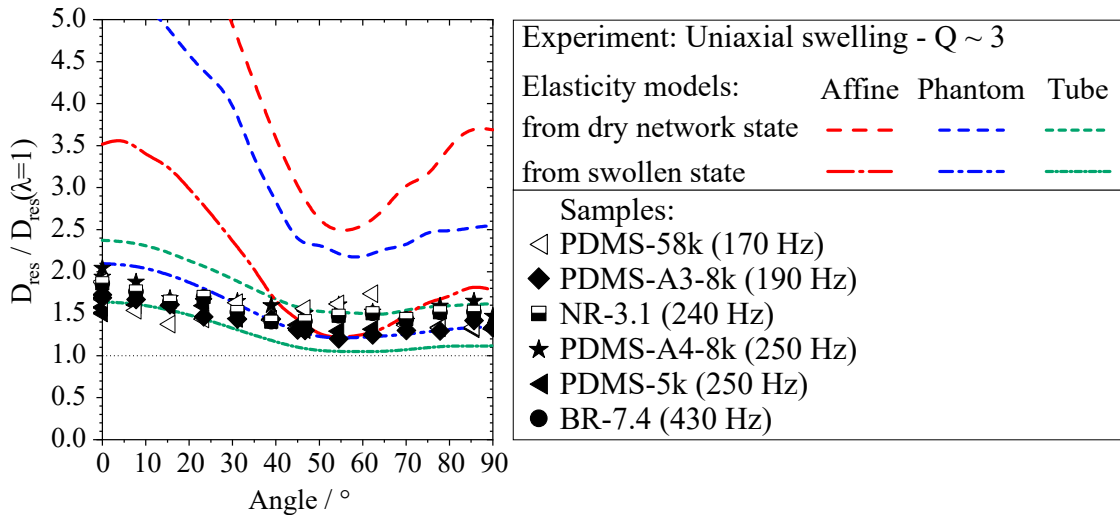


FIGURE 7.5: Angle dependence of normalized dipolar coupling for uniaxially swollen samples. All three models are shown for two initial conditions: non-swollen (dry network) and swollen states. Experimental data are normalized to the isotropically swollen state.

7.3. Anisotropic swelling

The experimental data shown by the black symbols in fig.7.5 represent the angle dependence of DQ NMR data for uniaxially swollen samples, considering only the normalization to the swollen state. Normalization to the dry state corresponding to the phantom reference state will be discussed for powder averaged data below. Both representations for the simulations are displayed for comparison: elasticity models for initial phantom reference (dry) and for initial swollen states. Measured dipolar coupling results are dispersed between tube and phantom models corresponding to swollen state. Due to the small amount of sample, the data are very noisy and could not be analysed in more detail. For clearer data we examined orientation averaged data, as described below.

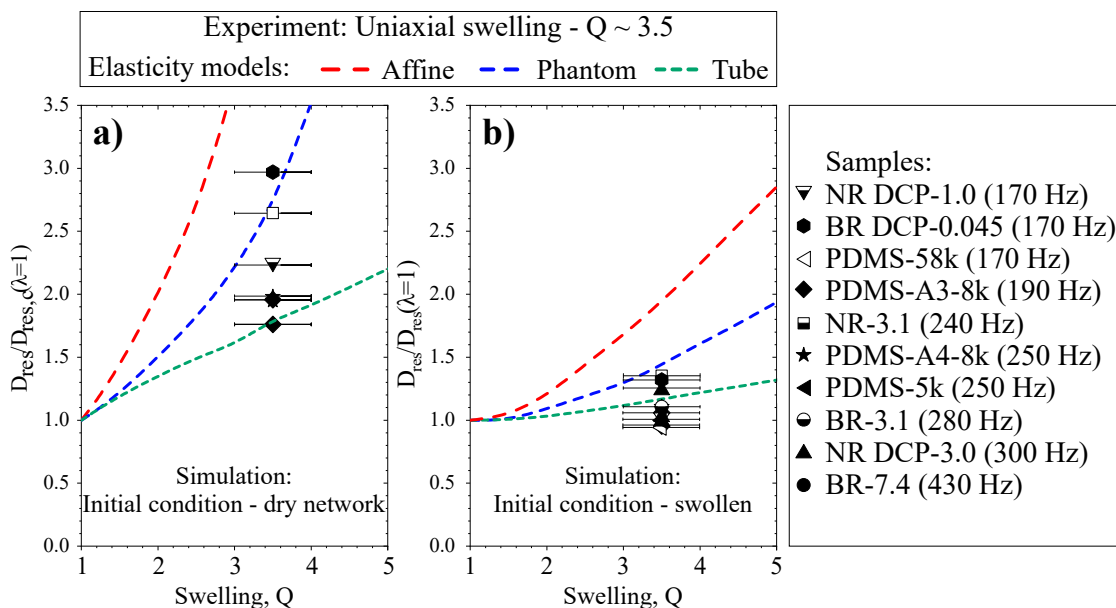


FIGURE 7.6: Artificial powder averaged DQ NMR results for uniaxially swollen samples and simulations a) for dry networks and b) for swollen networks as initial state. Experimental data are normalized accordingly by dipolar couplings of a) the phantom reference and b) the swollen state.

In fig.7.6a we show experimental data normalized to phantom reference and elasticity models simulations for "artificially powder averaged" data at different swelling degrees. Uncertainties of the swelling degree are shown for experimental data by error bars. All experimental data were normalized to the phantom reference dipolar coupling, which assumes that all entanglements and physical constraints are dissolved. This means that data with this normalization represent an upper border of the actual results. We can see that only the phantom model could be reached with the data, but affinity is clearly excluded. The dispersion of the data between the tube and the phantom models could also indicate that end-to-end

7.3. Anisotropic swelling

vectors follow to the phantom model behaviour with stretching of only a certain fraction of the chains(see section 6.4.2).

In fig.7.6b I show the same data, but normalized to the swollen state. The simulation is in this case corresponding to uniaxial elongation from the isotropically swollen state. The scatter of the data is wider, but an upper limit for the micro-deformation agrees with the other normalization procedure.

Chapter 8

Summary

In this work *microscopic deformation of polymer network chains* were investigated by DQ NMR experiments. Uniaxial deformation and compression, biaxial (pure-shear) deformation of dry and swollen NR, BR and PDMS rubbers of different crosslink densities were analysed and compared with three elasticity models (affine, phantom and nonaffine tube).

A new single-orientation Abragam-like (soAl) function for orientation dependent simulations was introduced in the current investigation. The new soAl function has an advantage over the previously used \sin^2 -function due to the absence of the oscillations on the long time scale. This enables to analyse experimental I_{nDQ} data for a longer DQ evolution time.

NMR results for uniaxial stretching of NR and BR samples in the dry state show that the tube model fits the experimental data quite well. For uniaxial compression and biaxial deformation, data for BR are closer to phantom network behaviour, whereas results for NR and PDMS samples are placed around the tube model prediction. This means that under deformation, the order parameter of BR chains increases relatively to its bulk state more than the order parameters for NR or PDMS. This could arise from the topology of chains due to the different chemical reactions of BR with the crosslinker in comparison to NR and PDMS.

Orientation-dependent DQ NMR data for different combinations of swelling and mechanical deformation of rubber were performed. These results were compared with the results for dry state and with the simulations. The overall deformation pattern for swollen samples is ascertained to be similar to dry samples with rather

weak microscopic deformation and angle dependency. However inhomogeneity of swollen samples is significantly increased. In comparison to the affine isotropic chain expansion for highly swollen network, their response to the mechanical deformation in the same swollen state appears to be well below the affine prediction.

The assumption of homogeneity of the network can overestimate the average microdeformation of network chains, i.e. average dipolar coupling. Taking into account the significant inhomogeneity of deformed networks, which becomes even more significant in the swollen state we proposed "reduced" models: coexistence of elastically active chains together with nondeformed and nonoriented chains. A comparison between the best fit of the "reduced" models for experimental data shows that the different models all provide similarly good fits at different reductions of elastic chains. Every model could be adjusted to experimental data by suitable reduction of stretched chains.

Even in the highly swollen state for uniaxially swollen samples, their polymer chains are weakly stretched and oriented. This means that for a dry and in particular for a swollen deformed samples inhomogeneity plays a crucial role and should not be ignored for the consideration of elasticity effects.

Appendix A

Samples

Densities of rubbers and solvents

Sample name	Density g/mL
NR	0.9093
BR	0.90
PDMS	0.97
toluene-d8	0.94
toluene	0.87
DBS	0.94
cyclohexanone	0.95

TABLE A.1: Densities of samples, used in this work. ρ_{BR} taken from <https://scientificpolymer.com/density-of-polymers-by-density/>. For other polymers data are taken from the polymer Handbook [104]. Densities of solvents were taken from the website: <https://www.sigmaaldrich.com/>.

Molecular weight M_c

The results for molecular weight measured by NMR in the table A.2 are not very exact, because the conversion factors between the measured D_{res} and molecular weight M_c are shown to be accurate only within about 30%. Defects column in the table A.2 shows the amount of defects in swollen state, and trapped defects are that part of defects, which is anisotropic in the dry state.

Sample	$M_c + M_e$ kg/mol	M_c kg/mol	Defects (swollen) %	Trapped Defects %	M_e kg/mol
NR-1.3	2.4	7.7	35	27	3.4
NR-3.1	1.3	2.8	9	5	2.4
NR-7.4	0.7	-	-	-	-
BR-1.3	1.9	-	44	27	-
BR-3.1	1.2	-	15	8	-
BR-7.4	0.8	-	5	3	-
NR DCP-0.5	2.6	-	50	37	-
NR DCP-1.0	1.9	6.2	32	24	2.8
NR DCP-1.5	1.5	3.4	17	11	2.8
NR DCP-2.0	1.3	2.8	13	8	2.4
NR DCP-3.0	1.0	-	9	5	-
BR DCP-0.045	1.9	4.1	46	32	3.6
PDMS-A3-7.8k	2.2	1.8	13	8	6.0
PDMS-A3-18.9k	8.4	-	58	22	-
PDMS-A4-7.8k	2.5	1.9	11	5	7.9
PDMS-A4-18.9k	13	-	58	19	-
PDMS-2003y-5k	2.5	-	5	1	-
PDMS-2003y-58k	3.3	-	12	8	-

TABLE A.2: Results for molecular weight of polymer strands between the crosslinks derived from DQ NMR analysis: M_e is average molecular weight between entanglements and M_c - between a neighbour crosslinks.

Bibliography

- [1] L. R. G. Treloar and D. J. Montgomery. The physics of rubber elasticity. *Physics Today*, 12:32–34, 1959.
- [2] B. Erman and J. E. Mark. Rubber-like elasticity. *Annual Review of Physical Chemistry*, 40:351–374, 1989.
- [3] E. Guth and H. M. James. Elastic and Thermoelastic Properties of Rubber-like Materials. *Industrial and engineering chemistry*, 36:624–629, 1941.
- [4] B. Erman. Chain dimensions in deformed networks: theory and comparison with experiment. *Macromolecules*, 20:1917–1924, 1987.
- [5] R. Ullman. Small-angle neutron scattering from elastomeric networks. application to labeled chains containing several crosslinks. *Macromolecules*, 15: 1395–1402, 1982.
- [6] P. T. Callaghan and E. T. Samulski. Biaxial deformation of a polymer network measured via deuteron quadrupolar interactions. *Macromolecules*, 36:724–735, 2003.
- [7] B. Deloche and E. T. Samulski. Short-range nematic-like orientational order in strained elastomers: a deuterium magnetic resonance study. *Macromolecules*, 14:575–581, 1981.
- [8] P. G. de Gennes. Reptation of a polymer chain in the presence of fixed obstacles. *The Journal of Chemical Physics*, 55:572–579, 1971.
- [9] M. Gottlieb and R. J. Gaylord. Experimental tests of entanglement models of rubber elasticity: 1. uniaxial extension-compression. *Polymer*, 24:1644–1646, 1983.
- [10] M. Gottlieb and R. J. Gaylord. Experimental tests of entanglement models of rubber elasticity. 2. swelling. *Macromolecules*, 17:2024–2030, 1984.

- [11] M. Gottlieb and R. J. Gaylord. Experimental tests of entanglement models of rubber elasticity. 3. biaxial deformations. *Macromolecules*, 20:130–138, 1987.
- [12] S. F. Edwards and T. A. Vilgis. The tube model theory of rubber elasticity. *Reports on Progress in Physics*, 51:243–297, 1988.
- [13] K. Urayama, T. Kawamura, and S. Kohjiya. Multiaxial deformations of end-linked poly(dimethylsiloxane) networks. 2. experimental tests of molecular entanglement models of rubber elasticity. *Macromolecules*, 34:8261–8269, 2001.
- [14] M. Zhong, R. Wang, K. Kawamoto, B. D. Olsen, and J. A. Johnson. Quantifying the impact of molecular defects on polymer network elasticity. *Science*, 353:1264–1268, 2016.
- [15] J. Wang, T.-S. Lin, Y. Gu, R. Wang, B. D. Olsen, and J. A. Johnson. Counting Secondary Loops Is Required for Accurate Prediction of End-Linked Polymer Network Elasticity. *ACS Macro Letters*, 7:244–249, 2018.
- [16] Michael Lang. Elasticity of phantom model networks with cyclic defects. *ACS Macro Letters*, 7:536–539, 2018.
- [17] T.-Sh. Lin, R. Wang, J. A. Johnson, and B. D. Olsen. Revisiting the elasticity theory for real gaussian phantom networks. *Macromolecules*, 52:1685–1694, 2019.
- [18] R. Ullman. Small angle neutron scattering from polymer networks. *The Journal of Chemical Physics*, 71:436–449, 1979.
- [19] J. Bastide, R. Duplessix, C. Picot, and S. Candau. Small angle neutron scattering and light spectroscopy investigation of polystyrene gels under osmotic deswelling. *Macromolecules*, 17:83–93, 1984.
- [20] K. Saalwächter and J.-U. Sommer. NMR reveals non-distributed and uniform character of network chain dynamics. *Macromolecular Rapid Communications*, 28:1455–1465, 2007.
- [21] W. Chassé, K. Saalwächter, and J.-U. Sommer. Thermodynamics of Swollen Networks As Reflected in Segmental Orientation Correlations. *Macromolecules*, 45:5513–5523, 2012.

- [22] K. Saalwächter, W. Chassé, and J.-U. Sommer. Structure and swelling of polymer networks: insights from NMR. *Soft Matter*, 9:6587–6593, 2013.
- [23] M. Ott, R. Pérez-Aparicio, H. Schneider, P. Sotta, and K. Saalwächter. Microscopic Study of Chain Deformation and Orientation in Uniaxially Strained Polymer Networks: NMR Results versus Different Network Models. *Macromolecules*, 47:7597–7611, 2014.
- [24] R. Pérez-Aparicio, M. Schiewek, J. L. Valentín, H. Schneider, D. R. Long, M. Saphiannikova, P. Sotta, K. Saalwächter, and M. Ott. Local Chain Deformation and Overstrain in Reinforced Elastomers: An NMR Study. *Macromolecules*, 46:5549–5560, 2013.
- [25] A. Naumova, C. Tschierske, and K. Saalwächter. Orientation-dependent proton double-quantum NMR build-up function for soft materials with anisotropic mobility. *Solid State Nuclear Magnetic Resonance*, 82-83:22–28, 2017.
- [26] A. Naumova, D. C. Agudelo, M. A. Villar, D. A. Vega, J. L. Valentin, and K. Saalwächter. Microscopic state of polymer network chains upon swelling and deformation. *Macromolecules*, 52:5042–5053, 2019.
- [27] Yu. V. Zelenev G. M. Bartenev. *Fizika i mekhanika polimerov (in Russian)*. Publisher "Vysshaya Shkola", Moscow, 1983.
- [28] S. Ya. Frenkel G. M. Bartenev. *Fizika polimerov (in Russian)*. "Khimiya", Leningrad, 1990.
- [29] A. D. Mitrofanov N. A. Kozlov. *Fizika polimerov (in Russian)*. Vladimir State University, Vladimir, 2001.
- [30] M. Rubinstein and R. H. Colby. *Polymer physics*. Oxford University Press, 2003.
- [31] A. R. Khokhlov A. Yu. Grosberg. *Statisticheskaya fizika makromolekul (in Russian)*. "Nauka", Moskva, 1989.
- [32] F. Tanaka. *Polymer Physics : Applications to Molecular Association and Thermoreversible Gelation*. Cambridge University Press, Cambridge New York, 2011.

- [33] Prof. J. Powers and R. S. Stein. *Topics in Polymer Physics*. Imperial College Pr, 2006.
- [34] C. P. Poole Jr. *Encyclopedic dictionary of condensed matter physics*. Elsevier, 2011.
- [35] B. Erman. Molecular aspects of rubber elasticity. In *Mechanics and Thermomechanics of Rubberlike Solids*, pages 63–89. Springer Vienna, 2004.
- [36] A.Y. Grosberg and A.R. Khokhlov. *Giant molecules : Here, There, and Everywhere*. World Scientific, 2011.
- [37] G. Hild. Model networks based on 'endlinking' processes: synthesis, structure and properties. *Progress in Polymer Science*, 23:1019–1149, 1998.
- [38] Zh. Wang, B. Zhang, H. Yu, G. Li, and Ya. Bao. Synthetic control of network topology and pore structure in microporous polyimides based on triangular triphenylbenzene and triphenylamine units. *Soft Matter*, 7:5723, 2011.
- [39] Y. Jochi, T. Seki, T. Soejima, K. Satoh, M. Kamigaito, and Y. Takeoka. Spontaneous synthesis of a homogeneous thermoresponsive polymer network composed of polymers with a narrow molecular weight distribution. *NPG Asia Materials*, 10:840–848, 2018.
- [40] C. M. Roland and M. L. Warzel. Orientation effects in rubber double networks. *Rubber Chemistry and Technology*, 63:285–297, 1990.
- [41] P. G. Santangelo and C. M. Roland. The mechanical behavior of double network elastomers. *Rubber Chemistry and Technology*, 67:359–365, 1994.
- [42] Zh. Zhuang, L. Wu, X. Ma, W. Diao, and Y. Fang. High-strength, tough, rapidly self-recoverable, and fatigue-resistant hydrogels based on multi-network and multi-bond toughening mechanism. *Journal of Applied Polymer Science*, 135:46847, 2018.
- [43] J. E. Mark, B. Erman, and C. M. Roland. *The Science and Technology of Rubber*. Academic Press, 2013.
- [44] V. P. Dorozhkin and E. M. Galimova. *Khimiya i fizika polimerov (in Russian)*. Nizhnekamsk Institute of Chemical Technology, Nizhnekamsk, 2013.
- [45] A. M. Shur. *Vysokomolekulyarnye soedineniya*. Vysshaya shkola, Moscow, 1981.

- [46] J. L. Valentín, J. Carretero-González, I. Mora-Barrantes, W. Chassé, and K. Saalwächter. Uncertainties in the determination of cross-link density by equilibrium swelling experiments in natural rubber. *Macromolecules*, 41: 4717–4729, 2008.
- [47] J. E. Mark, B. Erman, and F. R. Eirich. *Science and technology of rubber*. Elsevier Academic Press, 2005.
- [48] L. R. G Treloar. *The Physics of Rubber Elasticity*. Oxford University Press, 2005.
- [49] M. Doi and S. F. Edwards. Dynamics of concentrated polymer systems. part 1.—brownian motion in the equilibrium state. *J. Chem. Soc., Faraday Trans. 2*, 74:1789–1801, 1978.
- [50] H. M. James and E. Guth. Theory of the Elastic Properties of Rubber. *The Journal of Chemical Physics*, 11:455–481, 1943.
- [51] B. Erman and J. E. Mark. *Structures and properties of rubberlike networks*. Oxford University Press, New York, 1997.
- [52] M. Rubinstein and S. Panyukov. Nonaffine deformation and elasticity of polymer networks. *Macromolecules*, 30:8036–8044, 1997.
- [53] M. Rubinstein and S. Panyukov. Elasticity of polymer networks. *Macromolecules*, 35:6670–6686, 2002.
- [54] M. Doi. *Soft matter physics*. Oxford University Press USA, Oxford, 2013.
- [55] W. Chassé, S. Schlögl, G. Riess, and K. Saalwächter. Inhomogeneities and local chain stretching in partially swollen networks. *Soft Matter*, 9:6943–6954, 2013.
- [56] W. Kuhn und F. Grün. Beziehungen zwischen elastischen Konstanten und Dehnungsdoppelbrechung hochelastischer Stoffe. *Elastische Konstanten und Dehnungsdoppelbrechung*, 3:248–271, 1942.
- [57] K. Saalwächter, P. Ziegler, O. Spycykerelle, B. Haidar, A. Vidal, and J.-U. Sommer. 1h multiple-quantum nuclear magnetic resonance investigations of molecular order distributions in poly(dimethylsiloxane) networks: Evidence for a linear mixing law in bimodal systems. *The Journal of Chemical Physics*, 119:3468–3482, 2003.

- [58] J.-U. Sommer, W. Chassé, J. L. Valentín, and K. Saalwächter. Effect of excluded volume on segmental orientation correlations in polymer chains. *Physical Review E*, 78:051803, 2008.
- [59] J. P. Cohen-Addad, M. Domard, and J. Herz. NMR observation of the swelling process of polydimethylsiloxane networks. average orientational order of monomeric units. *The Journal of Chemical Physics*, 76:2744–2753, 1982.
- [60] J.P. Cohen-Addad, M. Domard, G. Lorentz, and J. Herz. Polymeric gels. NMR study of elementary chain swelling. effect of trapped topological constraints. *Journal de Physique*, 45:575–586, 1984.
- [61] F. Di Lorenzo and S. Seiffert. Nanostructural heterogeneity in polymer networks and gels. *Polymer Chemistry*, 6:5515–5528, 2015.
- [62] F. Di Lorenzo, J. Hellwig, R. von Klitzing, and S. Seiffert. Macroscopic and Microscopic Elasticity of Heterogeneous Polymer Gels. *ACS Macro Letters*, 4:698–703, 2015.
- [63] S. B. Clough, A. Maconnachie, and G. Allen. Small-angle neutron scattering from stretched polystyrene networks. *Macromolecules*, 13:774–775, 1980.
- [64] M. H. Wagner. Analysis of small-angle neutron scattering data on poly(dimethylsiloxane) network unfolding. *Macromolecules*, 27:5223–5226, 1994.
- [65] M. Beltzung, C. Picot, and J. Herz. Investigation of the chain conformation in uniaxially stretched poly(dimethylsiloxane) networks by small-angle neutron scattering. *Macromolecules*, 17:663–669, 1984.
- [66] D. J. Read and T. C. B. McLeish. Microscopic theory for the “lozenge” contour plots in scattering from stretched polymer networks. *Macromolecules*, 30:6376–6384, 1997.
- [67] M. Warner and S. F. Edwards. Neutron scattering from strained polymer networks. *Journal of Physics A: Mathematical and General*, 11:1649–1655, 1978.
- [68] E. Mendes, R. Oeser, C. Hayes, F. Boué, and J. Bastide. Small-angle neutron scattering study of swollen elongated gels: butterfly patterns. *Macromolecules*, 29:5574–5584, 1996.

- [69] E. Straube, V. Urban, W. Pyckhout-Hintzen, and D. Richter. SANS investigations of topological constraints and microscopic deformations in rubber-elastic networks. *Macromolecules*, 27:7681–7688, 1994.
- [70] S. Westermann, W. Pyckhout-Hintzen, D. Richter, E. Straube, S. Egelhaaf, and R. May. On the length scale dependence of microscopic strain by SANS. *Macromolecules*, 34:2186–2194, 2001.
- [71] W. Pyckhout-Hintzen, A. Botti, M. Heinrich, S. Westermann, D. Richter, and E. Straube. The length-scale dependence of strain in networks by SANS. *Applied Physics A: Materials Science & Processing*, 74:368–370, 2002.
- [72] M. Duer. *Solid-state NMR spectroscopy : principles and applications*. Blackwell Science, Malden, MA, 2002.
- [73] Malcolm Levitt. *Spin dynamics : basics of nuclear magnetic resonance*. John Wiley & Sons, Ltd, Chichester, England Hoboken, NJ, 2008.
- [74] H. Günther. *NMR spectroscopy : basic principles, concepts, and applications in chemistry*. Wiley-VCH, Weinheim, 2013.
- [75] S. Szymański and P. Bernatowicz. *Classical and quantum molecular dynamics in NMR spectra*. Springer, Cham, Switzerland, 2018.
- [76] R. Macomber. *A complete introduction to modern NMR spectroscopy*. Wiley, New York, 1998.
- [77] G. Kummerlöwe and B. Luy. Residual dipolar couplings for the configurational and conformational analysis of organic molecules. In *Annual Reports on NMR Spectroscopy*, pages 193–232. Elsevier, 2009.
- [78] Kay Saalwächter, Berta Herrero, and Miguel Angel López-Manchado. Chain order and cross-link density of elastomers as investigated by proton multiple-quantum NMR. *Macromolecules*, 38:9650–9660, 2005.
- [79] J. U. Sommer and K. Saalwächter. Segmental order in end-linked polymer networks: A monte carlo study. *The European Physical Journal E*, 18:167–182, 2005.
- [80] J. A. Losonczi, M. Andrec, M. W.F Fischer, and J. H. Prestegard. Order matrix analysis of residual dipolar couplings using singular value decomposition. *Journal of Magnetic Resonance*, 138:334–342, 1999.

- [81] P. T. Callaghan and E. T. Samulski. Molecular ordering and the direct measurement of weak proton-proton dipolar interactions in a rubber network. *Macromolecules*, 30:113–122, 1997.
- [82] J. Keeler. *Understanding NMR Spectroscopy*. WILEY, 2002.
- [83] J. Baum and A. Pines. NMR studies of clustering in solids. *Journal of the American Chemical Society*, 108:7447–7454, 1986.
- [84] K. Saalwächter. Proton multiple-quantum NMR for the study of chain dynamics and structural constraints in polymeric soft materials. *Progress in Nuclear Magnetic Resonance Spectroscopy*, 51:1–35, 2007.
- [85] K. Saalwächter, M. Gottlieb, Liu, and W. Oppermann. Gelation as studied by proton multiple-quantum NMR. *Macromolecules*, 40:1555–1561, 2007.
- [86] K. Saalwächter, F. Kleinschmidt, and J.-U. Sommer. Swelling heterogeneities in end-linked model networks: a combined proton multiple-quantum NMR and computer simulation study. *Macromolecules*, 37:8556–8568, 2004.
- [87] K. Saalwächter and A. Heuer. Chain Dynamics in Elastomers as Investigated by Proton Multiple-Quantum NMR. *Macromolecules*, 39:3291–3303, 2006.
- [88] W. Chassé, J. L. Valentín, G. D. Genesky, C. Cohen, and K. Saalwächter. Precise dipolar coupling constant distribution analysis in proton multiple-quantum NMR of elastomers. *The Journal of Chemical Physics*, 134:044907, 2011.
- [89] Jürgen Weese. A reliable and fast method for the solution of fredhol integral equations of the first kind based on tikhonov regularization. *Computer Physics Communications*, 69:99–111, 1992.
- [90] J. Weese. A regularization method for nonlinear ill-posed problems. *Comp. Phys. Commun.*, 77:429–440, 1993.
- [91] Y. Fukahori. *Use of natural rubber (NR) for vibration isolation and earthquake protection of structures*. Elsevier, 2014.
- [92] www.rubbercal.com.
- [93] Y. Hirata, H. Kondo, and Y. Ozawa. *Natural rubber (NR) for the tyre industry*. Elsevier, 2014.

- [94] <https://iisrp.com>.
- [95] Lars Friebe, Oskar Nuyken, and Werner Obrecht. Neodymium-based ziegler/natta catalysts and their application in diene polymerization. In *Advances in Polymer Science*, pages 1–154. Springer Berlin Heidelberg, 2006.
- [96] Frederikke Bahrt Madsen, Ivaylo Dimitrov, Anders Egede Daugaard, Søren Hvilsted, and Anne Ladegaard Skov. Novel cross-linkers for PDMS networks for controlled and well distributed grafting of functionalities by click chemistry. *Polymer Chemistry*, 4:1700, 2013.
- [97] J. de Jong, R. G. H. Lammertink, and M. Wessling. Membranes and microfluidics: a review. *Lab on a Chip*, 6:1125, 2006.
- [98] M.K. Jensen, A. Bach, O. Hassager, and A.L. Skov. Linear rheology of cross-linked polypropylene oxide as a pressure sensitive adhesive. *International Journal of Adhesion and Adhesives*, 29:687–693, 2009.
- [99] Paul Brochu and Qibing Pei. Advances in dielectric elastomers for actuators and artificial muscles. *Macromolecular Rapid Communications*, 31:10–36, 2010.
- [100] A. Vieyres, R. Pérez-Aparicio, P.-A. Albouy, O. Sanseau, K. Saalwächter, D. R. Long, and P. Sotta. Sulfur-cured natural rubber elastomer networks: Correlating cross-link density, chain orientation, and mechanical response by combined techniques. *Macromolecules*, 46:889–899, 2013.
- [101] J. L. Valentín, P. Posadas, A. Fernández-Torres, M. A. Malmierca, L. González, W. Chassé, and K. Saalwächter. Inhomogeneities and chain dynamics in diene rubbers vulcanized with different cure systems†. *Macromolecules*, 43:4210–4222, 2010.
- [102] W. Chassé, M. Lang, J.-U. Sommer, and K. Saalwächter. Cross-link density estimation of PDMS networks with precise consideration of networks defects. *Macromolecules*, 45:899–912, 2011.
- [103] Kay Saalwächter. Microstructure and molecular dynamics of elastomers as studied by advanced low-resolution nuclear magnetic resonance methods. *Rubber Chemistry and Technology*, 85:350–386, 2012.
- [104] J. E. Mark, editor. *Physical Properties of Polymers Handbook*. Springer, New York, 2006.

- [105] J. L. Valentín, D. López, R. Hernández, C. Mijangos, and K. Saalwächter. Structure of poly(vinyl alcohol) cryo-hydrogels as studied by proton low-field NMR spectroscopy. *Macromolecules*, 42:263–272, 2009.
- [106] W. Gronski, R. Stadler, and M. M. Jacobi. Evidence of nonaffine and inhomogeneous deformation of network chains in strained rubber-elastic networks by deuterium magnetic resonance. *Macromolecules*, 17:741–748, 1984.
- [107] H. M. James and E. Guth. Theory of rubber elasticity for development of synthetic rubbers. *Industrial and engineering chemistry*, 34:1365–1367, 1942.
- [108] H. M. James. Statistical properties of networks of flexible chains. *The Journal of Chemical Physics*, 15:651–668, 1947.
- [109] D.S. Pearson. Scattered intensity from a chain in a rubber network. *Macromolecules*, 10:696–701, 1977.
- [110] G. Heinrich, E. Straube, and G. Helmis. Rubber Elasticity of Polymer Networks – Theories. *Adv. Polym. Sci.*, 85:33–87, 1988.
- [111] P. H. Mott and C. M. Roland. Elasticity of natural rubber networks. *Macromolecules*, 29:6941–6945, 1996.
- [112] Paul J. Flory and Burak Erman. Theory of elasticity of polymer networks. 3. *Macromolecules*, 15:800–806, 1982.
- [113] Andrzej Kloczkowski, James E. Mark, and Burak Erman. A diffused-constraint theory for the elasticity of amorphous polymer networks. 1. fundamentals and stress-strain isotherms in elongation. *Macromolecules*, 28:5089–5096, 1995.
- [114] R. Everaers and K. Kremer. Elastic properties of polymer networks. *Journal of Molecular Modeling*, 2:293–299, 1996.
- [115] T.-P. Hsu and K. Kremer. Clustering of entanglement points in highly strained polymer melts.

Lebenslauf

Persönliche Daten

Name: Anna Naumova
Geburtsdatum: 20.07.1989
Geburtsort: Weliki Ustjug

Ausbildung

9.1996 - 8.2003 Bolschewistskaja-Schule, Blagoweschjenje, Russland
9.2003 - 8.2006 Gymnasium, Weliki Ustjug, Russland
Abschluss: Bachelor of Physics
6.2006 - 8.2010 Studium Bachelor Physik, Staatliche Universität Sankt Petersburg
Abschluss: Master of Physics
9.2010 - 8.2012 Studium Mater Physik, Staatliche Universität Sankt Petersburg
ab 12.2013 Promotion Physik, MLU Halle-Wittenberg

Halle (Saale), 26. Dezember 2019

Anna Naumova

Publikationsliste

1. A. Naumova, C. Tschierske and K. Saalwächter. Orientation-dependent proton double-quantum NMR build-up function for soft materials with anisotropic mobility, *Solid State Nuclear Magnetic Resonance*, **2017**, 82-83, 22-28
2. A. Naumova, D. C. Agudelo, M. A. Villar, D. A. Vega, J. L. Valentin and K. Saalwächter. Microscopic State of Polymer Network Chains upon Swelling and Deformation, *Macromolecules*, **2019**, 52: 5042-5053

Erklärung

Hiermit erkläre ich, dass ich die vorliegende Arbeit selbständig und ohne fremde Hilfe verfasst, andere als die von mir angegebenen Quellen und Hilfsmittel nicht benutzt und die den benutzten Werken wörtlich oder inhaltlich entnommenen Stellen als solche kenntlich gemacht habe.

Dissertation wurde an keiner anderen wissenschaftlichen Einrichtung zur Bewerbung eines Doktorgrades vorgelegt oder veröffentlicht.

Halle (Saale), 26. Dezember 2019

Anna Naumova

Thanks (Спасибо)

I would like to thank my thesis advisor Prof. Dr. Saalwächter for giving me the opportunity to conduct the research and write a thesis in his group, as well as his motivation and guidance throughout my PhD.

I am grateful to everyone from the NMR and BIO groups for providing a nice atmosphere and good working environment.

Thanks to my office mates: Ruth and Ricardo for pleasant time, helping me with the German language and interesting daily discussions. I am also grateful to my next door roommates: Mozhdeh, Mareen and Tiago for being interesting and helpful colleagues. I am thankful to my new neighbours: Anika and Lukas for spending nice time together. And not forgetting Maria for being a nice and pleasant person to talk to.

I am grateful to my friends: Anton and Zhanna for supporting me, especially at difficult times, as well as motivating me to write my thesis. I am also thankful to my cat: Masha for being cute and comforting me throughout difficult times. A very special thanks to Imran for being with me, even when I was totally negative and pessimistic, and for creating and sharing nice moments!

Особое спасибо моим родителям и сестре Танюше за поддержку и любовь, за воспитание меня, и за то, что принимают меня такой какая я есть.